THE UNIVERSITY OF CHICAGO

IMPROVING SUSTAINED RELEASE VACCINES VIA DELAYED BOOSTING AND IMMUNE POTENTIATORS FOR INCREASED IMMUNOLOGICAL CONTROL

A DISSERTATION SUBMITTED TO

THE FACULTY OF THE PRITZKER SCHOOL OF MOLECULAR ENGINEERING

IN CANDIDACY FOR THE DEGREE OF

DOCTOR OF PHILOSOPHY

BY

BRITTENY CASSAIDY

CHICAGO, ILLINOIS

AUGUST 2022

Table of Contents

List of Figures

List of Tables

Acknowledgments

First, I would like to thank my Ph.D. advisor, Prof Aaron Esser-Kahn, for allowing me to work in his lab at UC-Irvine and continue to do so at the University of Chicago. I have grown scientifically and professionally while being a member of your group. I would also like to extend thanks to my committee members, Dean Matthew Tirrell and Prof Jeffrey Hubbell, for all their support and feedback.

To my incredible lab members, both past and present: thank you so much for providing a fun and supportive lab environment. Dr. Brittany Moser, thank you so much for being an amazing mentor and Dr. Alfred Chon, Dr. Flora Kimani, Dr. Saikat Manna, Dr. Tyler Albin, Prof Zhao Wang, and Dr. Seong-Min Kim for being so helpful throughout my graduate school experience. Thank you so much, Jinjing and Qing, for helping me with my animal experiments and all those times we had to extract T cells. Thanks to Matt for being an excellent collaborator on the SARS-CoV-2 project. To Zoe Lockhart and Kristen Gotsis, thank you so much for being outstanding undergraduate researchers and helping me with my projects. Also, thanks to Adam and Brad for being fun and incredible lab mates. A special thanks to Jun, Yoseline, Jainu, Nihesh, and Jorge for being so supportive both professionally and personally. You have helped make all the tough times bearable.

Finally, thanks to my amazing and supportive husband, Kyle, and my mom for providing so much love and support. I could not have made it to this point without you.

Abstract

Effective vaccine adjuvants and formulations often fail to achieve FDA approval due to their adverse immunostimulation. In particular, over-activation of the NF-κB pathway via pattern recognition receptors results in excess inflammation and harmful side effects. Previous work in our lab has shown that our anti-inflammatory immune potentiators in solution with a TLR9 agonist, CpG ODN 1826, successfully increased antibody response while reducing inflammation in both Dengue, HIV, and lethal influenza challenge. We applied this model to the SARS-CoV-2 model and proved that the immune potentiators could be beneficial additives for improving coronavirus subunit vaccines. Although this method is suitable for initiating immune responses, it may not solve issues with long-term protection.

Controlled release particle vaccinations that discharge agonist and antigen encapsulants in a slow, continuous manner have been reported to produce higher and longer-lasting antibody titers than their unencapsulated counterpart. Our data displayed that depending on the immune potentiator selected, the immune potentiator could make higher antibody levels than CpG OVA microparticle vaccines and outperform their unencapsulated counterpart. By using particles as the delivery method, we can further control the release mechanism and timing of the payload to the immune system. To further prevent the release, we coated our microparticles with a secondary and tertiary polymer. Thus, once injected, the outer polymer coatings will eventually degrade, revealing the microparticle core and allowing the encapsulants to remain dormant inside the body. By using the proper polymer coatings, we may generate a single-dose vaccine. A single dose vaccination will reduce the need for multiple boost vaccinations, eliminating the need for numerous visits to the doctor. These repeat visits are a challenge for individuals living in low-access medical communities. Therefore, a single-dose vaccination can potentially increase the number of patients

receiving adequate protection. The coating procedure proposed in the study is a simple two-pot synthesis. It has the potential to generate single-dose vaccinations, increasing the availability of the vaccine for those in low-access medical assistance communities.

1. Introduction

1.1 Introduction

In the past century, vaccines have successfully decreased the cases of numerous diseases, including smallpox, rubella, mumps, and polio.[1] Today, vaccines have been a vital tool in combating coronavirus, estimated to reduce the number of deaths and hospitalizations in the United States by half in the first six months of 2021.[2] The success of vaccines as prophylactics has contributed to them being considered one of the most significant advancements in medicine.

In general, a vaccine is a biological material that can provide protection against a pathogen. The biological material must contain two parts to provide protection: a segment that the immune system builds a response against, known as an antigen, and a segment that stimulates the innate immune system.[3] The innate immune system comprises several different cell types: basophils, eosinophils, mast cells, natural killer cells, dendritic cells, and macrophages. Of these cell types, dendritic cells are vital in bridging the innate and the adaptive immune response.

Upon a dendritic cell endocytosing and processing the antigen from a vaccine, the dendritic cell may migrate to a lymph node and activate naïve lymphocytes. Naïve lymphocytes then become effector T and B cells responsible for generating cytotoxic T cells and antibodies against the virus of interest based on the antigen provided. Most of these effector lymphocytes eventually die off, but the remaining ones become memory cells. Memory cells can initiate a faster immune response against their respective antigen. These memory cells are responsible for providing long-term protection against a pathogen and the basis of the adaptive immune response's immunological memory.[4,5,6]

1.2 Different Types of Vaccines

Overall, there are six different categories of vaccines: live attenuated, inactivated, toxoid, messenger RNA, viral vector, and subunit.[7]

Live attenuated vaccines were the first vaccines developed. These vaccines are available against diseases like chickenpox, smallpox, yellow fever, measles, mumps, and rubella. A live attenuated vaccine is a weaker form of the pathogen of interest and can still replicate in the body after vaccination. As a result of the vaccine still being able to replicate, there are risks that the pathogen may be averse to individuals with weakened immune systems.

In contrast, to live attenuated vaccines, inactivated vaccines are deceased versions of the pathogen used for vaccination. Used in rabies, polio, and influenza vaccines, inactivated vaccines do not provide as vital of protection as live attenuated vaccines. Still, they provide less risk due to a lack of capacity to replicate.

Toxoid vaccines are like inactivated vaccines; however, the byproduct produced by the pathogen is inactivated and used for vaccination. Toxoid vaccines have limited use because not all pathogens produce toxins; thus, toxoid vaccines have been effective against bacterial diseases such as typhoid and diphtheria.

Messenger RNA or mRNA vaccines have gained widespread popularity since 2020 after the emergency FDA approval of Pfizer's and Moderna's COVID-19 vaccine. These vaccines contain the messenger RNA sequence for a portion of the pathogen to build immunity against. The host cells transfect the mRNA to the antigen of interest. The mRNA is delivered in a liposome to prevent pre-cellular degradation of the mRNA sequence.

Lastly, subunit vaccines immunize against a portion of the pathogen known as an antigen. The antigen alone is not usually immunogenic enough to generate an immune response. Therefore, subunit vaccines typically contain an adjuvant and require additional boosters. Adjuvants are substances that initiate a heightened pro-inflammatory immune response once administered. Consequently, an adjuvant combined with the desired antigen can significantly increase the vaccine's antibody production. However, numerous vaccine adjuvants such as Freud's Complete Adjuvant, Poly I: C, and various forms of CpG fail to receive FDA approval due to their adverse inflammatory side effects.[8,9]

1.3 Limitations of vaccines

Despite the success of vaccines in reducing the prevalence of infectious diseases, there are still limitations and challenges to their use. These limitations include the vaccine's need for cold storage, the number of doses required, and the need for new vaccines against existing deadly infectious diseases[10]. The multiple doses that are necessary for vaccines lead to difficulty in distributing the vaccine to low medical access communities. Historically, vaccines were developed without a solid mechanistic understanding of immunology. Thus, despite numerous vaccines available on the market, there is still the need to develop new vaccines against deadly infectious diseases such as dengue, tuberculosis, and HIV. We were particularly interested in helping create new vaccines by improving adjuvants in subunit vaccines. As previously mentioned, adjuvants struggle to reach approval due to adverse inflammatory side effects. Our lab had previously reported the ability to separate these inflammatory side effects while maintaining the antibody production effects of adjuvants. [11,12,13]Lastly we sought to decrease the dosing requirements

necessary via encapsulating subunit vaccines into polymer microspheres and control the release via additional polymer coating.

1.4 Immune Potentiators

Immune potentiators are a subclass of adjuvants that specifically target immune cells and modify the adaptive immune response[14,15]. Our lab has been specifically interested in immune potentiators that can suppress the inflammation generated by the NF-κB pathway. The NF-κB pathway can be activated by various receptors, including Pattern Recognition Receptors (PPR). Pattern Recognition Receptors commonly stimulate the NF-κB Pathway from the various PPRs expressed on innate immune cells. This subfamily of receptors includes NOD-like receptors, Toll-like receptors (TLR), and C-type lectin receptors. Many adjuvants stimulate the innate immune system via PPRs, including CpG. CpG is an adjuvant that stimulates TLR9, a Toll-like receptor located in the endoplasmic reticulum of mammalian cells. Upon stimulation in innate immune cells, the NF-κB pathway promotes the production of pro-inflammatory cytokines,

chemokines, and other acute phase reactants.[16,17]

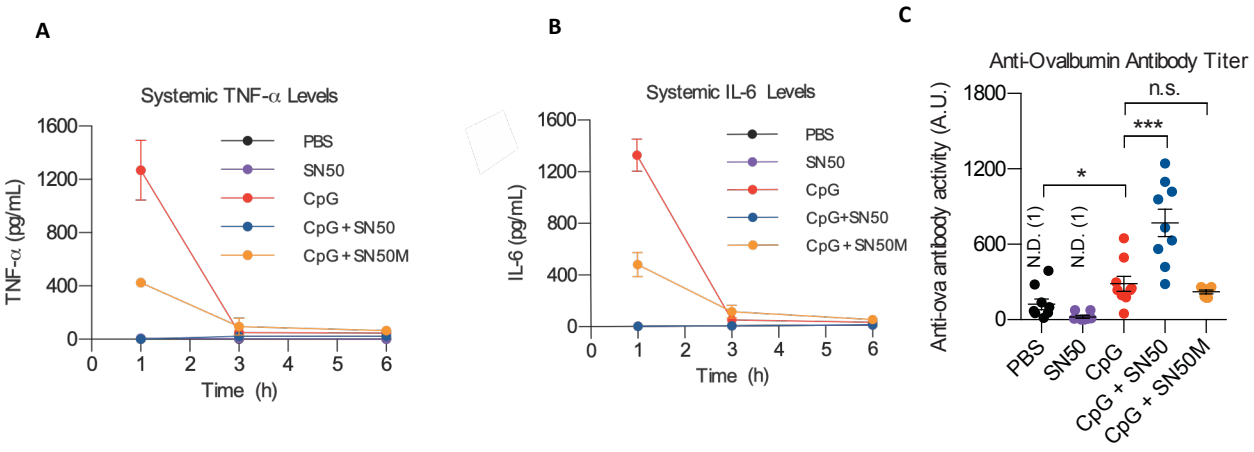

Figure 1.1. *In vivo* vaccination with OVA antigen and SN50. SN50M is similar to SN50 but has a different NLS sequence.

Figure 1.1 continued
(A) Serum cytokine levels of TNF-a measured at 1h, 3h, and 6h post-injection with: PBS (black line), SN50 alone (purple line), CpG (red line), CpG with SN50 (blue line), CpG and SN50M (yellow line) (B) Serum cytokine levels of IL-6. (C) Anti-ovalbumin antibody titer, day 21.

NF-κB has a group of transcription factor proteins that, when inactive, reside in the cell's cytoplasm and move into the nucleus via the nuclear pore complex once activated. These transcription factors reside as dimers, the most common being the p50/RelA dimer. The immune potentiators selected in this study can block these NF-κB transcription factors. As a result, when an agonist stimulates the receptors of the cells, the most significant portions of NF-κB, the dimers containing p50, are impaired from being translocated into the nucleus due to competition from the potentiators.[18,19] Previous work in the lab has shown that the SN50, honokiol, and capsaicin allotted in solution with an agonist, CpG, successfully increased antibody response compared to CpG while reducing the peak time-point of systemic inflammation at the 1-hour mark. (**Figure 1.1**). [13]

In addition to inhibiting the NF-κb pathway, our group was interested in generating innate immune cell memory via trained immunity. Molecules such as 1,3 β-glucan can cause epigenetic and metabolic changes that rewire innate immune cells.[21] These changes improve pathogen detection, and immune reactivity by the "trained" cells that can more readily respond to a second attack by both the same or an unrelated pathogen. This enhanced responsiveness conferred by innate cells, called trained immunity, can improve the first line of defense and subsequent adaptive immune responses by increasing antigen presentation and T-cell activation.[22] However, these changes exhibited by β-glucan have been short and transient, lasting no more than a week.

1.5 Controlled Release of Immune Potentiators

Although the half-life of SN50 is unknown, most peptides have an *in vivo* half-life of anywhere between 4 to 30 minutes.[20] β-glucan's short training effects may be due to its short half-life of around four hours.[23] Particle encapsulation approaches to vaccination have been able to extend the availability of the peptide payload and dose less than its unencapsulated counterpart due to the controlled release mechanism and protection of contents before cellular uptake.[24] Controlled release is a form of steady, constant release of encapsulants, typically exhibiting first-order kinetics.

Placing the immune potentiators into particles introduces several additional benefits: controlled release of the payload and easy uptake of particles by dendritic cells due to their resemblance to pathogens. In addition, particle vaccinations can ensure that all vaccine components reach the cells at once to achieve the optimal immune response.[25] It has been reported that particle vaccinations that discharge agonist and antigen encapsulants in a controlled release manner via microparticles produce a higher and longer antibody titer than its unencapsulated and nanoparticle counterpart.[26]

PLGA is a biocompatible polymer popular in particle vaccines. The copolymer has been successfully utilized to deliver proteins, DNA, and small molecules. PLGA degrades via hydrolysis of its ester backbone to nontoxic components. Both PLGA nanoparticles and microparticle have been shown to promote prolonged antigen presentation in dendritic cells. By resembling pathogens as particles, PLGA particles are more readily uptaken by antigen-presenting cells. Numerous studies using PLGA particles reported higher Th1 responses compared to their unencapsulated form. This holds for a wide range of antigens for diseases such as Hepatitis B, chlamydia, and tuberculosis. [24, 27]

1.6 Delayed Release

On top of having controlled release of the particles, we may also have a pulsatile release of the particles via a secondary coating of the particles. The secondary polymer coating will degrade first, then allow the core microparticles to degrade over time. Therefore, the thickness of the particles' coating can be optimized to have the desired release rate of the payload. Particles coated with different thicknesses of secondary polymer can be used to create dosages of the drug to be released at other time points. This pulsatile release behavior of the particles allows them to act as a single dose vaccination.

Few pulsatile release systems have been developed.[28] One of the most prominent endeavors was headed by the World Health Organization in creating a single dose tetanus vaccine. The project was abandoned due to difficulty upscaling all three of their double emulsion, spray drying, and coacervation techniques to clean-room good manufacturing practice (GMP) facilities.[29] Another recent study utilized expensive 3D printing to create particles with various molecular weights of PLGA. Therefore, particles with lighter molecular weight PLGA degraded before particles made with heavier PLGA.[30] With very few multiple dose delivery systems available, there is a critical need to develop new platforms that can broadly apply to different booster schedules. Such a broadly applicable platform could solve patient compliance with vaccines.

1.7 References

1. Plotkin, S. History of vaccination. *Proc. Natl. Acad. Sci.* **111**, 12283–12287 (2014).

2. Vilches, T. N. *et al.* Estimating COVID-19 Infections, Hospitalizations, and Deaths Following the US Vaccination Campaigns During the Pandemic. *JAMA Netw. Open* **5**, e2142725 (2022).

3. Pulendran, B. & Ahmed, R. Immunological mechanisms of vaccination. *Nat. Immunol.* **12**, 509–517 (2011).

4. Janeway CA Jr, Travers P, Walport M, et al. *Immunobiology: The Immune System in Health and Disease*. (Garland Science, 2001).

5. Alberts B, Johnson A, Lewis J, et al. *Molecular Biology of the Cell*. (Garland Science, 2002).

6. Pulendran, B. & Ahmed, R. Translating Innate Immunity into Immunological Memory: Implications for Vaccine Development. *Cell* **124**, 849–863 (2006).

7. Pollard, A. J. & Bijker, E. M. A guide to vaccinology: from basic principles to new developments. *Nat. Rev. Immunol.* **21**, 83–100 (2021).

8. Clem, A. Fundamentals of vaccine immunology. *J. Glob. Infect. Dis.* **3**, 73 (2011).

9. Petrovsky, N. & Aguilar, J. C. Vaccine adjuvants: Current state and future trends. *Immunol. Cell Biol.* **82**, 488–496 (2004).

10. Pambudi, N. A., Sarifudin, A., Gandidi, I. M. & Romadhon, R. Vaccine cold chain management and cold storage technology to address the challenges of vaccination programs. *Energy Rep.* **8**, 955–972 (2022).

11. Kurup, V. M. & Thomas, J. Edible Vaccines: Promises and Challenges. *Mol. Biotechnol.* **62**, 79–90 (2020).

12. Wilson-Welder, J. H. *et al.* Vaccine adjuvants: Current challenges and future approaches. *J. Pharm. Sci.* **98**, 1278–1316 (2009).

13. Moser, B. A. *et al.* Increased vaccine tolerability and protection via NF-κB modulation. *Sci. Adv.* **6**, eaaz8700 (2020).

14. Buonsanti, C. & D'Oro, U. Discovery of Immune Potentiators as Vaccine Adjuvants. in *Immunopotentiators in Modern Vaccines* 85–104 (Elsevier, 2017). doi:10.1016/B978-0-12-804019-5.00005-0.

15. O'Hagan, D. T. & Valiante, N. M. Recent advances in the discovery and delivery of vaccine adjuvants. *Nat. Rev. Drug Discov.* **2**, 727–735 (2003).

16. Liu, T., Zhang, L., Joo, D. & Sun, S.-C. NF-κB signaling in inflammation. *Signal Transduct. Target. Ther.* **2**, 17023 (2017).

17. Scheiermann, J. & Klinman, D. M. Clinical evaluation of CpG oligonucleotides as adjuvants for vaccines targeting infectious diseases and cancer. *Vaccine* **32**, 6377–6389 (2014).

18. Tse, A. K.-W., Wan, C.-K., Shen, X.-L., Yang, M. & Fong, W.-F. Honokiol inhibits TNF-α-stimulated NF-κB activation and NF-κB-regulated gene expression through suppression of IKK activation. *Biochem. Pharmacol.* **70**, 1443–1457 (2005).

19. Singh, S., Natarajan, K. & Aggarwal, B. B. Capsaicin (8-methyl-N-vanillyl-6-nonenamide) is a potent inhibitor of nuclear transcription factor-kappa B activation by diverse agents. *J. Immunol. Baltim. Md 1950* **157**, 4412–4420 (1996).

20. Penchala, S. C. *et al.* A biomimetic approach for enhancing the *in vivo* half-life of peptides. *Nat. Chem. Biol.* **11**, 793–798 (2015).

21. Netea, M. G. *et al.* Defining trained immunity and its role in health and disease. *Nat. Rev. Immunol.* **20**, 375–388 (2020).

22. Netea, M. G. *et al.* Trained immunity: A program of innate immune memory in health and disease. *Science* **352**, (2016).
23. Rice, P. J. *et al.* Pharmacokinetics of fungal (1–3)-β-d-glucans following intravenous administration in rats. *Int. Immunopharmacol.* **4**, 1209–1215 (2004).

24. Allahyari, M. & Mohit, E. Peptide/protein vaccine delivery system based on PLGA particles. *Hum. Vaccines Immunother.* **12**, 806–828 (2016).

25. Joshi, V. B., Geary, S. M. & Salem, A. K. Biodegradable Particles as Vaccine Delivery Systems: Size Matters. *AAPS J.* **15**, 85–94 (2012).

26. Kanchan, V. & Panda, A. K. Interactions of antigen-loaded polylactide particles with macrophages and their correlation with the immune response. *Biomaterials* **28**, 5344–5357 (2007).

27. Keles, H., Naylor, A., Clegg, F. & Sammon, C. Investigation of factors influencing the hydrolytic degradation of single PLGA microparticles. *Polym. Degrad. Stab.* **119**, 228–241 (2015).

28. Jain, D., Raturi, R., Jain, V., Bansal, P. & Singh, R. Recent technologies in pulsatile drug delivery systems. *Biomatter* **1**, 57–65 (2011).

29. Johansen, P., Gómez, J. M. M. & Gander, B. Development of synthetic biodegradable microparticulate vaccines: a roller coaster story. *Expert Rev. Vaccines* **6**, 471–474 (2007).

30. McHugh, K. J. *et al.* Fabrication of fillable microparticles and other complex 3D microstructures. *Science* **357**, 1138–1142 (2017).

2. Application of Immune Potentiators to Improve SARS-CoV-2 Subunit Vaccine

2.1 Summary

The SARS-CoV-2 outbreak has caused a global pandemic that is being successfully combated with global vaccination campaigns. One of the most popular vaccines that are being developed is subunit vaccines. Immune potentiators can be beneficial additives to subunit vaccines by reducing the side effects of the adjuvant entailed while maintaining or improving the vaccine's efficacy. In this study, we designed two different subunit vaccines with immunomodulators SN50 and honokiol. Both immunomodulators successfully decreased systemic cytokines when paired with CpG and improved the number of neutralizing antibodies. In a viral challenge with Syrian hamsters, the honokiol formulation was the most successful immunomodulator in that it had the least amount of weight loss after inoculation, the lowest viral titer in nasal washes, and consistently had low viral titers in tissue. With numerous subunit vaccines in development against SARS-CoV-2, we believe that an immune potentiator such as honokiol could not help the vaccine have fewer side effects but also improve the vaccine's ability to combat SARS-CoV-2.

2.2 Introduction

Since first being reported in December 2019, SARS-CoV-2 has caused over half a billion infections and millions of deaths worldwide.[1] Vaccination have significantly helped curtail the spread of SARS-CoV-2 and reduce the number of hospitalizations.[2] However, as SARS-CoV-2 continues to progress through communities, several new variants have emerged. These new variants are more resistant to current mRNA vaccines available.[3,4,5] Therefore, there is a need to continue to develop effective vaccines against SARS-CoV-2.

Many different forms of SARS-CoV-2 vaccines have been developed and reached clinical trials: from inactivated vaccines to virus-like particles.[6] As of June 2022, of the 166 vaccines to enter clinical trials, over half of the vaccines have been subunit vaccines.[7] In general, subunit vaccines are safer than attenuated and inactivated vaccines since a piece of the virus, an antigen is used for vaccination. However, vaccinating with an antigen alone usually results in less immunogenicity. As a result, an adjuvant is added to increase the immune response to the antigen. [8,9] However, numerous vaccine adjuvants such as Freud's Complete Adjuvant, Poly I: C, and various forms of CpG fail to receive FDA approval due to their adverse inflammatory side effect.[10] One of the leading subunit vaccines, SCB-19, uses the S trimer and two different adjuvants, CpG 1018 and alum.[11] Data from the vaccine's phase 1 clinal trial reported that almost a third of participants reported local and systemic side effects, including injection site pain with their medium dosage.[12]

To help improve the safety of these vaccines, we propose to add immune potentiators that reduce systemic side effects while maintaining vaccine efficacy. We selected SN50 and honokiol as our immune potentiators because our previous studies displayed that these NF-κB inhibitors successfully repressed systemic cytokines when paired with an adjuvant while maintaining or improving the adaptive immune response.[13,14] In this study, we investigated our immune modulators with CpG and the Spike (S) protein. CpG was selected as the adjuvant since it is a popular adjuvant for SARS-CoV-2 subunit vaccines. We hypothesized that our immune potentiators combined with the Spike protein and CpG could reduce side effects generated by CpG and help create more protection from SARS-CoV-2.

2.3 Results and Discussion

For our first trial, we first applied our vaccine to BALB/c mice in a short, three-week experiment. We hypothesized that our immune potentiator formulations would be able to suppress systemic cytokines while improving the T cell activity and antibody levels. PBS was used to formulate all vaccine groups except for honokiol, where AddaVax was used to assist in dissolving the small molecule. Mice were vaccinated intramuscularly on day 0 with either S protein (20 μg), CpG-1826 (50 μg), SN50 (500 μg), and honokiol (400 μg). One hour after primary vaccination, serum was collected to measure systemic cytokines, IL-6 and TNF-α. Boost vaccination was delivered on day 14 before serum and splenocytes were collected on day 24. To measure T cell activity, splenocytes were re-stimulated ex-vivo with an S protein peptide mix, and the media was analyzed for cytokines 48 hours after incubation. As expected, one-hour bleeds revealed that SN50 paired with CpG successfully suppressed IL-6 and TNF- α cytokine productions. However, honokiol failed to do so (**Figure 2.1A-B**). We believe this is a result of honokiol being formulated in AddaVax. IFN- γ, and IL-17A were the only group of significant cytokines detected between groups. In both cases, the vaccines containing honokiol had higher IFN- γ and IL-17A levels than the CpG and S protein vaccine (**Figure 2.1C-D**). High levels of IFN- γ and IL-17A expression may indicate the helper T cells expressing a TH1/TH17 response. Therefore, the honokiol vaccine formulation may be trafficking and promoting CD8 + T cell activity and the recruitment of neutrophils to combat bacterial and fungal infections,[15,16]. However, IL-17A has been documented to be secreted by variety of T cells, including CD8+ T cells, for unknown biological reasons.[17]

Honokiol and SN50 formulations had higher IgG antibody levels than the S and CpG vaccine (**Figure 2.1E**). Since the IgG levels measured were not specific for SARS-CoV-2, we were

curious if the antibodies generated were neutralizing. The neutralization assay results indicated that the S+ CpG had a fifty percent neutralization dilution, ND50, of 1:320. SN50 and honokiol each had exceptionally high neutralizing antibodies that we did not dilute the serum enough to determine the ND50 value (**Figure 2.1F**). Therefore, SN50 could suppress systemic side effects while improving neutralization. Despite honokiol failing to stop systemic cytokines in our murine experiment, honokiol provided the highest average IgG antibody levels and potentially the strongest neutralization titer.

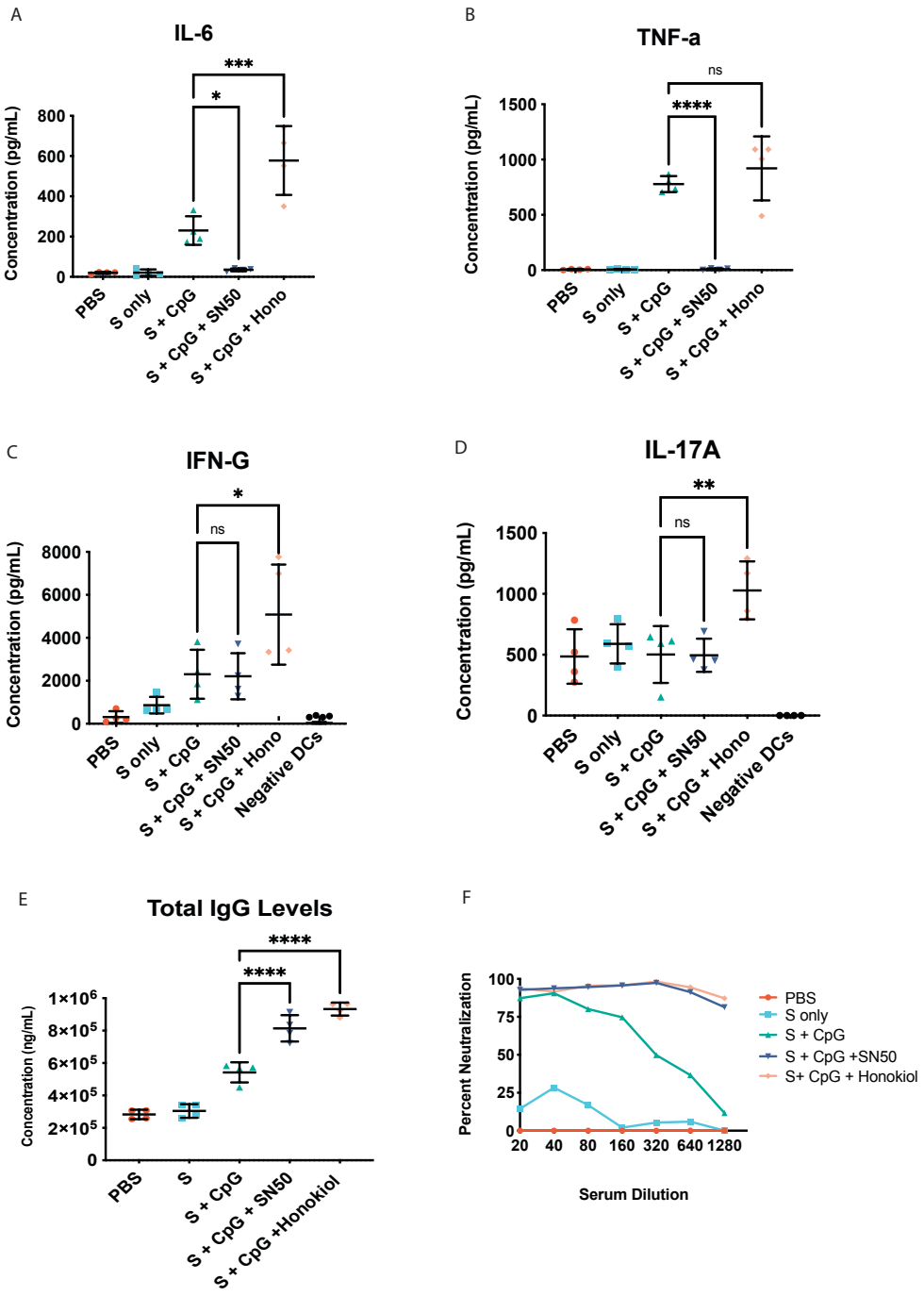

Figure 2.1 Murine Vaccination Experiment A) IL-6 B) TNF-α cytokine levels measured from 1-hour bleeds post-primary vaccination. N=4. C) IFN- γ D) IL-17A cytokine levels secreted from spike peptide mixture stimulated splenocytes harvested on day 24. N=4. E) Total IgG levels measured from serum on day 24. F) Neutralization assay using 2019-nCoV virus against day 24 serum. Mean reported with error bars representing the standard deviation. Statistics were One-Way Anova analysis with Dunnett's multiple comparison test.* $p<0.05$, **$p<0.01$, ***$p<0.001$.

The promising murine experiment led us to apply our vaccine to a more relevant model for a challenge study. Syrian hamsters are susceptible to SARS-CoV-2 and experience similar patterns of infections as humans do.[18,19] For the hamster challenge, all doses were delivered in PBS-including the honokiol formulation, to avoid the contribution of AddaVax to the vaccine's performance. Honokiol was solubilized in a small portion of dimethyl sulfoxide before being diluted with PBS with S protein and CpG. We were unsure of what immune modulators concentration to use for hamsters, so we tested two different concentrations: high dose (HD) and low dose (LD). Hamsters were vaccinated on days 0 and day 21. Serum was collected one hour after the primary boost to measure IL-6 levels and on day 31 to measure antibody levels. Three weeks later, hamsters were challenged intranasally with a high dose of SARS-CoV-2 (5×10^4 $TCID_{50}$). Body weight and clinical signs were measured after injections and viral challenge to assess vaccine and viral side effects.

After vaccination, no significant changes in body temperature were observed (**Figure 2.2A**). The lack of change in body temperature post vaccination may indicate that the vaccinations did not have an adverse effect on the hamsters. Serum samples taken from day 31 revealed that the immunomodulators had statistically similar anti-RBD IgG antibody levels to the CpG-1018 + Spike (**Figure 2.2B**). Honokiol formulations had similar microneutralization titers to CpG-1018 +Spike. In contrast, the SN50 formulations had statistically significantly less microneutralization titers (**Figure 2.2C**).

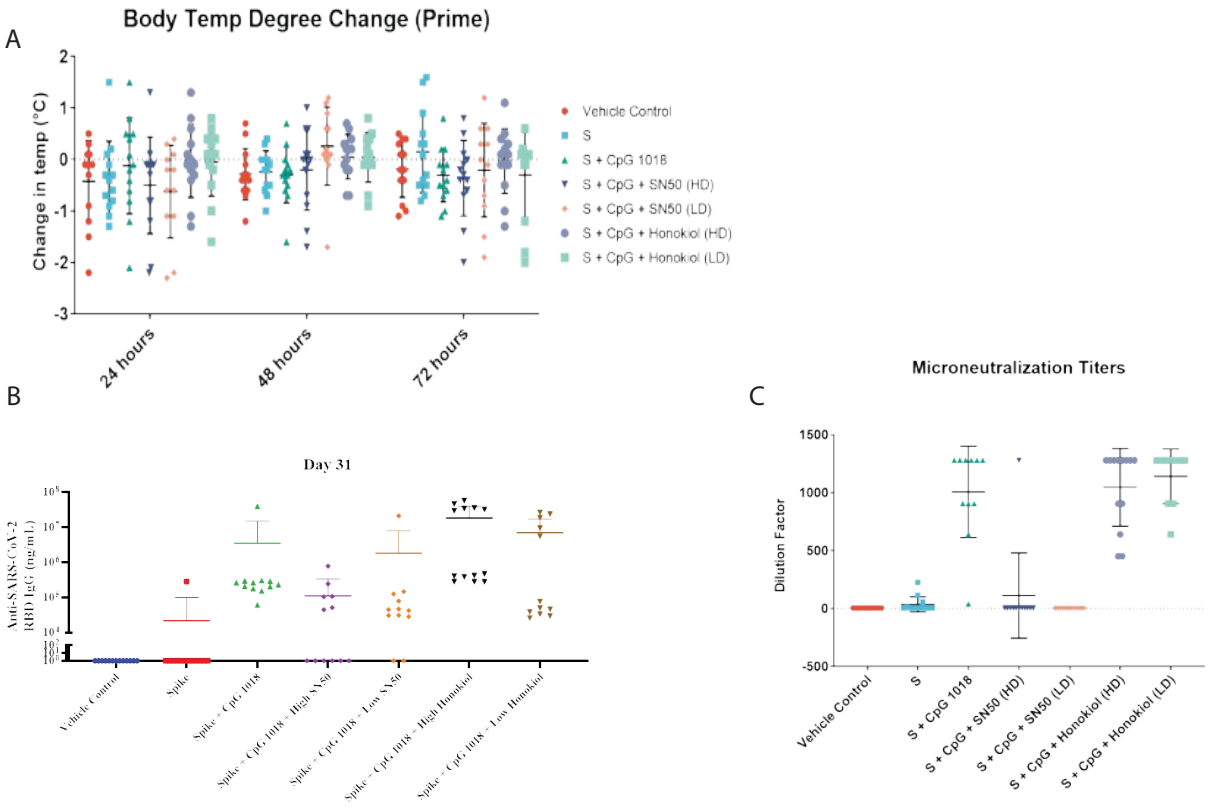

Figure 2.2 Syrian Hamster body temperature change post prime-boost and D31 Antibody Levels A) Syrian hamster body temperature changes (oC) measured post-primary vaccination over 72 hours. B) Anti-RBD IgG concentration measured from hamster's day 31 collected serum C) Microneutralization titers from hamster's day 31 serum. The highest dilution that is positive for neutralization is reported above. Mean reported with standard deviation error bars—no statistical significance between formulations with immune potentiator and S+CpG formulation.

After the challenge, the honokiol HD formulation resisted body weight changes the most and almost fully recovered after six days. Both SN50 formulations body weight changes post-challenge was similar to the CpG-1018+Spike group (**Figure 2.3A**). Genome titers taken on day 44 (2 days post-challenge), showed that honokiol LD had less virus detected in nasal washes than the CpG-1018 + Spike (**Figure 2.3B**). This statistical significance was gone by the day 45 nasal washes (**Figure 2.3C**). Surprisingly, despite the SN50 formulations having poor

microneutralization titers, both SN50 groups had similar genome titers to the CpG-1018+ S group.

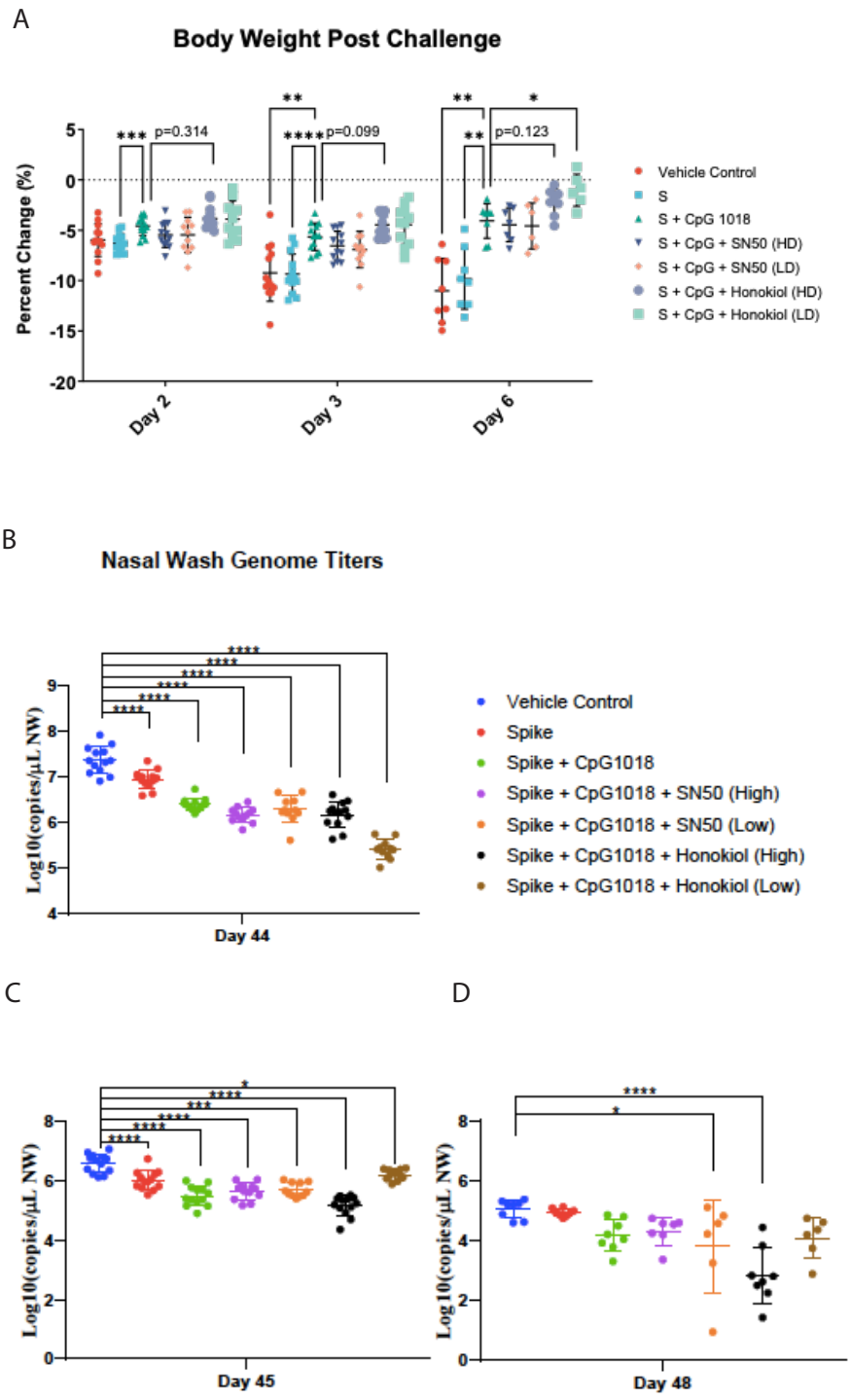

Figure 2.3 Post challenge body weight change and Nasal Genome Titers A) Syrian hamster's mean body weight changes post-challenge. Error bars are standard deviations.

Figure 2.3 continued
One-Way Anova analysis with Tukey's multiple comparison test. $p<0.05$, $^{**}p<0.01$, $^{***}p<0.001$, $^{****}p<0.0001$ B) Day 44 C) Day 45 D) Day 48 Genome titers in hamster nasal wash samples. Mean reported with standard deviation error bars. Statistics were One-Way Anova analysis with Dunnett's multiple comparison test. $p<0.05$, $^{**}p<0.01$, $^{***}p<0.001$, $^{****}p<0.0001$.

Post challenge genome titers were collected from several organs to quantify SARS-CoV-2 presence. Due to the strong neutralization titers measured in serum in the murine experiment, we hypothesized that our immune potentiator formulations could generate mucosal antibodies that could suppress the replication and eradicate the virus. Lung genome titers measured on day 45 and 48 revealed that the honokiol formulations had the lowest average viral concentration; however, it was not significant compared to the SN50 and CpG-1018+Spike groups (**Figure 2.4A & 2.4B**). The same trend was observed for the viral titers in nasal turbinates (**Figure 2.4C& 2.4D**). There were no significant differences in genome titer in the trachea (**Figure 2.4E & 2.4F**). All groups tested outside of the vehicle control successfully suppressed viral replication in the kidneys on day 45. By day 48, the kidney's viral load was low for all groups, and there was no statistical difference between them (**Figure 2.4H & 2.4I**).

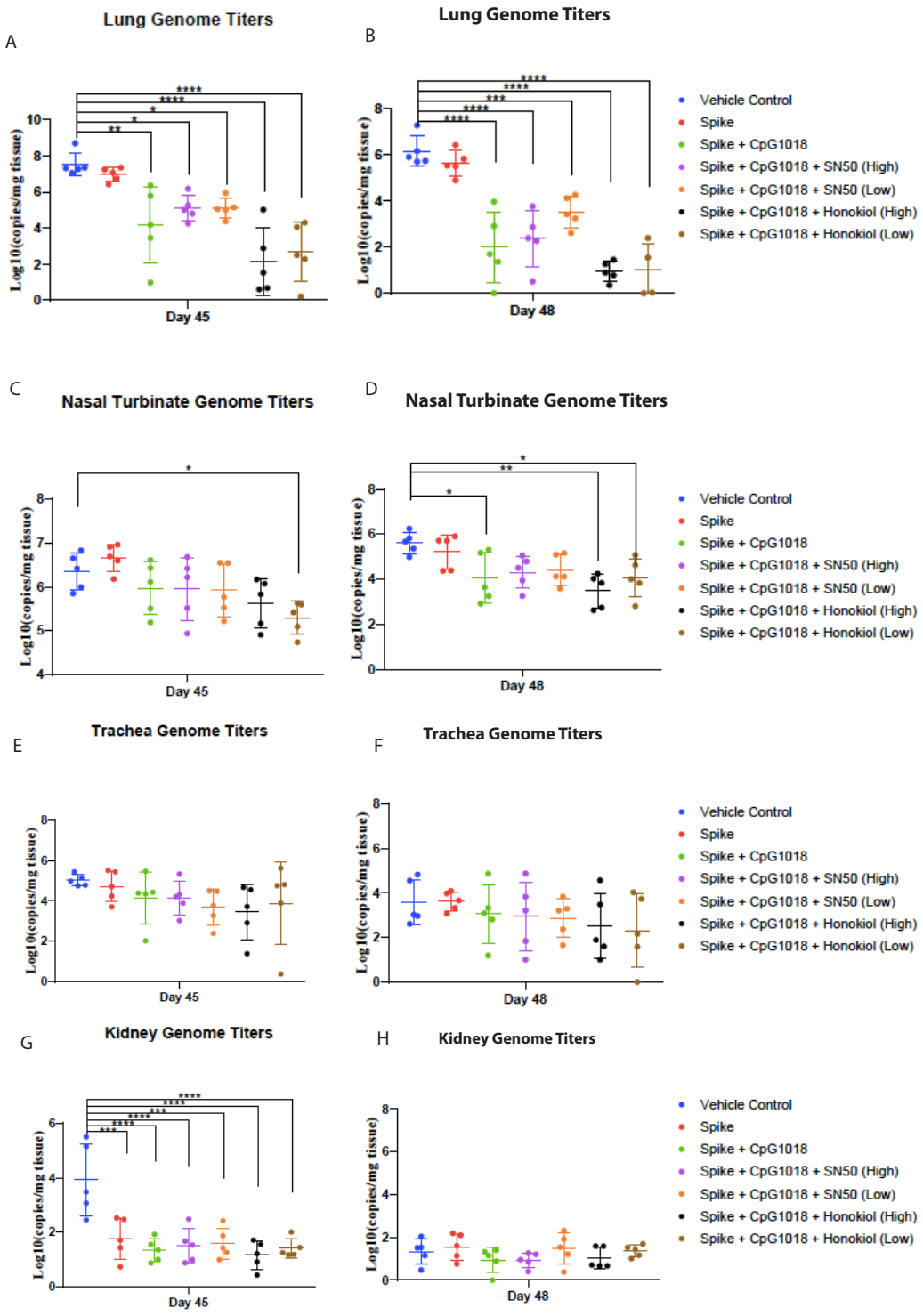

Figure 2.4 Viral genome titer in organs of interest A) Day 45 nasal turbinate B) Day 48 nasal turbinate C) Day 48 lung genome titer. D) Day 45 E) Day45 F) Day 48 trachea genome titer. N=5. Mean reported with standard deviation error bars Statistics were One-Way Anova analysis with Dunnett's multiple comparison test. $p<0.05$, $^{**}p<0.01$, $^{***}p<0.001$, $^{****}p<0.0001$.

2.4 Conclusion

Immunomodulators can be beneficial additives to subunit vaccines by improving their safety while maintaining efficacy. In murine studies, SN50 and honokiol both successfully decreased systemic cytokines while paired with CpG but improved the number of neutralizing antibodies. In the viral challenge with Syrian hamsters, the honokiol LD was the most successful immunomodulator in that it had the least amount of weight loss after inoculation, the lowest viral titer in nasal washes, and consistently had low viral titers in tissue. With numerous subunit vaccines in development against SARS-CoV-2, we conclude that an immunomodulator such as honokiol could help the vaccine have fewer side effects and improve the vaccine's ability to combat SARS-CoV-2.

2.5 Materials and Methods

Animals

6-8 weeks BALB/c mice were purchased from Jackson Laboratory. All animal procedures and protocols were performed under the approval of the Institutional Animal Care and Use Committee (IACUC) at the University of Chicago. 5-8 week Syrian Golden hamsters were purchased from Envigo (Indianapolis, IN) for the challenge study. All animal procedures were performed under a protocol approved by the Illinois Institute of Technology Research Institute (IITRI) Animal Care and Use Committee (IACUC).

Vaccination

Mice were vaccinated intramuscularly with a combination of 50 μg of CpG-1826 (IDT), 20 μg of Spike protein (Raybiotech), 500 μg of SN50, and 400 μg of honokiol (TCI Chemicals) in 50 μL of PBS. Honokiol was formulated with AddaVAx (Invivogen). Depending on the group,

hamsters were vaccinated intramuscularly with 150 μg of CpG-1018 (IDT), 20 μg of Spike protein, 1.5 mg of SN50 (high dose), 0.5 mg SN50 (low dose), 1.2 mg honokiol (high dose), and 0.4 mg honokiol (low dose).

Challenge Study:

USA-WA1/2020 (SARS-CoV-2) virus was used to challenge the hamsters. Hamsters were anesthetized and inoculated with an estimated 5 x 104 TCID50 of the virus dropwise into the nares. Post-virus exposure, all hamsters were observed twice daily for mortality, moribundity, and clinical scoring. Hamsters were weighed before challenge then on Days 44, 45, and 48. The remaining animals will have body weight collected on Days 49 – 56. Temperature readings were collected via subcutaneously implanted transponder daily on Days -1 through Day 5 and before challenge (Day 42). Following the challenge, the hamsters'' temperature measurements were collected on Days 44, 45, and 48. The remaining animals will have temperatures collected daily on Days 49 – 56.

Nasal Wash Collection:

Hamsters were anesthetized before 0.160 ml of sterile PBS containing penicillin (100 U/ml), streptomycin (100 μg/ml), and gentamicin (50 μg/ml) were injected into the nostrils and collected. The volume of each sample was recorded, and an equal volume of PBS was added to dilute (1:1) to get sufficient volume for TCID50 and RT-qPCR assays.

Blood Collections:

Mice were bled on day 24 from the submandibular vein. For the hamster challenge, whole blood was collected on Days -1, 0 (1hr post-vaccination), 14, 31, 42, and 48 in a blood collection tube (i.e., 1.0 mL Serum-Gel Sarstedt tube). Blood was allowed to clot for 30 minutes at room

temperature, followed by centrifugation to separate the clotted blood and serum. The serum will be aliquoted in approximately 200 □l aliquots and stored frozen at -80 ºC until further use.

Necropsy and Histopathology:

On Days 45 and 48, five hamsters from each group were euthanized, and tissues to be collected include nasal turbinate, lung (left and right lung lobes), trachea, and kidneys. Each tissue was examined for macroscopic (gross pathology) and microscopic (histopathology) changes. All tissues collected were quantitated for viral genome copy using RT-qPCR. The left lung was collected into a 7 mL tube prefilled with 2.8 mm beads and weighed to determine the net weight of the lung. The TCID50 assay analyzed the left lung lobe for viral titers and RT-qPCR. In contrast, the right lung was fixed by being inflated with 10% neutral-buffered formalin (NBF) and immersed in 10% NBF. Following fixation, the tissue was processed for histopathological evaluation.

TCID50 Assay

Nasal Wash and lung tissue samples viral titers were determined using the TCID50 assay. Briefly, clarified tissue supernatants and a portion of nasal wash samples will be diluted 1:10 followed by seven 2-fold serial dilutions and added to a 96-well plate pre-seeded with VeroE6 cells. Samples were plated in triplicate and incubated for 72hr (±4hr. The cytopathic effect was scored (+ or -) for each well for each dilution.

RT-qPCR Assay:

Following tissue homogenization, the homogenate supernatant was collected after a brief centrifuge. The concentration of virus in harvested tissue supernatants and nasal wash samples was determined by RT-qPCR assay. Briefly, RNA was extracted from the supernatant of

homogenized tissue samples and nasal wash. RT-qPCR was performed using the iTaq universal probes One-Step RT-qPCR Kit (BioRad). The following RT-PCR cycling conditions were used: 50 °C for 15 min (RT), then 95 °C for 2 min (denature), then 40 cycles of 10s at 95 °C, 45s at 62 °C. Virus titer by RT-qPCR will be performed according to IITRI SOPs.

Primers used for SARS-CoV-2 detection:

2019-nCoV_N1-F 5'-GACCCCAAAATCAGCGAAAT-3'

2019-nCoV_N1-R 5'-TCTGGTTACTGCCAGTTGAATCTG -3'

Probe: 2019-nCoV_N1-P: 5'-FAM-ACCCCGCATTACGTTTGGTGGACC-BHQ1-3'

Microneutralization Assay

Serum samples collected on Days -1 and 31 were analyzed for neutralizing antibody titers determined using the microneutralization assay. Individual samples were heat inactivated (56 °C for 30 ±5 min) and initially diluted 1:10, followed by seven two-fold serial dilutions (final dilution scheme 1:10 to 1:1280). Each dilution is then mixed with a standard virus concentration, incubated for 75 minutes, and added to a 96-well plate with Vero E6 cells (1x104 – 1x105 cells per well). Plates were incubated for 48 hours at 37 °C with 5% CO_2.After incubation, plates were fixed with 80% cold acetone for 30 minutes, and cells were stained by anti-mouse SARS-CoV-2 nucleoprotein IgG (Sino Biological) followed by peroxidase-conjugated goat anti-mouse IgG (SeraCare). Wells were developed using ABTS Substrate Solution, and the reaction was stopped by acidification. The plates were read at 450 nm on a microplate reader's spectrophotometer setting. To calculate wells positive for at least 50% virus infection were determined using virus (VC) and cell (CC) control wells using the following calculation:

(VCOD Mean + CCOD Mean)/2. The sample's neutralization is based on the last dilution that generated an OD value above (negative for neutralization) or below (positive for neutralization) this cut-off value. The highest dilution positive for neutralization is the estimated titer for the sample. Each sample is tested in duplicate, and the geometric mean is reported.

ELISA

Serum samples collected on Day -1, 0 were analyzed for IL-6 using a commercially available ELISA kit (MyBioSource.com) following the manufacturer's recommendations. Mice serum samples from D24 and hamster serum samples collected on Days 0, 14, and 31 were quantitated for antigen-specific IgG using a commercially available ELISA kit (Eagle Biosciences) following the manufacturer's recommendations.

Statistics

Statistics were determined using Prism 9 software with One-Way ANOVA with multiple comparison tests.

2.6 References

1.World Health Organization. WHO Coronavirus (COVID-19) Dashboard. https://covid19.who.int.

2. Moghadas, S. M. *et al. The impact of vaccination on COVID-19 outbreaks in the United States*. http://medrxiv.org/lookup/doi/10.1101/2020.11.27.20240051 (2020) doi:10.1101/2020.11.27.20240051.

3. Center of Disease Control. SARS-CoV-2 Variant Classifications and Definitions. *Variants Being Monitored* https://www.cdc.gov/coronavirus/2019-ncov/variants/variant-classifications.html#anchor_1632158775384 (2022).

4. Harvey, W. T. *et al.* SARS-CoV-2 variants, spike mutations, and immune escape. *Nat Rev Microbiol* **19**, 409–424 (2021).

5. Ramesh, S. *et al.* Emerging SARS-CoV-2 Variants: A Review of Its Mutations, Its Implications and Vaccine Efficacy. *Vaccines* **9**, 1195 (2021).

6. P, N., R., N., B., V., S., R. & A., S. COVID-19: Invasion, pathogenesis and possible cure – A review. *Journal of Virological Methods* **300**, 114434 (2022).

7. World Health Organization. COVID-19 vaccine tracker and landscape. (2022).

8. Pulendran, B., S. Arunachalam, P. & O'Hagan, D. T. Emerging concepts in the science of vaccine adjuvants. *Nat Rev Drug Discov* **20**, 454–475 (2021).

9. Kallon, S., Samir, S. & Goonetilleke, N. Vaccines: Underlying Principles of Design and Testing. *Clin. Pharmacol. Ther.* **109**, 987–999 (2021).

10. Petrovsky, N. & Aguilar, J. C. Vaccine adjuvants: Current state and future trends. *Immunology & Cell Biology* **82**, 488–496 (2004).

11. Pollet, J., Chen, W.-H. & Strych, U. Recombinant protein vaccines, a proven approach against coronavirus pandemics. *Advanced Drug Delivery Reviews* **170**, 71–82 (2021).

12. Richmond, P. *et al.* Safety and immunogenicity of S-Trimer (SCB-2019), a protein subunit vaccine candidate for COVID-19 in healthy adults: a phase 1, randomised, double-blind, placebo-controlled trial. *The Lancet* **397**, 682–694 (2021).

13. Moser, B. A. *et al.* Small Molecule NF-κB Inhibitors as Immune Potentiators for Enhancement of Vaccine Adjuvants. *Front. Immunol.* **11**, 511513 (2020).

14. Moser, B. A. *et al.* Increased vaccine tolerability and protection via NF-κB modulation. *Sci Adv* **6**, eaaz8700 (2020).

15. Bhat, P., Leggatt, G., Waterhouse, N. & Frazer, I. H. Interferon-γ derived from cytotoxic lymphocytes directly enhances their motility and cytotoxicity. *Cell Death Dis* **8**, e2836–e2836 (2017).

16. Zenobia, C. & Hajishengallis, G. Basic biology and role of interleukin-17 in immunity and inflammation. *Periodontol 2000* **69**, 142–159 (2015).

17. Xu, S. & Cao, X. Interleukin-17 and its expanding biological functions. *Cell Mol Immunol* **7**, 164–174 (2010).

18. Francis, M. E. *et al.* SARS-CoV-2 infection in the Syrian hamster model causes inflammation as well as type I interferon dysregulation in both respiratory and non-respiratory tissues including the heart and kidney. *PLoS Pathog* **17**, e1009705 (2021).

19. Sia, S. F. *et al.* Pathogenesis and transmission of SARS-CoV-2 in golden hamsters. *Nature* **583**, 834–838 (2020).

3. Immune Potentiation of PLGA Controlled Release Vaccines for Improved Immunological Outcomes

3.1 Summary

With the emergence of SARS-CoV-2 and the continued emergence of new infectious diseases, there is a need to improve and expand current vaccine technology. Controlled release subunit vaccines provide several benefits over current vaccines on the market, including the use of less antigen and fewer boost doses. Previously, our group reported that molecules that alter NF-κB signaling could be used to improve the vaccine's efficacy and reduce adjuvant-related side effects. In this report, we test how these immune potentiators will influence responses when included as part of a controlled release poly(lactic-co-glycolic) vaccine formulation. Depending on the immune potentiator selected, these formulations can increase the antibody levels and T-cells generated by the controlled release vaccine. In addition, when applied to a SARS-CoV-2 vaccine, the immune modulator can generate high antibody levels, which have improved neutralization compared to the standard controlled release formulation.

3.2 Introduction

Particle encapsulation approaches to vaccination extend the availability of the antigen payload and dose of adjuvant compared to the unencapsulated counterpart. This extension is from the steady, controlled release mechanism and protection of contents before cellular uptake. [1, 2, 3] Controlled release formulations via microparticles produce a higher and longer antibody titer than their unencapsulated and nanoparticle counterparts[4].

Many polymers have been used to achieve controlled release, but poly(lactic-co-glycolic) acid (PLGA) remains the most common, owing to its ease of formulation and degradation of its ester backbone to nontoxic component. [5-8] Both PLGA nanoparticle and microparticles promote prolonged antigen presentation by macrophages and dendritic cells[9]. However, a remaining challenge is that at the local level, these particles still require the activation of inflammatory innate pathways. Despite producing minimal systemic inflammation, the local environment still results in cells which might respond as though in a highly inflammatory environment. We conjectured that immune potentiators, such as SN50, might offer the potential to enhance the local innate response resulting in better vaccine responses. As we previously demonstrated, SN50 and other potentiators alter innate pathways to promote antigen presentation through a novel mechanism[10]. Previous work in the lab has showed that the SN50 peptide when included with a model vaccination using, CpG, a TLR9 agonist, successfully increased antibody response by over 2-fold compared to CpG including vaccines for HIV, influenza, and dengue[11]. We have also reported small molecule immune potentiators, honokiol and capsaicin that result in the same outcome but do not have the risk of eliciting peptide antibodies.[12]

Immune potentiators might also benefit from controlled release methodologies as current vaccine formulations have limitations. Both SN50 and honokiol, require between 200 to 500 micrograms to achieve their activity. The effective concentration of free capsaicin causes side effects including hyperalgesia and temporary loss of thermal homeostasis[12,13]. With these two principles in mind, we set out incorporating immune potentiators into controlled release formulations.

Although, subunit vaccines encapsulated into PLGA microparticles are effective, we hypothesized that immune potentiators would improve sustained release formulations. In this study, we tested three different immune potentiators, SN50, honokiol, and capsaicin. Each immune potentiator when co-formulated with a model vaccine within the particles exhibited higher antibody levels in serum with longer durability compared to particle formulations without immune potentiators. The longer durability of our immune potentiator particle implies the need for less frequency of booster vaccinations, T cells obtained from the draining lymph node exhibited a strong MHC-II response resulting in increased antibody responses that also persisted for a greater period of time. In this case, it appears the potentiators simply amplify the particle response rather than alter it. Lastly, the microparticle vaccine was successfully applied to a SARS-CoV-2 vaccine subunit model. These findings display that immune potentiators can be beneficial additives to sustained release particle vaccines against infectious diseases.

3.3 Results and Discussion

In order to create sustained release PLGA microparticles, we used the double emulsion technique[14]. In brief, each subunit component was fully dissolved separately in a fixed amount of phosphate buffered saline (PBS) and then combined to give the desired ratio. Subunit component within each particle vaccine were co-encapsulated to ensure equal exposure of agonist, antigen, and immune potentiator *in vivo.* Fifty percent more of CpG-1826 was loaded with the immune potentiator containing microparticles to ensure a comparable amount of CpG-1826 would be loaded in comparison to the CpG-1826 OVA microparticles. Each of the formulation details can be found in the SI. The aqueous layer, containing the subunit components, was then added to 100 mg of PLGA dissolved in 2 mL of DCM. The resulting mixture was then subjected to

ultrasonication (40 khz) for 3 cycles of sonication (30 seconds sonication, 30 seconds of rest) before being vortexed after the addition of 8 mL of 5% polyvinyl alcohol (PVA). The resulting emulsion was left stirring for 6 hours in a total volume of 200mL 0.5% PVA stabilizing solution. The resulting precipitated microparticles were washed three times with DI water and lyophilized overnight prior to further characterization.

SEM analysis confirmed that each of the particles possess a sphere like morphology with an average diameter of at least 11 um (**Figure 3.1A-3.1D**). The components loaded into the particles, CpG 1826, OVA, and immune potentiators, were quantified via a previous published extraction technique[15]. Most of components encapsulated by the particles were loaded with more than 30% encapsulation efficiency (for complete details **Table A1**). Of note, different particles did appear to have slightly different morphologies upon formulation with the honokiol and capsaicin particles each resulting in the enhancement of observable pore-like structures. We attribute this subtle difference to the small molecule nature of these two compounds in contrast to the protein and peptide nature of OVA and SN50. While it's difficult to confirm the reason for this difference, we conjecture that the small molecules slight already the solvent exchange process resulting in enlargement of the pores that are also observable in the particles containing only CpG 1826 and OVA (**Figure 3.1A**).

Initially, we were concerned that these subtle differences in morphology might alter the release rate of the particles. We sought to test this hypothesis and to measure the rate of release of the contents from the particles. We conducted vitro release experiments of the microparticles using a

standard in vitro release protocol.[16] All of the particles exhibited a sustained release profile *in vitro* over a 40-day period (**Figure 3.1E**).

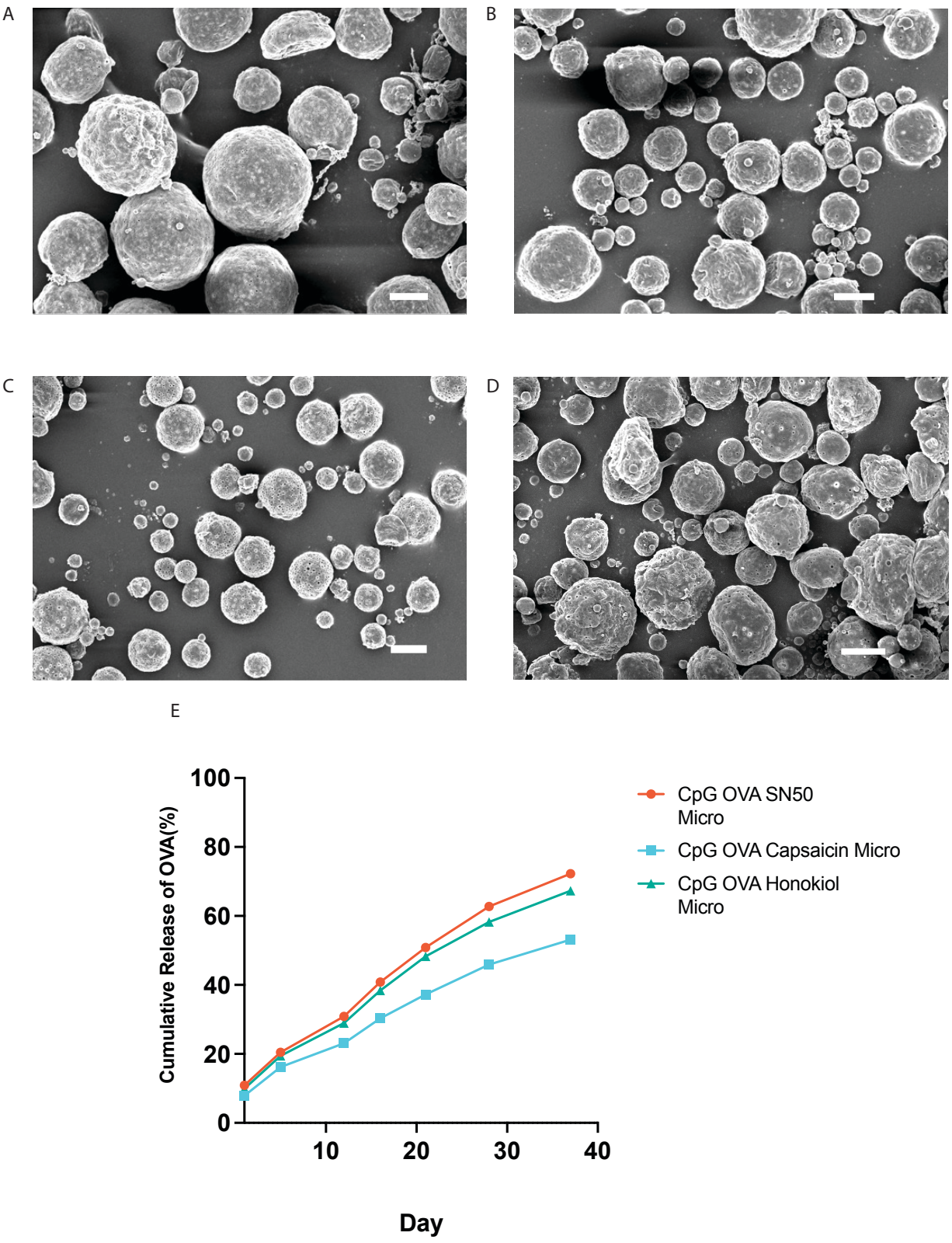

Figure 3.1 SEM images of microparticles created by the double emulsion technique. A)CpG OVA Microparticles B) SN50 CpG OVA Microparticles C) Honokiol CpG OA Microparticles

Figure 3.1 continued
D) Capsaicin CpG OVA Microparticles. (scale bar is 10 μm). E) *in vitro* release kinetics of particles stirred in PBS at 37 ºC over a 4-week period.

After observing promising loading and *in vitro* release data, we next wanted to test the sustained-release potentiation *in vivo*. However, with the loading of up to three different components within a particle, we needed to consider the balance of antigen, adjuvant, and potentiator and make sure we had an accurate comparison between groups. In formulation of particles, it is very difficult to standardize the concentration of two components across multiple formulations. Previous studies on antigen sparing have reported that the amount of adjuvant contributes more than the amount of antigen especially at low antigen concentrations[17,18, 19]. Therefore, we concluded that when standardizing a concentration for the particles, the adjuvant, CpG-1826, should be kept standard across injections. For injections where additional PLGA mass was required, microparticles composed only of PLGA (**Appendix A**) were injected to keep the overall amount of injected PLGA the same between groups.

With the appropriate formulations ready, we conducted a series of vaccination experiments to test how potentiator particles would perform. Each vaccination was administered subcutaneously in the right flank in 150 μL of PBS on day 0, and the same formulation was used for a boost on day 14. Microparticle content ranged from 1 mg for CpG OVA microparticles to 1.13 mg for CpG OVA SN50 microparticles (**Appendix A**). Seven days after the boost, draining lymph nodes were harvested and cells isolated and separately stained with $OVA_{323-339}$ and $OVA_{257-264}$ tetramers. There was no significant number of CD8/$OVA^{257-264}$Tetramer+ with all having levels similar to levels observed in PBS control groups (**Figure 3.2A**). However,

microparticles containing SN50 had significantly higher CD4/ $OVA^{323-339}$Tetramer+ staining than microparticles containing no immune potentiator (**Figure 3.2B**).

The CD8/$OVA^{323-339}$Tetramer+ staining indicated a more robust MHC-II response in the presence of the SN50 immune potentiator particle vaccines. This was substantiated by the strong antibody levels exhibited by the immune potentiator particle vaccine, which was six times greater than the CpG-1826 OVA microparticle vaccine (**Figure 3.2C**). The high antibody levels peaked at day 56 for the microparticles containing SN50, and these antibody levels persisted at higher levels for the entirety of the measured 98 days than the unencapsulated formulations. However, larger variability decreased the statistical significance after day 56. (**Figure 3.D**).

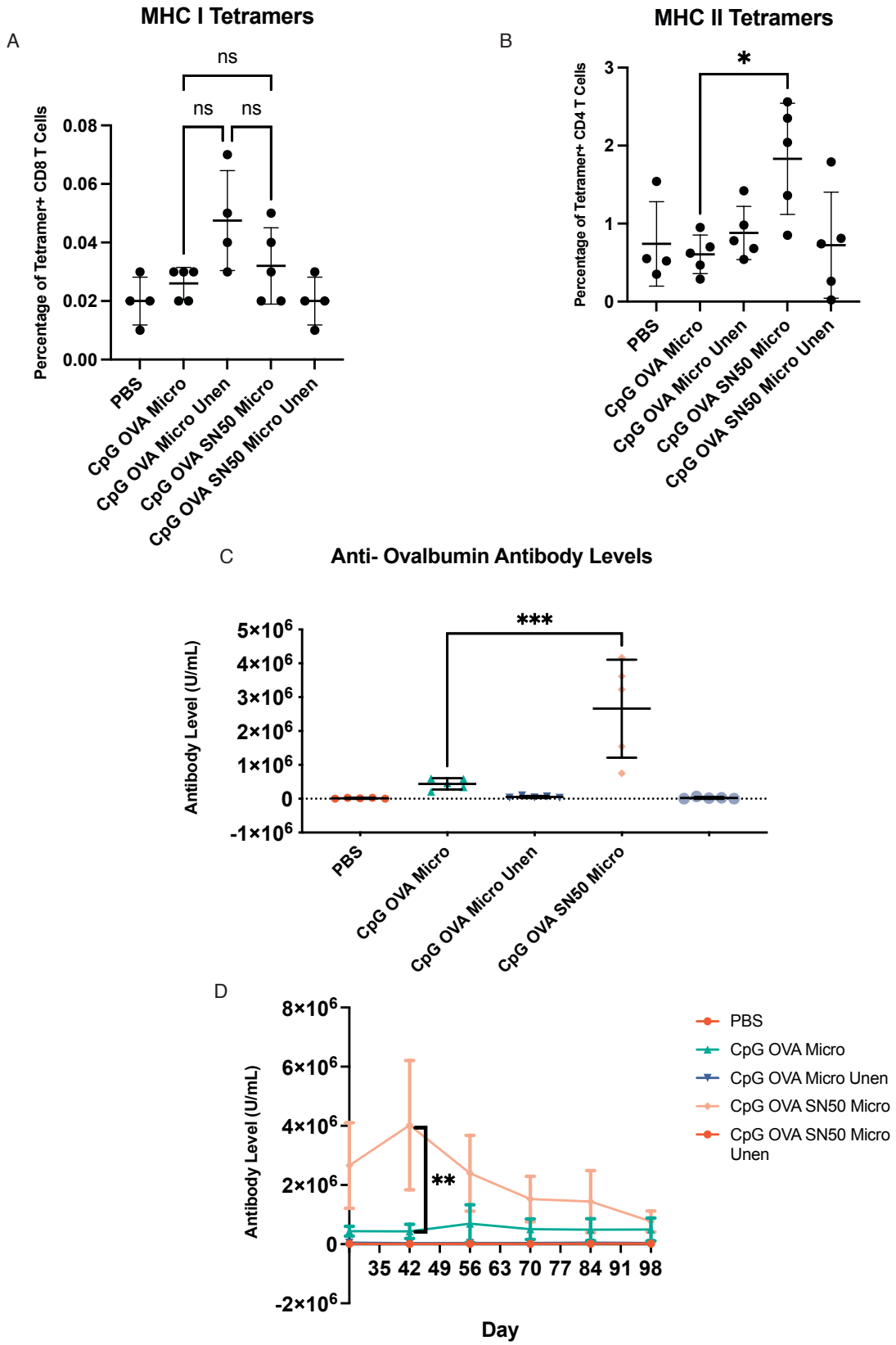

Figure 3.2: *in vivo* performance of controlled release subunit vaccine containing SN50

Figure 3.2 continued
A) $OVA^{257-264}$MHC I B) $OVA^{323-339}$MHC II tetramers staining performed on lymphocytes harvested on day 21. N=5. Some groups were removed due to not harvesting enough lymphocytes for staining. C) Day 28 anti-ovalbumin Ig's (IgG+IgM+IgA) antibody levels measured from day 28 serum. N=5 D) Anti-ovalbumin Ig's (IgG+IgM+IgA) antibody levels were measured over time from serum collected every two weeks after day28. N=5. Mean reported with standard deviation as the error. One-Way-Anova performed with Dunnett's test. $*P < 0.05$, $**P < 0.01$, and $***P < 0.001$. n.s., not significant.

The success of microparticles containing SN50 led us to try encapsulating our previously published small molecule immune potentiators. Previously, our group has reported that honokiol and capsaicin were similar to SN50 in that they successfully suppressed systemic cytokines generated by subunit vaccines containing CpG-1826 while improving antibody levels[12]. Identical to our experiment with SN50-containing particles, honokiol and capsaicin particles were injected using the same route, volume, and balance of particles on days 0 and 14 (**Appendix A**). Draining lymph nodes were harvested on day 21, and antibody levels were measured on day 28 and day 42.

Upon examination, in parallel to the SN50 experiment, CD8/$OVA^{257-264}$Tetramer+ showed that capsaicin and honokiol did not significantly improve t-cell activity compared to the CpG-1826 OVA microparticle formulation (**Figure 3.3A**). The same conclusion was proper for the CD4/ $OVA^{323-339}$Tetramer+ staining, where no significant tetramers were observed (**Figure 3.3B**). While tetramer data was not substantial for antigen-specific CD4+ and CD8+ T cells, honokiol and capsaicin microparticles showed increased antibody levels on day 28 (**Figure 3.3C**). However, honokiol was the only group significantly higher than the CpG-1826 OVA microparticles. These results suggest that improving CpG-1826 OVA microparticles may be highly dependent on the immune potentiator selected.

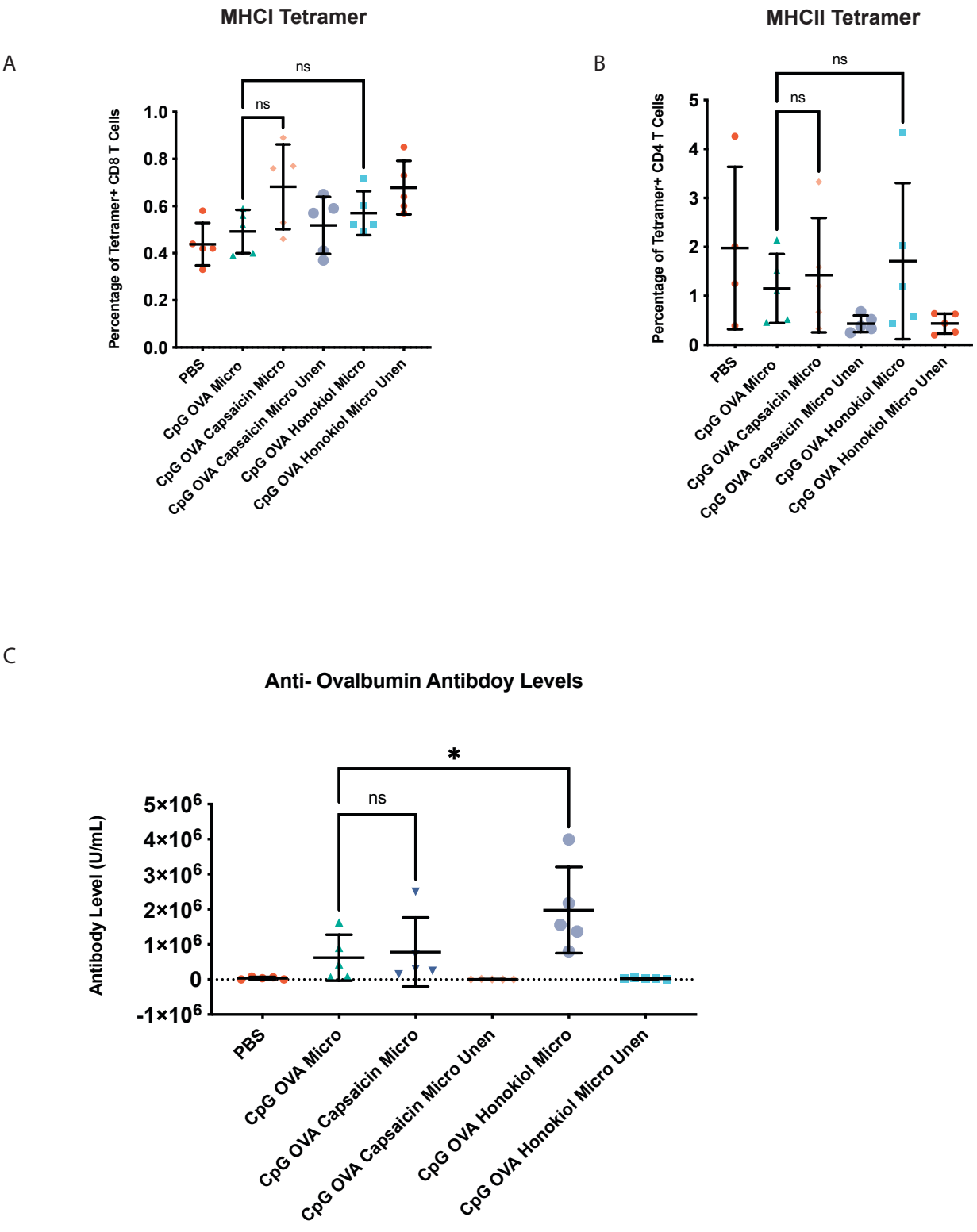

Figure 3.3: *in vivo* performance of controlled release subunit vaccine containing Capsaicin and Honokiol

Figure 3.3 continued
A) $OVA^{257-264}$ MHC I B) $OVA^{323-339}$MHC II tetramers staining on lymphocytes. Some groups were removed due to not harvesting enough lymphocytes for staining N=5. C) Day 28 anti-ovalbumin Ig's (IgG+IgM+IgA) antibody levels measured from day 28 serum. N=5. Mean reported with standard deviation as the error. One-Way-Anova performed with Dunnett's test. $*P < 0.05$, $**P < 0.01$, and $***P < 0.001$. n.s., not significant.

Based on the success of the immune potentiator vaccine coupled with OVA, we wanted to apply our approach to a disease-relevant antigen. Developing novel vaccine responses for the SARS COV-2 virus remains a priority for improved vaccine design. [20] A key parameter of a successful COVID-19 vaccine is generating a strong level of neutralizing antibodies.[21] Given the strong humoral response profiled from our immune potentiator microparticles, we wanted to apply our vaccine model with a SARS COV-2 antigen. The spike protein is a transmembrane protein found on the surface of the virus. It is responsible for assisting the virus in attaching and infiltrating host cells and its neutralization leads to reduced infectivity. [22]

We encapsulated the spike protein from 2019-nCoV, CpG-1826, and honokiol into microparticles and compared them *in vivo* to microparticles without an immune potentiator. Day 28 serum samples showed microparticle formulations had higher antibody levels than unencapsulated formulations (**Figure 3.4A**). However, there was no statistical significance between microparticles containing honokiol and microparticles containing no immune potentiator. Therefore, improving antibody levels with immune potentiators may depend on the antigen selected.

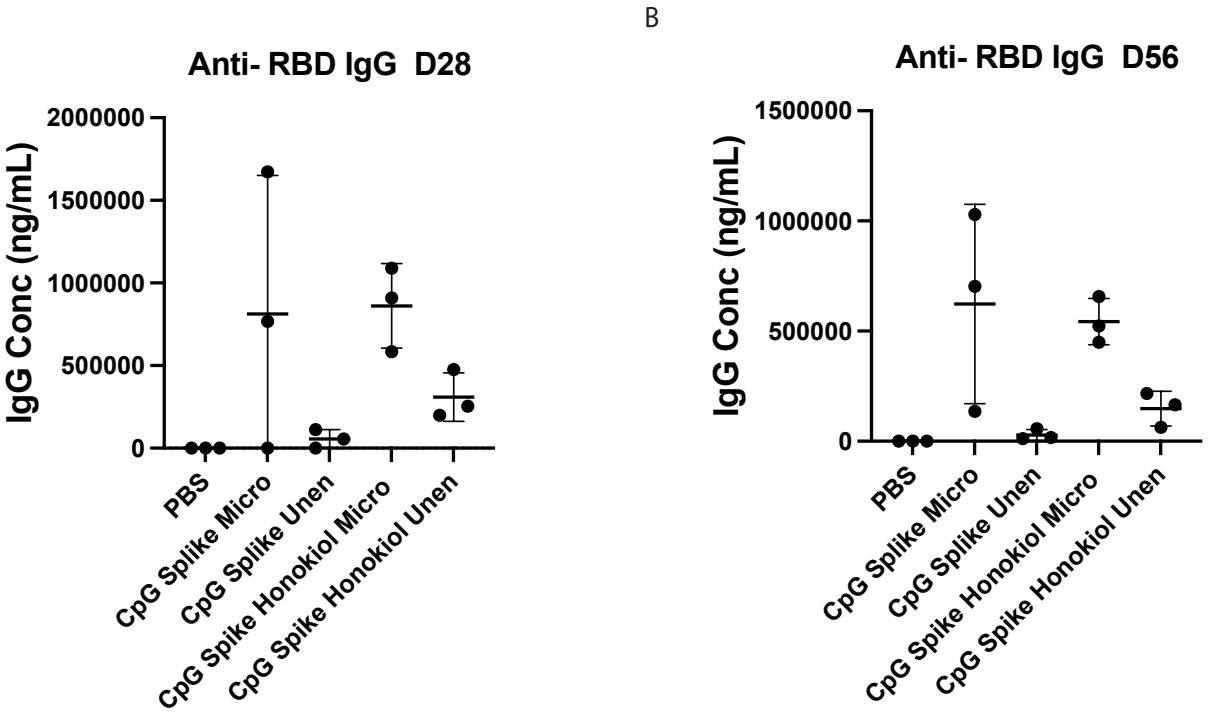

Figure 3.4: SARS-COV-2 subunit vaccine with honokiol A) Anti-RBD IgG conc in serum taken from day 28 B) day 56. N=5. Truncated mean reported with standard deviation as the error. One-Way-Anova performed with Dunnett's test. *$P < 0.05$, **$P < 0.01$, and ***$P < 0.001$. n.s., not significant.

3.4 Conclusion

In conclusion, we examined how immune potentiators could alter and improve sustained release vaccine formulations. Sustained release formulations that included immune potentiators improved adjuvanted subunit microparticle vaccines by increasing antibody levels which appeared to occur through an increased CD4/MHC-II mediated mechanism for SN50 microparticle formulations. This increased response generally worked for both the peptide potentiator, SN50, and the small molecular potentiator, honokiol. The potentiators increased the absolute level of antibodies produced – sometimes as much as 6X. They also increased the persistence of the high levels of antibodies. In the case of immune potentiators like capsaicin, the sustained release mechanism can reduce pain responses exhibited by unencapsulated vaccines.

The method of modulating a sustained release particle was also applied to a current antigen of interest, SARS-CoV-2 resulting in increased responses from the unencapsulated formulation though not increases from the particles lacking potentiators. Overall, these immune potentiator particle vaccines display a robust humoral response. While this may not be the best fit for every vaccination strategy, we note that the potentiators simply act to amplify the pre-existing Th2 skew of the particle formulation. This study is a preliminary set of data that shows that potentiators can be used in particle formulations and that they do not alter the inherent immune bias of the particle formulation.

3.5 Materials and Methods

Particles Synthesis

The payload was added in 300 μL to 2 mL of 100 mg/mL of PLGA in methylene chloride. The mixture was ultrasonicated at 40% amplitude for 3 minutes (30 seconds stirring following 30 seconds of rest). After ultrasonification, a determined amount of 5% (w/v) PVA solution was added to the primary w/o emulsion and vortexed for 30 seconds to produce the w/o/w double emulsion. The w/o/w emulsion was poured into 100 mL of chilled 1% (w/v) PVA and stirred at room temperature for 6 hours. The microspheres were either centrifuged, and the pellet was washed three times with ultrapure deionized water and then lyophilized.

Scanning Electron Microscopy

Lyophilized particles were sputter coated with 10nm of Pt/Pd (Ted Pella Cressington 208HR) and then imaged on a Scanning Electron Microscope(Carl Zeiss Merlin) for shape and morphology analysis.

Loading Analysis

Loading analysis was performed in triplicate using a previously reported extraction method. [15] CpG and immune potentiators concentrations were measured on reverse-phase high-performance liquid chromatography (HPLC). Protein levels were calculated with Qubit Fluorometer.

In-vitro Release

Gram vials containing 2 mg of OVA-loaded particles were treated with 0.5 mL of pH 7.45 PBS. The vials were gently stirred at 200 rpm at 37 ºC. The particle solution was collected by centrifuging the vials at 4000 rpm for ten minutes and stored at -20 ˚C. The ova concentration was determined by using a Qubit Protein Assay.

Cytokine Profile

Serum was collected at 1 hour, 3 hours, 6 hours, 24 hours, 48 hours, day 5, and day 28. The serum was centrifuged at 2000 x g for ten minutes. The supernatants were collected and stored at -80 ºC until testing. The cytokine levels were measured using the BioLegend Legendplex kit.

Serum Antibody Levels

Cheek bleeds were collected on days 28, 42, 56, 70, 84, and 98. Samples were clotted for 30 minutes at room temperature before being centrifuged at 2000 x g for ten minutes. The supernatants were collected and stored at -80 ºC until testing. An Alpha Diagnostic International mouse anti-ovalbumin (Gal d 2) Ig's (IgG, IgA, IgM) ELISA Kit, 96 tests were used following the manufacturer's instructions to quantify the serum's antibody titer.

T cell response

Murine lymphocytes from the radial, auxiliary, and inguinal lymph nodes were harvested on day 21. Lymph nodes were treated with 5mg/ml collagenase-d for 30 minutes before being mashed with a syringe plunger. The lymphocytes were washed with RPMI and resuspended in T cell media. The lymphocytes were counted on a hemocytometer, and one million cells from each sample were plated on two 96 well plates. For each tetramer staining, the $OVA_{323-339}$ and $OVA_{257-264}$ Tetramer staining was conducted according to the manufacturer's protocol and processed using flow cytometry.

SARS CoV-2 Vaccination Experiment

On day 0 and day 14, mice were subcutaneously injected with the appropriate vaccine. By day 28 and day 56 serum was collected, and an anti-RBD IgG ELISA (Eagle's Bioscience) was executed according to manufacturer's protocol

3.6 References

1. Allahyari, M. & Mohit, E. Peptide/protein vaccine delivery system based on PLGA particles. *Hum. Vaccines Immunother.* **12**, 806–828 (2016).

2. Nie, T. *et al.* Sustained Release Systems for Delivery of Therapeutic Peptide/Protein. *Biomacromolecules* **22**, 2299–2324 (2021).

3. Higuchi, T. Mechanism of sustained-action medication. Theoretical analysis of rate of release of solid drugs dispersed in solid matrices. *J. Pharm. Sci.* **52**, 1145–1149 (1963).

4. Kanchan, V. & Panda, A. K. Interactions of antigen-loaded polylactide particles with macrophages and their correlation with the immune response. *Biomaterials* **28**, 5344–5357 (2007).

5. Lagreca, E. *et al.* Recent advances in the formulation of PLGA microparticles for controlled drug delivery. *Prog. Biomater.* **9**, 153–174 (2020).

6. Keles, H., Naylor, A., Clegg, F. & Sammon, C. Investigation of factors influencing the hydrolytic degradation of single PLGA microparticles. *Polym. Degrad. Stab.* **119**, 228–241 (2015).

7. Han, F. Y., Thurecht, K. J., Whittaker, A. K. & Smith, M. T. Bioerodable PLGA-Based Microparticles for Producing Sustained-Release Drug Formulations and Strategies for Improving Drug Loading. *Front. Pharmacol.* **7**, (2016).

8. Fu, Y. & Kao, W. J. Drug release kinetics and transport mechanisms of non-degradable and degradable polymeric delivery systems. *Expert Opin. Drug Deliv.* **7**, 429–444 (2010).

9. Koerner, J., Horvath, D. & Groettrup, M. Harnessing Dendritic Cells for Poly (D,L-lactide-co-glycolide) Microspheres (PLGA MS)—Mediated Anti-tumor Therapy. *Front. Immunol.* **10**, 707 (2019).

10. Lin, Y.-Z., Yao, S., Veach, R. A., Torgerson, T. R. & Hawiger, J. Inhibition of Nuclear Translocation of Transcription Factor NF-κB by a Synthetic Peptide Containing a Cell Membrane-permeable Motif and Nuclear Localization Sequence. *J. Biol. Chem.* **270**, 14255–14258 (1995).

11. Moser, B. A. *et al.* Increased vaccine tolerability and protection via NF-κB modulation. *Sci. Adv.* **6**, eaaz8700 (2020).

12. Moser, B. A. *et al.* Small Molecule NF-κB Inhibitors as Immune Potentiators for Enhancement of Vaccine Adjuvants. *Front. Immunol.* **11**, 511513 (2020).

13. Kobayashi, A. *et al.* Capsaicin activates heat loss and heat production simultaneously and independently in rats. *Am. J. Physiol.-Regul. Integr. Comp. Physiol.* **275**, R92–R98 (1998).

14. Bailey, B. A., Ochyl, L. J., Schwendeman, S. P. & Moon, J. J. Toward a Single-Dose Vaccination Strategy with Self-Encapsulating PLGA Microspheres. *Adv. Healthc. Mater.* **6**, 1601418 (2017).

15. Saez, V. *et al.* Extraction of PLGA-Microencapsulated Proteins Using a Two-Immiscible Liquid Phases System Containing Surfactants. *Pharm. Res.* **30**, 606–615 (2013).

16. D'Souza, S. S. & DeLuca, P. P. Methods to Assess in Vitro Drug Release from Injectable Polymeric Particulate Systems. *Pharm. Res.* **23**, 460–474 (2006).

17. Reisinger, K. S., Holmes, S. J., Pedotti, P., Arora, A. K. & Lattanzi, M. A dose-ranging study of MF59 ® -adjuvanted and non-adjuvanted A/H1N1 pandemic influenza vaccine in young to middle-aged and older adult populations to assess safety, immunogenicity, and antibody persistence one year after vaccination. *Hum. Vaccines Immunother.* **10**, 2395–2407 (2014).

18. Jiang, J. *et al.* Antigen sparing and enhanced protection using a novel rOv-ASP-1 adjuvant in aqueous formulation with influenza vaccines. *Vaccine* **32**, 2696–2702 (2014).

19. Kuo, T.-Y. *et al.* Development of CpG-adjuvanted stable prefusion SARS-CoV-2 spike antigen as a subunit vaccine against COVID-19. *Sci. Rep.* **10**, 20085 (2020).

20. World Health Organization. WHO Coronavirus (COVID-19) Dashboard. https://covid19.who.int.

21. Khoury, D. S. *et al.* Neutralizing antibody levels are highly predictive of immune protection from symptomatic SARS-CoV-2 infection. *Nat. Med.* **27**, 1205–1211 (2021).

22. Huang, Y., Yang, C., Xu, X., Xu, W. & Liu, S. Structural and functional properties of SARS-CoV-2 spike protein: potential antivirus drug development for COVID-19. *Acta Pharmacol. Sin.* **41**, 1141–1149 (2020).

4. Temporal Control of Trained Immunity via Encapsulated Release of β-glucan Improves Therapeutic Applications

This Chapter has been published in Wiley's Advanced Healthcare Materials

4.1 Summary

Emerging diseases require generating new vaccines, which can often be time-consuming. An alternate method to boost host defense is inducing nonspecific innate immune memory, called trained immunity, to develop novel prophylactics. Many molecules, most notably β-glucan, induce trained immunity, but their effects are often short-lived and uncontrolled. This lack of temporal control limits both the therapeutic ability of training and provides fundamental questions about its nature. To achieve temporal control of trained immunity, we engineered controlled release nanoparticles encapsulating only 3.5% of the standard dose of β-glucan to attain sustained release over a month. Nanoparticle-trained mice exhibited prolonged training effects and improved resistance to a B16F10 tumor challenge compared to mice that received an equivalent amount of free β-glucan. We further fine-tuned the duration of trained immunity by synthesizing nanoparticles composed of different molecular weights to modulate the release kinetics. These results demonstrate that dosing and temporal control can substantially alter the trained response to unanticipated levels. As such, this approach using sustained release platforms might lead to a novel prophylactic strategy for improved disease resistance against a wide variety of diseases

4.2 Introduction

Innate immune cells form the first line of defense against pathogens. [1] Recent work has revealed that innate immune cells experience nonspecific "memory," which allows modulation of responses against repeated pathogenic insult, which was previously not considered an innate function. This enhanced responsiveness conferred by innate cells, called trained immunity, can improve the first line of defense and subsequent adaptive immune responses by increasing antigen presentation and T-cell activation.[2] Certain pathogenic stimuli, such as whole-cell inactivated mycobacteria, induces epigenetic and metabolic changes that rewire innate immune cells.[3] This rewiring improves pathogen detection and immune reactivity of the "trained" cells to better respond to a second attack by both the same or an unrelated pathogen.

Many whole-pathogen vaccines, such as *Bacillus* Calmette-Guérin (BCG)[4], polio[5], and measles[6], have been reported to induce trained immunity and protect against several unrelated viral and bacterial infections.[4,7,8] Less active trained immunity inducers, such as the yeast-derived β-glucan, are functional substitutes and protect mice against a diverse range of pathogens.[9–12] However, their protective effects are transient – lasting for only a few days – and the high dosages have raised concerns about inducing adverse responses.[10,13] Therefore, methods to control and extend trained immunity could help provide new tools for generating durable disease resistance. This paper demonstrates using conventional materials methods to control trained immunity responses over time and its application to a disease model.

Since macrophages and monocytes have a relatively short lifespan, methods to prolong trained immunity have thus far focused on targeting the bone marrow to generate trained myeloid precursors.[14,15] Priem et al. developed high-density lipoprotein (HDL) based nano-biologics

encapsulating trained immunity-inducing muramyl tripeptide (MTP) that suppressed tumor growth in mice.[16] However, bone marrow targeted nanomaterials do not provide precise temporal control over trained immunity and can potentially lead to unwanted side effects due to accumulation in the liver.[17] We sought to employ an efficient method of controlling the kinetics of trained immunity through a more generalizable approach using the sustained release of trained immunity-inducing molecules from biodegradable nanoparticles. Poly (lactic-co-glycolic acid) (PLGA) is a widely used FDA-approved polymer that exhibits slow degradation via hydrolysis of ester bonds with broad applications.[18] PLGA nanoparticles can be easily formulated to deliver the encapsulated cargo to their intended target cells. Moreover, the release kinetics can be controlled by modulating the properties of PLGA. [19,20] Therefore, to test the hypothesis of if sustained release would alter the temporal control of trained immunity - PLGA nanoparticles were an excellent test-bed.

We investigated if the sustained release of β-glucan from PLGA nanoparticle formulation would prolong trained immunity effects by controlling release kinetics (**Figure 4.1**). We synthesized and characterized PLGA nanoparticles varying the rate of release of β-glucan over 30 days. We observed enhanced pro-inflammatory cytokine production in nanoparticle trained bone-marrow-derived macrophages (BMDMs) challenged with lipopolysaccharide (LPS) in a 7-day *in vitro* assay. To better capture slow release and its effect on inducing trained immunity, we tested the synthesized nanoparticles in an *in vivo* model. While the standard dose of 1 mg of free β-glucan conferred trained immunity for more than a week, nanoparticle-trained mice demonstrated peak systemic effects extending over a month of training. This prolonged response enabled the nanoparticle-trained mice to resist tumor growth better than conventionally trained animals when challenged with B16.F10 melanoma three weeks after training. We demonstrated

that different molecular weight PLGA could fine-tune the duration of training for various applications by controlling release kinetics. We report for the first time that sustained release from biodegradable polymer nanoparticles can be used for temporal control of trained immunity over a predictable window of a week to a month. This work can potentially lead to the development of a new class of prophylactics for safe, effective, and improved disease resistance against a wide range of pathogens.

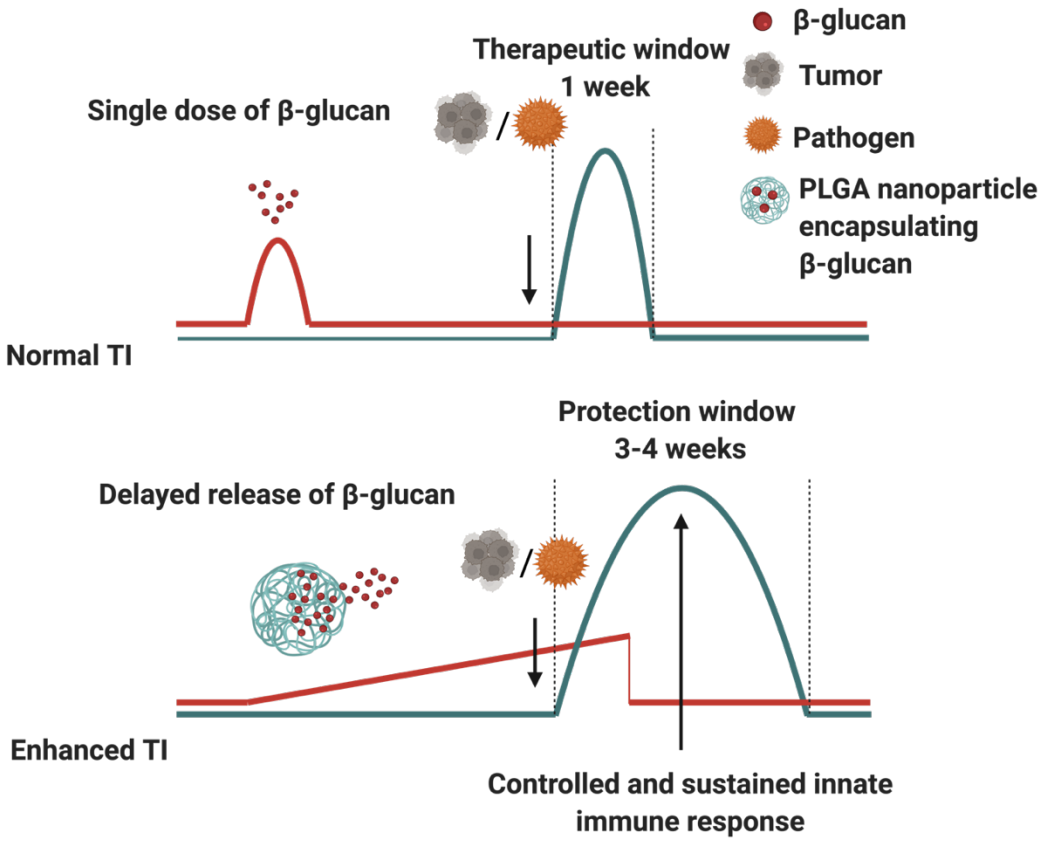

Figure 4.1: Schematic representation of the proposed mechanism of action of PLGA nanoparticles encapsulating β-glucan.
Trained immunity mediated by free β-glucan confers protective effects that last only one week. Sustained release of β-glucan from engineered PLGA nanoparticles enable prolonged trained immunity effects that can last up to four weeks depending on the release profile. (created with BioRender.com)

4.3 Results

To test the hypothesis that sustained release can prolong trained immunity, we first synthesized nanoparticles composed of PLGA encapsulating β-glucan. Nanoparticles were synthesized using a modified version of a previously reported double emulsion technique,[21] owing to its ease and consistency in creating homogenous nanospheres that degrade in a controlled release fashion. In brief, nanoparticles were synthesized by ultrasonication of an aqueous solution of β-glucan and PLGA dissolved in dichloromethane. The solution was ultrasonicated again after adding 5% PVA and left stirring for 6 hours in a 0.5% PVA stabilizing solution. The resulting precipitated nanoparticles were washed and lyophilized for characterization.

In examining the consistency of nanoparticles, scanning electron microscopy (SEM) images revealed nanosphere morphology of particles that were around 67 ± 20 nm in diameter (**Figure 4.2A**). However, we detected larger radiuses under DLS measurements suggesting that the particles significantly aggregate in aqueous solutions (**Appendix B1**). The amount of β-glucan encapsulated within the nanoparticles was quantified using a total carbohydrate assay.[22] Encapsulation efficiency was determined by the percentage of β-glucan as measured by the carbohydrate assay divided by the amount of β-glucan initially loaded in each formulation. Synthesized nanoparticles had a high encapsulation efficiency of 73%. We also evaluated the *in vitro* release profile at pH 7.4, which showed a sustained release profile of b -glucan over the 4-week period of testing (**Figure 4.2B**). We confirmed that the synthesized nanoparticles were devoid of endotoxin using a HEK-mTLR4 reporter assay (**Appendix B2**). Concluding that the particles were loaded with β-glucan and devoid of any other immuno-stimulatory materials, we next tested them for their ability to train innate cells.

As previous work had shown that PLGA nanoparticles exhibit slow-release, we first tested if the synthesized nanoparticles encapsulating β-glucan improved trained immunity using a standard BMDM training model.[23] In this model, macrophages are trained with added material (e.g., β-glucan) and later challenged with a conventional secondary stimulant (e.g., LPS). If training occurs, the macrophages increase the transcription of pro-inflammatory cytokines like IL-6 and TNF-a. Following a standard 7-day training assay, murine BMDMs at a density of 100,000 cells per well were incubated for 24 h with a set of "training material." Each group of cells were trained for 24 h, rested for four days, and later challenged with 10 ng/mL of LPS in a total volume of 200 mL. We compared how the release of β-glucan affected training by using nanoparticles containing either β-glucan (100 mg/ml) or administering the free form of an equivalent amount of β-glucan (3.7 mg/mL). We included an untrained (or PBS trained) group as our negative control. Some nanoparticles were found to stick to the well plate even after washing with PBS after 24 h (**Appendix B3a**). We observed significantly higher IL-6 and TNF-a levels confirming that nanoparticles enhanced trained immunity *in vitro* (**Figure 4.2C**). In fact, encapsulating the β-glucan in nanoparticles resulted in an approximately 1.5-fold increase in both IL-6 and TNF-a produced by BMDMs in response to the same stimulus compared to the unencapsulated equivalent. In addition, we observed that nanoparticles with no β-glucan did not induce training (**Appendix B3b**). Together, these results suggested that encapsulation of the training material, β-glucan, could strongly enhance the training effect in preliminary *in vitro* assays. Additionally, the remaining nanoparticles after the 24 h wash period, might also contribute to slow release of β-glucan and enhanced training.

While the initial *in vitro* data was promising, one important consideration was if encapsulation affected the mechanism of action of trained immunity mediated by β-glucan. In previous experiments, others established that β-glucan induces epigenetic and metabolic changes via histone methylation and acetylation to control transcription of pro-inflammatory cytokines.[24] We tested if the nanoparticles activated similar pathways in trained immunity using our *in vitro* assay. To do this, BMDMs were pre-treated with small-molecule epigenetic and metabolic inhibitors for 30 min before exposing them to each training material in the standard 7-day BMDM training assay used in the previous experiment.[23,25] All the epigenetic inhibitors reduced trained immunity induced by free β-glucan, as reported previously – validating the assays. Histone demethylase inhibitor-pargyline hydrochloride significantly reduced training by nanoparticles, whereas histone methyltransferase inhibitor (methylthioadenosine or MTA) did not affect training. Histone acetyltransferase inhibitor (Epigallocatechin-3-gallate or EGCG) reduced nanoparticle-induced training *in vitro*; however, the difference was not significant ($p = 0.073$) (**Figure 4.2D**). The results confirm that the nanoparticles induce training through an epigenetic mechanism. However, the results also suggest that nanoparticle-based training operates through a slightly different overall temporal process, perhaps owing to the timing and delivery of the β-glucan. This may bear further examination in fundamental studies in the future.

Apart from epigenetics, metabolic changes also contribute to β-glucan induced training. Dectin-1 activation by β-glucan results in phosphorylation of Akt, thereby activating the mammalian target of rapamycin (mTOR). Akt inhibitor- wortmannin reduced trained immunity mediated by free β-glucan but not by nanoparticles. Inhibiting mTOR by pre-treating cells with rapamycin significantly reduced training effects in both the free β-glucan equivalent and nanoparticle groups.

Trained innate cells switch from oxidative phosphorylation to glycolysis to meet the energy demands to induce epigenetic changes for higher effector function, such as secretion of pro-inflammatory cytokines. This process also generates metabolites that further modulate their epigenetic profile.[26,27] To test the metabolic effects of training with nanoparticles, we depleted glucose by pre-treating cells with 2-deoxy D-glucose and observed reduced training effects by all training materials tested, confirming that glycolysis is a key to trained immunity effects by nanoparticles. (**Figure 4.2E**). Taken together, these results demonstrate that nanoparticles mediate trained immunity through much the same pathways targeted by free β-glucan encompassing both metabolic and epigenetic reprogramming of BMDMs. However, they show distinctive differences in how the particles may alter the pathways, perhaps in the kinetics of the overall dose of β-glucan, which may explain the resulting improvements in training observed in the preliminary *in vitro* results.

While β-glucan stimulates Dectin-1 and complement receptors, previous reports have shown that trained immunity mediated by β-glucan is not fully dependent on this receptor-ligand interaction.[25,43] One potential explanation for these subtle mechanistic differences observed with our nanoparticle system would be the kinetics and delivery of β-glucan to the cells. We reasoned that better uptake of nanoparticles by BMDMs might be one reason for better training *in vitro* compared to an equivalent amount of free β-glucan. To test this hypothesis, we labeled β-glucan with fluorescein isothiocyanate (FITC) and monitored their uptake by BMDMs at the end of 24 h, mimicking the *in vitro* training assay using flow cytometry. After 24 h of training, we observed higher levels of FITC+ cells in the nanoparticle trained groups than the free equivalent group (**Figure 4.2F**, **Appendix B4**). We performed the 7-day *in vitro* assay by pre-treating BMDMs with

known inhibitors targeting caveolae and clathrin-mediated endocytosis pathways to test if endocytosis is involved.[28] We observed a significant reduction in nanoparticle-mediated training with inhibitors of both caveolae-specific endocytosis (filipin) and both caveolae and clathrin-dependent endocytosis (dynasore). (**Figure 4.2G**). Clathrin inhibitor (chlorpromazine) did not cause any change in nanoparticle-mediated training. These results strongly support that nanoparticle-induced trained immunity *in vitro* proceeded through increased uptake by BMDMs revealing an alternate method for inducing trained immunity.

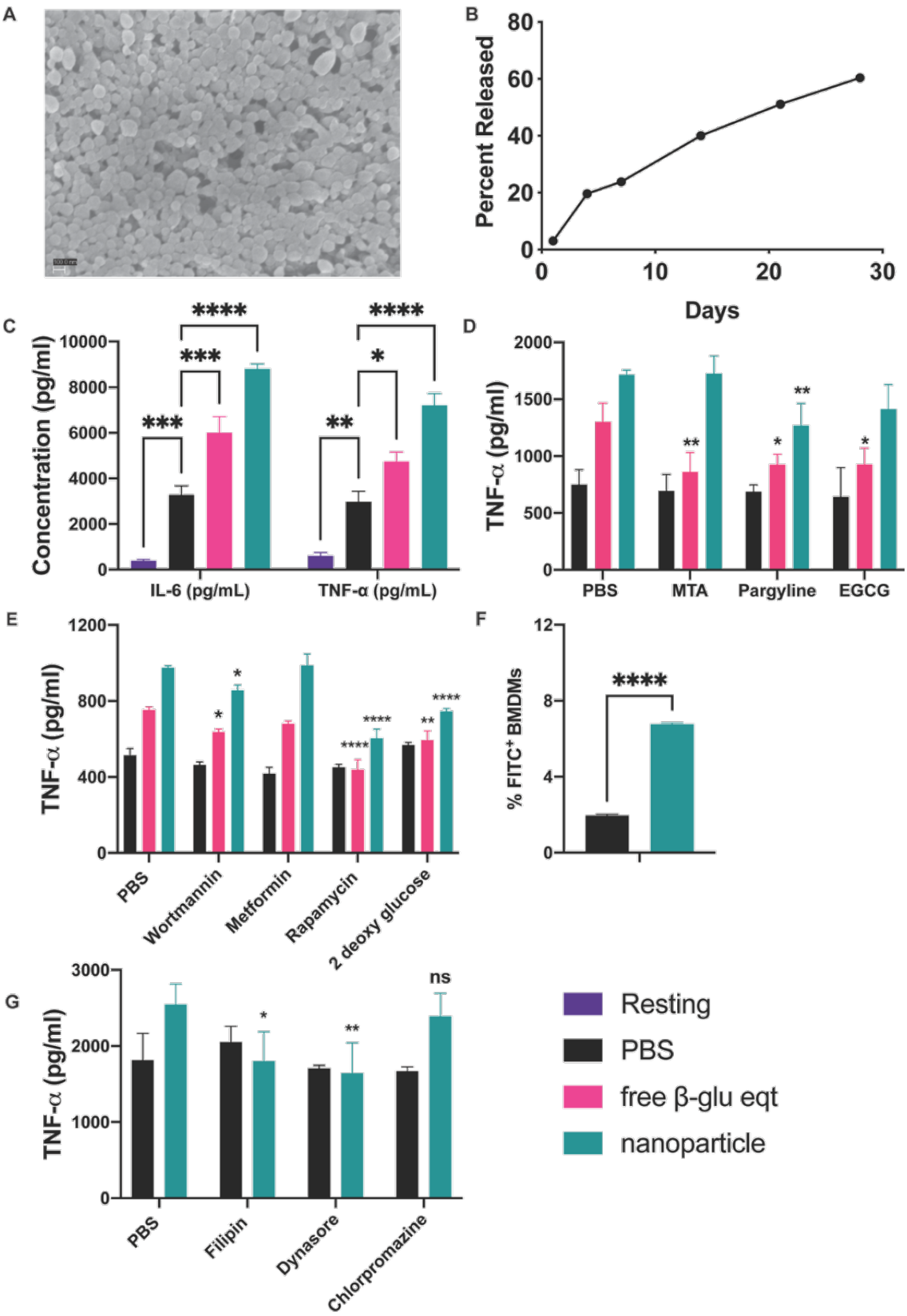

Figure 4.2: Nanoparticle characterization and *in vitro* TI assays

Figure 4.2 continued
a) Scanning electron microscopy image of PLGA nanoparticles synthesized by double emulsion technique. (scale bar = 100 nm)
b) 7-day *in vitro* release kinetics of encapsulated β-glucan from the synthesized PLGA nanoparticles at pH 7.4.
c) *in-vitro* trained immunity assay comparing cytokine levels in resting cells (purple bar) or following an LPS challenge in BMDMs trained with either PBS (black bar), the free equivalent amount of β-glucan (pink bar) or PLGA nanoparticles encapsulating β-glucan (green bar), n=3, significance compared with PBS.
d) Assay determining changes in epigenetic training response. BMDMs were pretreated for 30 min with inhibitors targeting epigenetic modifications, namely MTA (histone methyltransferase inhibitor), EGCG (histone demethylase inhibitor), or pargyline hydrochloride (histone acetyltransferase inhibitor). Cytokine levels were measured after an LPS challenge on day 5 with BMDMs trained with PBS (black bar), the free equivalent amount of β-glucan (pink bar), or PLGA nanoparticles (green bar) n=3, significance compared with PBS (no inhibitor) group.
e) Assay determining changes in metabolic training response. BMDMs were pretreated for 30 min with inhibitors targeting metabolic pathways, namely wortmannin (Akt inhibitor), metformin (AMPK activator), rapamycin or 2-deoxy D-glucose (glycolysis inhibitor). Cytokine levels were measured after an LPS challenge on day 5 with BMDMs trained with– PBS (black bar), the free equivalent amount of β-glucan (pink bar), or PLGA nanoparticles (green bar), n=3, significance compared with PBS (no inhibitor) group.
f) BMDMs were treated with either free FITC-labelled β-glucan (pink bars) or nanoparticles encapsulating FITC- β-glucan (green bars) for 24 h. BMDMs were analyzed by flow cytometry to measure the percentage of cells that were FITC+. Statistics was conducted using an unpaired student's T-test.
g) BMDMs were pre-treated for 30 min with inhibitors targeting endocytosis pathways, namely dynasore (caveolae and clathrin inhibitor), filipin (caveolae inhibitor), or chlorpromazine (clathrin inhibitor). IL-6 levels were measured after an LPS challenge on day 5 with BMDMs trained with– PBS (black bar), the free equivalent amount of β-glucan (pink bar), or PLGA nanoparticles (green bar), n=3, significance compared with PBS (no inhibitor) group.
All values are expressed as mean ± SEM. n=3 and statistics were conducted using a two-way ANOVA with Dunnett's multiple comparisons test (significance compared with PBS group) or student's T-test. *$P < 0.05$, **$P < 0.01$, ***$P < 0.001$, ****$P < 0.0001$, n.s., not significant.

To accurately test how controlled release might affect trained immunity in a prophylactic model, we tested the particles using an *in vivo* model (**Figure 4.3A**). Mice were trained twice with either nanoparticles or an equivalent amount of free β-glucan. To account for the potential effects of age and injection, we included an "untrained" (PBS) group. For comparison, we also included a conventional standard training regimen –1 mg of free β-glucan. To determine the increase in innate response from training, mice were then challenged intraperitoneally with a secondary stimulus-

LPS, at defined time points after the training regimen. In a standard training assay, LPS challenge results in systemic pro-inflammatory cytokines (IL-6 and TNF-a). Higher cytokine response indicates better trained mice. Since the synthesized nanoparticles exhibit slow release of the encapsulated β-glucan over thirty days, we hypothesized that the training response in the nanoparticle-trained group would coincide with its release profile, peaking after 30 days of training. To test this hypothesis, we analyzed systemic cytokines following an LPS challenge at two different time points– 7 and 28 days after the first training material was administered. In previous work, mice trained with standard 1 mg free β-glucan elicited peak systemic cytokines after 7 days of training.[13] At 7 days, for the β-glucan (1 mg) group, systemic cytokines following an LPS challenge were highest, matching previous work. The group trained with the free equivalent amount of β-glucan (35 mg/mouse) did not show any systemic responses. This result may be due to the very low dosage – only 3.5% of a responsive amount. Also, mice trained with nanoparticles at 7 days somewhat surprisingly showed no systemic response (**Figure 4.3B**). However, when challenged 28 days after the first training, nanoparticle-trained mice showed higher peak systemic responses than mice trained with 1 mg of β-glucan or the nanoparticle-free equivalent dosage. Of note, the level was nearly as high as that of the standard training at day 7 with only 3.5 % as much β-glucan added. This result provided strong support for our initial hypothesis. Additionally, we observed no increase in cytokines in any category when mice were challenged with LPS 35 days after training (**Appendix B5**)- indicating the transient nature of training. To rule out innate immune priming effects, we analyzed serum cytokines before the LPS challenge on day 28. We observed no significant differences between untrained and nanoparticle trained mice (**Appendix B6**), indicating that the system was not actively responding to previous stimulation. Taken together, these results strongly support that the controlled release

from nanoparticles prolonged training, but only peak around 28 days. They did not extend training beyond a predictable time window- preventing potential uncontrolled inflammation.

A critical question remained: how long do the particles persist upon injection, and how does that timing impact the controlled training regimen? To assess the biodistribution of the synthesized nanoparticles, mice were injected intra-peritoneally with NIR-labelled PLGA nanoparticles with the same formulation of encapsulated β-glucan (**Appendix Table B1**). The injected nanoparticles localized to the peritoneal cavity 30 min after injection (**Figure 3C**). To confirm that nanoparticles exhibited sustained release, we monitored the fluorescence intensity emitted from the nanoparticles. Fluorescence intensity measurement was reduced to zero by three weeks post-training and followed first-order kinetics. (**Figure 4.3C** and **Figure 4.3D**). After confirming the absence of residual nanoparticles, we challenged the mice with LPS and observed higher systemic cytokines from the nanoparticle-trained mice (**Appendix B7**). These results add further support to our hypothesis that it is the sustained release of β-glucan from the nanoparticles which increases the effect of training. We also confirm that peak training effects induced in the nanoparticle-trained group occurred after the nanoparticles appeared fully dispersed.

After confirming that the nanoparticles localized at the peritoneal cavity, we examined if peritoneal macrophages contributed to the response of nanoparticle-induced training when peak systemic responses were induced at day 28. To test this hypothesis, we isolated peritoneal macrophages from mice that received training material four weeks earlier. The isolated trained peritoneal macrophages were challenged ex-vivo with LPS, and pro-inflammatory cytokines were quantified. We observed 77% higher IL-6 levels from peritoneal macrophages isolated from nanoparticle-

trained mice than those isolated from unencapsulated free equivalent β-glucan trained mice (**Figure 3E**). We performed an adoptive transfer experiment to determine if peritoneal macrophages could act as a sole mediator of training. After 28 days of training in mice administered standard nanoparticles, the free-equivalents of β-glucan, or 1 mg of β-glucan, peritoneal macrophages were adoptively transferred to naïve mice. The recipient mice were challenged with LPS 1 day later, and systemic cytokines were quantified. Analogous to the *ex vivo* challenge experiment, we observed that peritoneal macrophages isolated from nanoparticle trained mice conferred naïve mice with improved training effects against LPS challenge compared to all other groups tested (**Figure 3F**). Mice that received peritoneal macrophages from nanoparticle trained mice produced a 2-fold increase in IL-6 compared to the group with an unencapsulated amount of free β-glucan. This result provided evidence that peritoneal macrophages are one of the primary cellular mediators of training for nanoparticle-induced training and that sustained-release platforms can target macrophages to improve training effects.

We then explored if nanoparticle trained mice exhibit localized training effects, particularly at the administration site, i.e., the peritoneal cavity, at earlier times (one week after training). In previous work, inflammation in the peritoneal cavity was observed to induce the recruitment of monocyte-derived small peritoneal macrophages (SPMs).[9,29] Mice were trained with the same regiment of desired training materials, challenged with LPS after 7 days and their peritoneal cavity cells were harvested. We observed that mice trained with nanoparticles had much higher populations of SPMs (40 %) than the free β-glucan groups (**Figure 3G**, **Appendix B8**), confirming that the particles induced localized effects. However, training may also modulate immune cell populations at the spleen. Analysis of splenic cell populations between nanoparticles and other free

formulations revealed a slight but non-significant increase in the percent of macrophages in mice trained with nanoparticles. We observed no changes in other cell types like neutrophils which were upregulated in mice trained with 1 mg free β-glucan (**Appendix B9**). These results were inconclusive but indicated that the nanoparticles might exert some localized effects at the injection site, and further study of the localized effects of controlled release is warranted.

To explore if the dosing regimen would alter the activity and cellular makeup at the site of action in nanoparticle-induced training at earlier time points (day 7), mice were trained with either two doses of 0.5 mg spaced four days apart or a single dose of 1 mg of nanoparticles. In this case, both groups would ultimately release an equivalent amount of β-glucan. Yet, the distributions would differ, resulting, theoretically, in different cellular compositions in the injection site and altered training responses. After a standard training injection of either 0.5 mg of nanoparticles at intervals of 4 days or 1 mg of nanoparticles, we collected cells from the peritoneal cavity, spleen, and bone marrow. Cells were challenged with LPS *ex vivo*, and cytokines released into the supernatant were analyzed.[13,30,31] We observed a single dose of 1 mg nanoparticles resulted in better training in peritoneal macrophages. (**Figure 4.3H**) However, two doses of 0.5 mg of nanoparticles resulted in better-trained immunity effects in splenic macrophages (**Figure 4.3I**). No significant differences were observed in bone marrow-derived macrophages (BMDMs) harvested from nanoparticle trained mice, confirming that the site of action was restricted to the peritoneal cavity and spleen at earlier time points (**Appendix B10**). These results indicate that the dosing regimen of nanoparticles could provide more spatial control over the site of training at earlier time points. Taken together, these results indicate that the training with nanoparticles occurs mainly within the local tissue but can be altered via dosing and distribution. Future therapeutic approaches might

take that timing and dose into consideration. However, further experiments are needed to evaluate the extent of local vs. systemic training thoroughly.

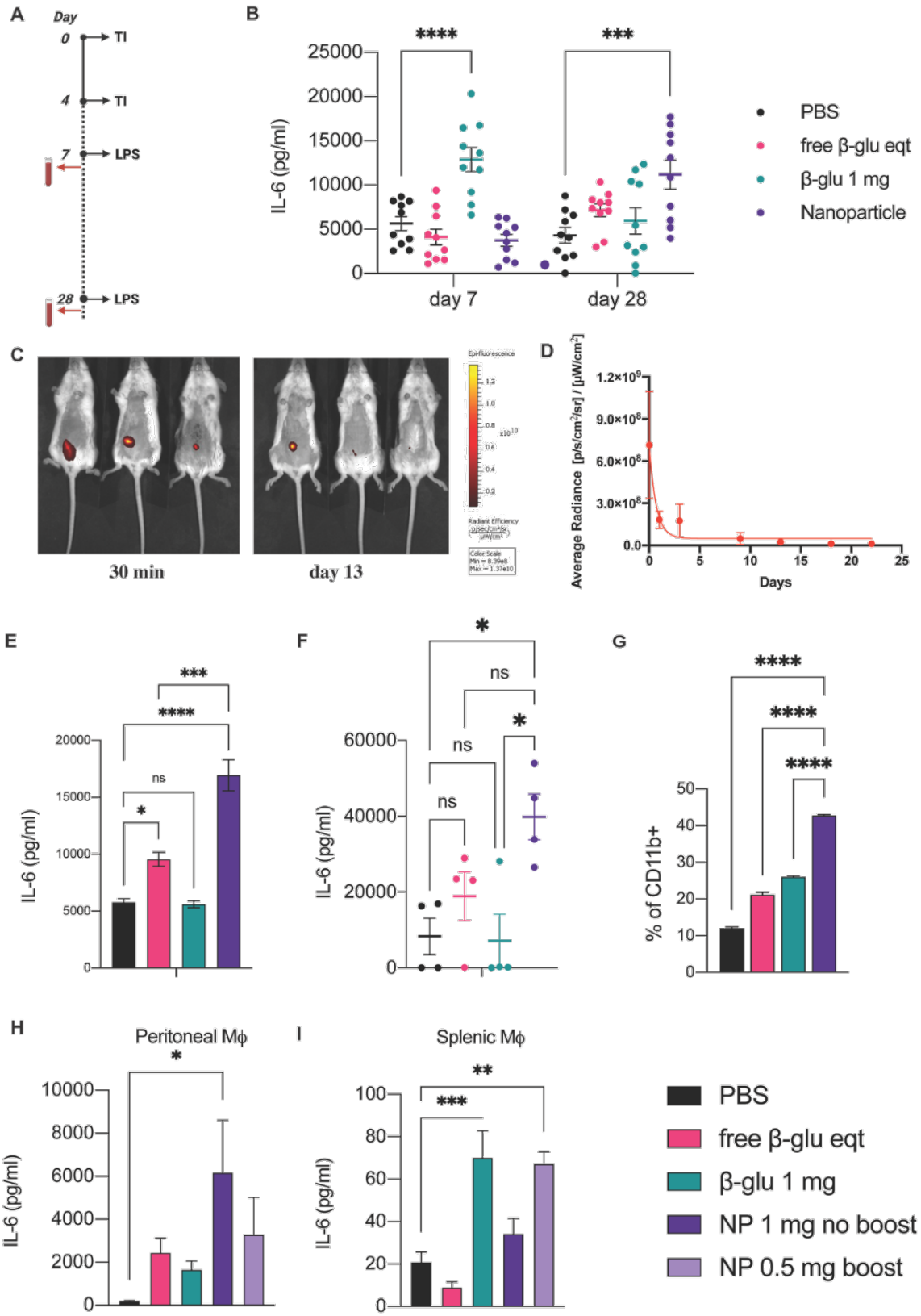

Figure 4.3: Altering the temporal response of trained immunity *in vivo* results in changes in trained macrophage populations

Figure 4.3 continued
a) *in-vivo* trained immunity schematic. Training materials were administered on day 0 and day four, and separate sets of mice were challenged 7 or 28 days later. Systemic cytokines were measured 1 h after the LPS challenge
b) Systemic IL-6 levels 1 h after LPS challenge on day 7 and day 28 with mice trained with PBS (black), the free equivalent amount of β-glucan (pink), 1 mg of β-glucan (green) or nanoparticles (purple), n=10, significance compared with PBS (untrained) group.
c) *in vivo* biodistribution assay of NIR-labelled PLGA nanoparticles encapsulating β-glucan at 30 min and 13 days measured by IVIS, n=3.
d) PLGA degradation profile *in vivo* measured by fluorescence intensity over time. Data was fitted to one-phase decay characteristic of reported PLGA degradation kinetics.
e) Analysis of trained immunity phenotype in peritoneal macrophages isolated from mice 28 days after training. Training was administered on day 0 and day 4 with PBS (black), the equivalent amount of β-glucan (pink), 1 mg of β-glucan (green), or nanoparticles (purple). After 28 days, peritoneal macrophages were harvested and challenged ex-vivo with LPS (10 ng/mL), and IL-6 levels were quantified, n= 5
f) Analysis of the effect of adoptive transfer of peritoneal macrophages from trained mice in conferring trained immunity phenotype in naïve mice. Training was administered on day 0 and day 4 with PBS (black), the equivalent amount of β-glucan (pink), 1 mg of β-glucan (green), or nanoparticles (purple). After 28 days, peritoneal macrophages were harvested and cultured for 1 day. 1 million peritoneal macrophages per group were adoptively transferred (i.p) to naïve mice. After 24 h, these mice were challenged with LPS, and serum cytokines were analyzed 3 h post-challenge; n= 4
g) Analysis of percentage of SPMs in the peritoneal cavity after LPS challenge after 7 days of training. Training was administered on day 0 and day 4 with PBS (black), the equivalent amount of β-glucan (pink), 1 mg of β-glucan (green), or nanoparticles (purple). After one week, mice were challenged with LPS, and peritoneal cells were harvested 2 h later. The percentage of small peritoneal macrophages (SPMs) (CD11b+ F4/80-) was analyzed by flow cytometry, n=5,
h) Analysis of trained immunity phenotype in peritoneal macrophages after 7 days. Training was administered on day 0 and day 4 with PBS (black), the equivalent amount of β-glucan (pink), 1 mg of β-glucan (green), 1 mg only on day 0 (purple) or 0.5 mg nanoparticles on both day 0 and day 4 (lilac). Peritoneal macrophages were harvested on day 7 and challenged ex-vivo with LPS. Cell supernatants were analyzed for inflammatory cytokines – IL-6, n=5, significance compared with PBS (untrained) group,
i) Analysis of trained immunity phenotype in splenic macrophages after 7 days. Training was administered on day 0 and day 4 with PBS (black), the equivalent amount of β-glucan (pink), 1 mg of β-glucan (green), 1 mg only on day 0 (purple), or 0.5 mg nanoparticles on both day 0 and day 4 (lilac). Splenic macrophages were harvested and challenged ex-vivo with LPS. Cell supernatants were analyzed for inflammatory cytokines- IL-6. n=5, significance compared with PBS (untrained) group,
All values are expressed as mean ± SEM. n= 3-5, Statistics was conducted using one or two way ANOVA with Dunnett's multiple comparison testing to compare groups to PBS group or Tukey's multiple comparison testing to compare all groups as indicated. $*P < 0.05$, $**P < 0.01$, $***P < 0.001$, $****P < 0.0001$, n.s., not significant.

Trained immunity has been proposed and demonstrated to be useful in both infectious diseases and immune therapy. In initial experiments, we explored how altering the temporal persistence of trained immunity could be applied to cancer immuno-therapy owing to the potential to generate a long-lived response. Generating durable responses against tumor growth is an oft-cited goal to sustain therapeutic effects. We tested to see if nanoparticle-trained mice would provide greater resistance to a tumor challenge owing to its sustained release. Using a similar setup to previous experiments, mice were injected intra-peritoneally, either with nanoparticles containing β-glucan, an equivalent amount of unencapsulated free β-glucan, or a standard training dose of β-glucan at 1 mg. In this experiment, injections were given twice, 4 days apart, indicated as day 0 and day 4. Mice were challenged with B16.F10 tumors three weeks (day 21) after the training. Tumors take about a week to form a visible mass (day 28) which we had previously measured to be the time by which nanoparticles elicited complete release of encapsulated β-glucan (**Figure 4.4A**). Measuring tumor volume, we observed that the nanoparticle trained mice significantly resisted tumor growth compared to the free β-glucan trained groups (**Figure 4.4B**). Looking for a mechanism, analysis of the tumor-infiltrating innate immune cells at the end of the experiment revealed increased neutrophils and macrophages in the tumor microenvironment, confirming that the anti-tumor effects in nanoparticle trained mice were due to changes in the tumor microenvironment [32] (**Figure 4.4C**, **Figure 4.4D**, **Figure 4.4E**, **Appendix B11**). In previous work, β-glucan was shown to skew TAMs into an inflammatory M1 phenotype and train neutrophils to improve tumor resistance.[33–35] From this preliminary examination, we conjecture that the nanoparticles may sustain this same result for a more extended period, resulting in the observed phenotype. Additionally, spleen weights corresponded with tumor size as well – splenomegaly was observed for both the PBS and 1 mg free β-glucan groups (**Appendix B12**). Beyond this model, we also tested the anti-tumor

effects of the nanoparticles in an EG7.OVA tumor model. We observed similar effects with nanoparticle-trained mice exhibiting the highest tumor resistance. (**Appendix B13**) These results suggest that sustained-release training platforms could potentially be combined with existing anti-cancer therapies, including checkpoint blockade, to prolong protection as they provide an alternate method to influence the tumor micro-environment.[37]

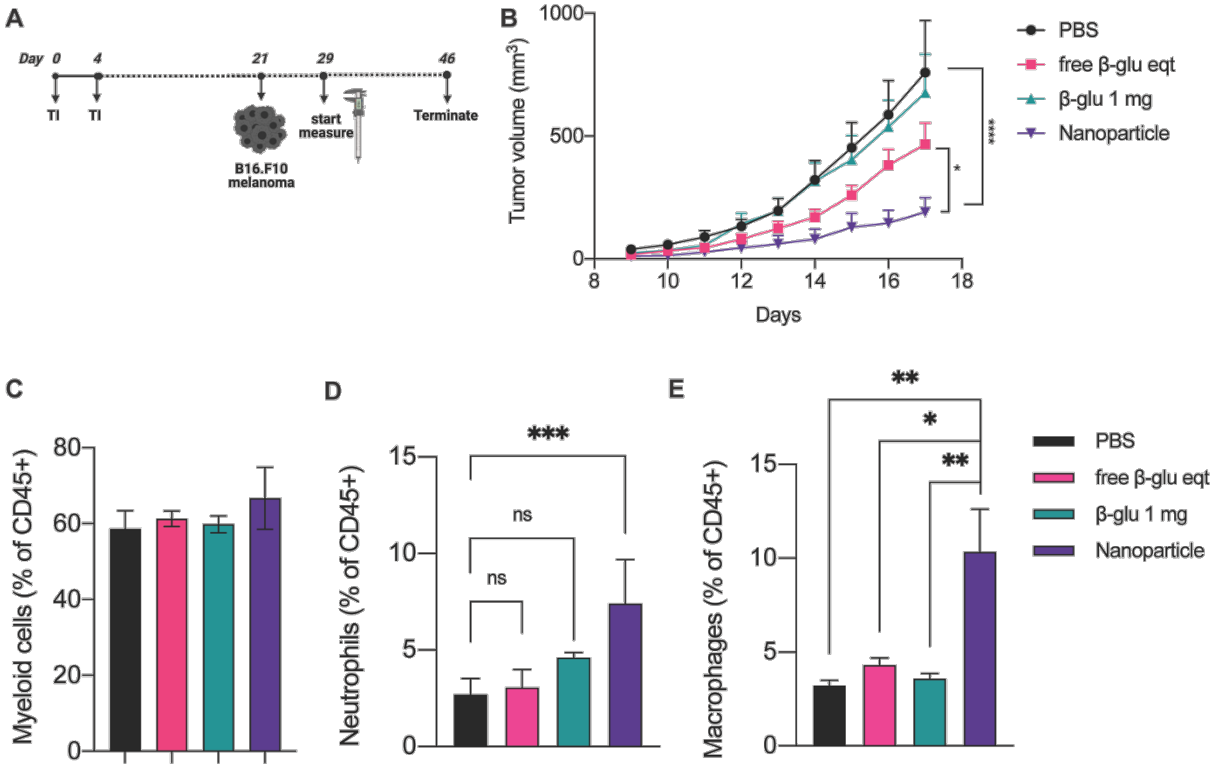

Figure 4.4: Tumor challenge
a) Experimental scheme for B16.F10 tumor challenge. (created with BioRender.com)
b) Mice were trained on day 0 and day 4 with the indicated training materials- PBS (black bars), the free equivalent amount of β-glucan (pink bars), 1 mg β-glucan (green), or PLGA nanoparticles encapsulating β-glucan (purple bars). Mice were then challenged subcutaneously with B16.F10 tumor cells. Tumor volume was recorded after the tumors were palpable – day 29 onwards.
c) Tumors were excised at the end of the experiment on day 46, and the percentage of myeloid cells (Cd45+Cd11b+) was analyzed using flow cytometry.
d) Tumors were excised at the end of the experiment on day 46, and the percentage of neutrophils (Cd45+Cd11b+Ly6g+) was analyzed using flow cytometry, significance compared to the PBS group.

Figure 4.4 continued
e) Tumors were excised at the end of the experiment on day 46, and the percentage of macrophages (Cd45+Cd11b+Ly6g-F4/80+) was analyzed using flow cytometry, significance compared to the PBS group.
Statistics was conducted using one-way ANOVA with Dunnett's multiple comparison testing to compare groups as indicated. All values are expressed as mean ± SEM. n= 5 ,*$P < 0.05$, **$P < 0.01$, ***$P < 0.001$, ****$P < 0.0001$, n.s., not significant.

One of the well-established properties of PLGA is its control over the release kinetics of encapsulated cargo.[19] Increasing the molecular weight of PLGA decreases diffusion of the encapsulated cargo, thereby prolonging the duration of release and vice versa.[20,37] We hypothesized that this property might be uniquely suited to improve temporal control of trained immunity. Additionally, PLGA end groups can also affect release kinetics- carboxylic acid end groups degrade faster than those with ester end groups.[38] To test this hypothesis, we encapsulated β-glucan using two different molecular weight PLGA polymers of molecular weights ranging from 7kDa-17kDa and 35kDa-55kDa. We also used PLGA with two different end groups- acid terminated and ester terminated. For simplicity, the formulations are hereby categorized as low acid/ester and high acid/ester, respectively. SEM characterization revealed a spherical morphology for all the PLGA nanoparticles. Encapsulation efficiency was in the range of 72-41% for all the synthesized nanoparticles (**Appendix B14**, **Appendix Table B1**). *In vitro* release data confirmed that nanoparticles composed of smaller molecular weight PLGA degraded faster than higher molecular weight PLGA nanoparticles. (**Figure 5A**) Because our experiment was solely focused on the temporal control of the training and not on inducing a specific magnitude of training, we proceeded with this level of control over loading and release.

To study the kinetics of training, we tested the different molecular weight nanoparticles in an *in vivo* model with a time-course analysis of serum cytokines following an LPS challenge (**Figure**

4.5B). Mice were trained as previously described with the various molecular weight nanoparticles and challenged with LPS at increasing time points- 7, 21, 25, or 30 days after the first training. We observed peak systemic IL-6 responses at day 7 for both the acid and ester terminated low molecular weight nanoparticles. By day 21, the high molecular weight acid terminated group demonstrated significantly higher systemic IL-6 levels after LPS challenge. However, the high molecular weight ester terminated group peaked at day 25 (**Figure 4.5C**) suggesting that controlled release could be achieved by modulating both molecular weight as well as polymer end groups used. Continued analysis through day 30 confirmed the absence of sustained inflammatory responses (**Appendix B15**). These results further supported our hypothesis that fine-tuning the properties of sustained-release platforms can be used for precise temporal control over the duration of trained immunity. These results suggest that with different formulations, it is possible to partially control the timing of training and lengthen or shorten the window over which higher innate responses are induced via training. Controlled training is an important step to preventing potential over-inflammatory or chronic-inflammatory responses which might cause adverse reactions.

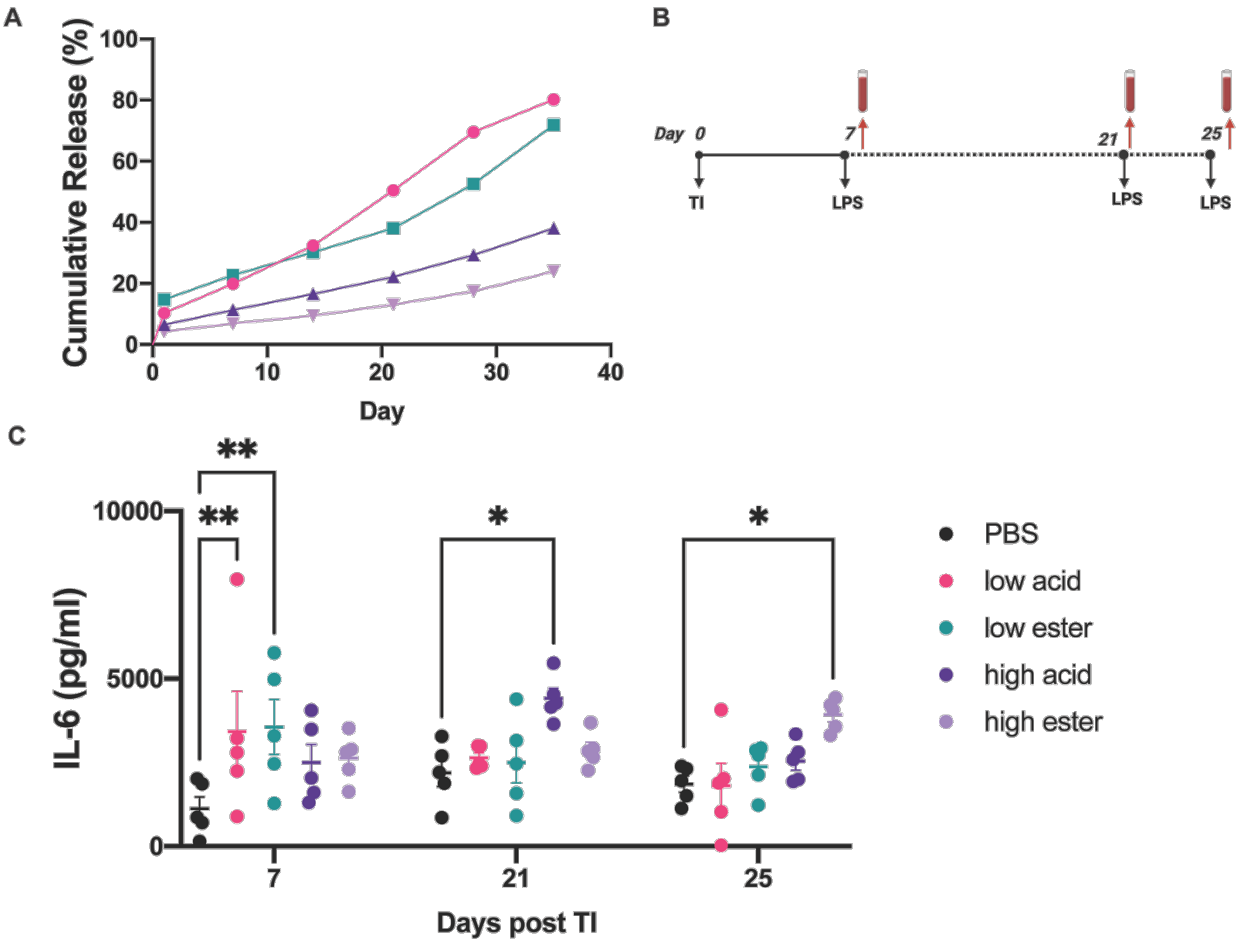

Figure 4.5: Modulating PLGA properties for temporal control of trained immunity
a) 7 day *in vitro* release profile of low molecular weight ester-terminated PLGA nanoparticles (green), high molecular weight acid-terminated nanoparticles (purple), or high molecular weight ester-terminated nanoparticles (lilac) at pH 7.4, n=3
b) *in vivo* experimental protocol. (created with BioRender.com)
c) Mice were trained with either PBS (black) low molecular weight acid-terminated PLGA nanoparticles (pink), low molecular weight ester-terminated PLGA nanoparticles (green), high molecular weight acid-terminated nanoparticles (purple), or high molecular weight ester-terminated nanoparticles (lilac) on day 0. Different sets of mice (n=5) were challenged with LPS on the indicated days (7, 21, or 25), and systemic cytokines were quantified. Significance compared with PBS group.
All values are expressed as mean ± SEM. n= 3-5 and statistics were conducted using a two-way ANOVA with Dunnett's multiple comparisons test ,*$P < 0.05$ and **$P < 0.01$,

4.4 Conclusion

Trained immunity improves the innate immune response to pathogenic challenge and tumor burden. However, current methods only provide transient approaches to induce training due to the short lifespan of the trained cells. While methods to direct training at the bone-marrow level ensure long-term effects, this approach suffers from the potential disadvantage of inducing long-term adverse inflammatory responses. Precise control of timing and dosage of innate immune cell activation may provide a method to improve training duration while managing unwanted adverse reactions due to prolonged activation.

We report on a nanoparticle-based sustained delivery platform for temporal control over training. Controlled release of training material, β-glucan, resulted in both more sustained and higher training than a comparable injection of standard-dose β-glucan or an equivalent amount of β-glucan to that in the particle. Of note, only 3.5% of the standard dose of β-glucan was incorporated in the nanoparticles. We observed that particle training proceeded through similar pathways and mechanisms as free β-glucan training with the potential difference that some kinetic elements are altered. These results indicate that the enhanced training effect resulted mainly from the altered timing of the release. We further studied the pharmaco-kinetics by examining the release in animals using IVIS imaging, concluding that sustained-release occurred for at least the first 14 days. This altered and improved training resulted in differences in the location of training and the degree of trained cells in the peritoneal cavity and spleen, demonstrating that control of cell training can be achieved through material programming.

To demonstrate the potential of temporal control for trained immunity, we also demonstrated that training-induced by nanoparticles improved tumor resistance in mice than those trained with free β-glucan. This approach can be potentially used in conjunction with current immune therapies such as checkpoint blockade therapies to prolong anti-tumoral effects and prevent recurrence. Finally, to show the potential of this technology for future application, we showed that different training windows could be achieved with different molecular weights and end-groups of nanoparticle formulation PLGA. This novel nanoparticle-based delivery platform reduces bulk inflammation and provides effective temporal control of trained immunity.

In this study, we focused on an intraperitoneal route of training which has been extensively explored in the field. The use of PLGA based delivery platforms makes it easy to translate to other clinically relevant routes of training to target specific tissues that are key to disease resistance.[39] For example, detailed aerosolized techniques for PLGA nanoparticle delivery have been documented and explored to target pulmonary macrophages [40] that are important in resisting respiratory diseases. Trained immunity also enhances anti-tumor effects, and surface modification of PLGA with suitable ligands can help target specific tumors such as those affecting pancreas. [44,45] Similarly, local release platforms can be leveraged to decrease trained immunity to decrease allograft rejection for prolonged periods of time. For example, myeloid cell targeting high-density lipoprotein nanobiologics delivered intravenously were recently shown to reduce training to ensure prolonged allograft survival in a heart transplant model in mice. [14] It is also important to eliminate training after achieving the desired outcome to reduce unwanted inflammation. [17] Taken together, our nanoparticle-based delivery system offers two advantages. Firstly, our platform enables easy surface modifications to achieve targeted delivery. Secondly, our sustained release formulations

utilizes significantly less β-glucan that releases slowly over time, thereby eliminating any adverse immunostimulation. We present this work as its potential for biomaterials and formulations methods employed in drug delivery to modulate and improve trained immune responses. This work can potentially lead to the development of novel, safe, and effective prophylactics for improved resistance against a variety of diseases.

4.5 Materials and Methods

HEK mTLR4, B16F10 and EG7.OVA cells were obtained from InvivoGen. All cell culture reagents were obtained from Thermo Fisher Scientific. mTLR4 cells were cultured in DMEM supplemented with 10% FBS and selective antibiotics. Cells were maintained at 37°C and 5% CO2. C57Bl/6J mice were obtained from Jackson Laboratories and acclimatized for 1 week prior to experimentation. All animal experiments were conducted with approval from the University of Chicago Institutional Animal Care and Use Committee. All statistical analyses were performed using GraphPad Prism.

Formulation of nanoparticles

β-glucan was purchased from Sigma (G5011). The payload was added in 200 mL to 2 mL of 100 mg/mL of PLGA in methylene chloride. The mixture was ultrasonicated at 40% amplitude for 3 minutes (30 seconds stirring following 30 seconds of rest). After ultra-sonification, a determined amount of 5% (w/v) PVA solution was added to the primary w/o emulsion and ultrasonicated for 60 seconds to produce the w/o/w double emulsion. The w/o/w emulsion was poured into 200 mL of chilled 1% (w/v) PVA and stirred at room temperature for 6 hours. The microspheres were

centrifuged at 4000 rpm for 40 minutes and the pellet were washed three times with ultrapure deionized water and then lyophilized.

Characterization of nanoparticles

For SEM imaging, nanoparticles were first sputter coated with 12 nm of Pt/Pd using Sputter Coater - Cressington 208HR. SEM images were taken with Carl Zeiss Merlin SEM at 3.0 kV. Particles were immersed in PBS at 1 mg/mL concentration for DLS measurements. Measurements were taken with 10 acquisitions with 5 seconds for each acquisition.

in-vitro Release

A graham vials containing 20 mg of β-glucan nanoparticles were treated with 0.5 mL of pH 7.45 PBS buffer. The vials were gently stirred at 90 rpm at 37 ºC. The particle solution was collected by centrifuging the vials at 4000 rpm for five minutes and stored at -20 ºC. The β-glucan concentration was determined by using a total carbohydrate assay kit (Millipore Sigma).

BMDM harvest and culture

Bone marrow derived macrophages (BMDMs) were harvested from the femurs of 6-week old C57BL/6 mice (Jackson Laboratory). BMDMs were cultured in primary medium: RPMI 1640 (Life Technologies), 10% heat inactivated fetal bovine serum (HIFBS) 2 mM L-glutamine (Life Technologies), antibiotic antimycotic (1×) (Life Technologies) and 10 % MCSF (mycoplasma free L929 supernatant) for 5 days at 37 ºC and 5% CO_2. The cells were then released with 5 mM EDTA in PBS, counted and plated at desired densities.

In-vitro training assays

BMDMs were plated at a density of 100,000 cells/well in flat bottom 96-well plates (Corning) at a final volume of 200 mL) and rested for a few hours to adhere at 37 ºC and 5% CO_2. After the cells were adherent, training material was added at desired concentration and incubated for 24 h. (Nanoparticle concentration used was 100 mg/mL unless otherwise stated) Then cells were washed and rested for 3 days. On day 4, BMDMs were washed again and primed with 25 ng/mL IFN-γ (BD Biosciences) for 24 hr. On day 5, a final wash was performed, and cells were stimulated with 10 ng/mL standard Escherichia coli LPS (serotype O55:B5; Invivogen). Cell supernatant was collected after 24 h to measure IL-6 and TNF-a levels using ELISA (BioLegend) according to manufacturer's instructions.

For inhibition studies, BMDMs were pre-incubated for 30 min with inhibitors before stimulating with training materials and were left in the media during the 24 h training period.[23] For epigenetic pathway analysis, cells were pre-treated with 500 μM 5′-deoxy-5′-(methylthio)adenosine (MTA), 6 μM pargyline and 50 μM (-)-epigallocatechin-3-gallate (EGCG) (all from Sigma Aldrich). For metabolic pathway analysis, cells were pre-treated with 100 nM rapamycin (Invivogen), 10 mM Wortmannin, 30 mM Metformin and 1 mM 2' deoxyglucose (all from Sigma). For testing different pathways contributing to endocytosis, cells were pre-treated with 5 mM Filipin (Sigma), 100 mM Dynasore (Abcam) and 3 mM chlorpromazine hydrochloride (Sigma).

To quantify uptake, β-glucan was labelled with fluorescein isothiocyanate (FITC) using a previously described protocol.[41, 40] BMDMs were treated with an equivalent amount of free FITC-labelled β-glucan or 100 mg/mL nanoparticles encapsulating FITC-labelled β-glucan for 24 h. Then, media was removed and cells were released by gentle scraping and the cells were analyzed by flow cytometry (NovoCyte Benchtop Flow Cytometer).

After *in vitro* training assay, the cells were incubated in 100 mL PBS and 10 mL of cell counting kit-8 (CCK-8) solution was added to each well and incubated at 37 ºC. Absorbance was measure at 540 nM using Multiskan FC plate reader (Thermo Scientific).

HEK mTLR4 cells were passaged and plated in a 96 well plate at 100,000 cells/well in 180 µL DMEM containing 10% HI-FBS and selective antibiotics. The cells were stimulated with the synthesized nanoparticles for 24 h at 37 °C and 5% CO_2. TLR4 binding was measured by a QUANTI-Blue (Invivogen) assay and the absorbance was measured at 620 nm using a Multiskan FC plate reader (Thermo Scientific).

In-vivo training assay

Mice were trained intra-peritoneally either once or twice on days -7 and/or day -4 with indicated amount of nanoparticles, equivalent amount of free β-glucan or 1 mg free β-glucan. Sterile PBS was always used as a control. After training, different set of mice were challenged intra-peritoneally with 5 mg LPS (serotype O55:B5; Invivogen) at desired time points and serum was collected after 1 h or 3 h. None of the mice received repeated LPS challenges. Serum cytokines were analyzed using Legendplex Mouse Inflammation Panel (BioLegend) according to the manufacturer's protocol. 2 h after LPS challenge, mice were euthanized and peritoneal cells were harvested by lavage. Cells were flow cytometry analysis was performed to determine the percentage of small peritoneal macrophages. All antibodies were purchased from BioLegend or BD Biosciences. Anti-mouse phycoerythrin (PE) CD11b, APC- MHC2, Pe/Cy7-F4/80, Brilliant violet 570- Ly6G, APC/fire 750-CD11c, Alexa fluor 700- Ly6C, APC- NK1, PE-cd115, PerCP/Cy5.5- cd19, Alexa flour 488- CD3, Brilliant violet 788- MHC2, Brilliant violet 711 CD8a, Brilliant violet 650- F4/80, BUV 395 CD45R/B220. In other experiments, spleens and peritoneal

exudate cells were isolated prior to LPS challenge. Spleens were homogenized, and cells were filtered through a 70 μm strainer. Red blood cells were lysed by incubating with ACK Lysing Buffer for 5 min at 25 °C. Cells were plated in petri dishes for 2 h and washed to remove non-adherent cells. Peritoneal cells were harvested by lavage according to previously described protocol. [40] Briefly, the skin was peeled off and clamped, followed by injection of 5 mL PBS containing 3% heat- inactivated fetal bovine serum (HIFBS) into the peritoneal cavity. The peritoneal content was then collected and centrifuged (400 g for 10 min). Peritoneal cells were plated in petri dishes for 2 h and washed to remove non-adherent cells. Peritoneal and splenic macrophages (0.1 million cells) were plated in a 96-well plate and allowed to adhere for 2 h before being challenged with LPS.

Training was administered on day 0 and day 4 with the desired material. After 28 days, mice were euthanized and cells were harvested by peritoneal lavage. The peritoneal macrophages were split for two sets of experiments. In one set, 100,000 cells were plated in 96 well flat bottom plates in a final volume of 200 mL. These cells were allowed to adhere for 3 h and then challenged with LPS (10 ng/mL). Supernatant was collected after 24 h and IL-6 levels were quantified. In a second set of experiments, 1 million peritoneal macrophages per group was adoptively transferred (ip) to naïve mice. After 24 h, these mice were challenged with LPS (5 mg/mouse) and serum cytokines were analyzed 3 h post challenge using Legendplex Mouse Inflammation Panel (BioLegend).

To determine the biodistribution, nanoparticles were synthesized using NIR-labelled PLGA (Poly(lactide-co-glycolide)-Flamma Fluor near-IR, Millipore Sigma). Fluorescence intensity was measured using Xenogen IVIS 200 Imaging System at F stop=2, 1 second Exposure, Ex= 745 nm, and Em= 800 nm.

Tumor Challenge

Mice were anesthetized and shaved of hair from their right-side using clippers. Following grooming, the mice were injected with 200,000 B16F10 melanoma cells or 1 million EG7OVA cells in 50 mL of PBS subcutaneously. For B16.F10 tumor model, mice were first trained with indicated materials and rested for three weeks. After three weeks, all the animals were challenged with B16.F10 tumor. For EG7.OVA tumor model, mice were trained first and were vaccinated with CpG (50 mg) and OVA (100 mg) a week later. Tumor cells were injected two weeks after vaccination. Tumor progression was monitored and measured with a caliper, recording the width, length and height of the tumor every other day throughout the experiment. Mice with tumor sizes exceeding 20 mm along any direction was sacrificed.

Statistical Analysis

Pre-processing was not performed for any of the data. All values are expressed as mean ± SEM. Sample size is as indicated in figure captions in all *in vivo* and *in vitro* experiments. Student's T-test was applied for comparing two groups. Data were analyzed by and one- or two-way analysis of variance (ANOVA) followed by Tukey's or Dunnett's multiple comparisons for comparison of multiple groups (indicated in the figure captions) using the GraphPad Prism 9 software. P values less than 0.05 were considered statistically significant. Significance $*P < 0.05$, $**P < 0.01$, $***P < 0.001$, $****P < 0.0001$, n.s., not significant.

4.6 References

1. T. Kawai, S. Akira, *Nature Immunology* **2010**, *11*, 373.
2. M. G. Netea, L. A. B. Joosten, E. Latz, K. H. G. Mills, G. Natoli, H. G. Stunnenberg, L. A. J. O'Neill, R. J. Xavier, *Science* **2016**, *352*, DOI 10.1126/science.aaf1098.

3. M. G. Netea, J. Domínguez-Andrés, L. B. Barreiro, T. Chavakis, M. Divangahi, E. Fuchs, L. A. B. Joosten, J. W. M. van der Meer, M. M. Mhlanga, W. J. M. Mulder, N. P. Riksen, A. Schlitzer, J. L. Schultze, C. Stabell Benn, J. C. Sun, R. J. Xavier, E. Latz, *Nature Reviews Immunology* **2020**, *20*, 375.

4. P. Aaby, A. Roth, H. Ravn, B. M. Napirna, A. Rodrigues, I. M. Lisse, L. Stensballe, B. R. Diness, K. R. Lausch, N. Lund, S. Biering-Sørensen, H. Whittle, C. S. Benn, *J Infect Dis* **2011**, *204*, 245.

5. N. Lund, A. Andersen, A. S. K. Hansen, F. S. Jepsen, A. Barbosa, S. Biering-Sørensen, A. Rodrigues, H. Ravn, P. Aaby, C. S. Benn, *Clin Infect Dis* **2015**, *61*, 1504.

6. P. Aaby, B. Samb, F. Simondon, A. M. Seck, K. Knudsen, H. Whittle, *BMJ* **1995**, *311*, 481.

7. J. C. Spencer, R. Ganguly, R. H. Waldman, *The Journal of Infectious Diseases* **1977**, *136*, 171.

8. E. Butkeviciute, C. E. Jones, S. G. Smith, *Future Microbiol* **2018**, *13*, 1193.

9. E. Ciarlo, T. Heinonen, C. Théroude, F. Asgari, D. Le Roy, M. G. Netea, T. Roger, *J Infect Dis* **2020**, *222*, 1869.

10. S. J. C. F. M. Moorlag, N. Khan, B. Novakovic, E. Kaufmann, T. Jansen, R. van Crevel, M. Divangahi, M. G. Netea, *Cell Reports* **2020**, *31*, 107634.

11. V. Vetvicka, J. Vetvickova, *Ann Transl Med* **2015**, *3*, DOI 10.3978/j.issn.2305-5839.2015.01.08.

12. D. Muramatsu, A. Iwai, S. Aoki, H. Uchiyama, K. Kawata, Y. Nakayama, Y. Nikawa, K. Kusano, M. Okabe, T. Miyazaki, *PLOS ONE* **2012**, *7*, e41399.

13. P. Garcia-Valtanen, R. M. Guzman-Genuino, D. L. Williams, J. D. Hayball, K. R. Diener, *Immunology & Cell Biology* **2017**, *95*, 601.

14. M. M. T. van Leent, A. E. Meerwaldt, A. Berchouchi, Y. C. Toner, M. E. Burnett, E. D. Klein, A. V. D. Verschuur, S. A. Nauta, J. Munitz, G. Prévot, E. M. van Leeuwen, F. Ordikhani, V. P. Mourits, C. Calcagno, P. M. Robson, G. Soultanidis, T. Reiner, R. R. M. Joosten, H. Friedrich, J. C. Madsen, E. Kluza, R. van der Meel, L. A. B. Joosten, M. G. Netea, J. Ochando, Z. A. Fayad, C. Pérez-Medina, W. J. M. Mulder, A. J. P. Teunissen, *Science Advances* **2021**, *7*, eabe7853.

15. M. S. Braza, M. M. T. van Leent, M. Lameijer, B. L. Sanchez-Gaytan, R. J. W. Arts, C. Pérez-Medina, P. Conde, M. R. Garcia, M. Gonzalez-Perez, M. Brahmachary, F. Fay, E. Kluza, S. Kossatz, R. J. Dress, F. Salem, A. Rialdi, T. Reiner, P. Boros, G. J. Strijkers, C. C. Calcagno, F. Ginhoux, I. Marazzi, E. Lutgens, G. A. F. Nicolaes, C. Weber, F. K.

Swirski, M. Nahrendorf, E. A. Fisher, R. Duivenvoorden, Z. A. Fayad, M. G. Netea, W. J. M. Mulder, J. Ochando, *Immunity* **2018**, *49*, 819.

16. B. Priem, M. M. T. van Leent, A. J. P. Teunissen, A. M. Sofias, V. P. Mourits, L. Willemsen, E. D. Klein, R. S. Oosterwijk, A. E. Meerwaldt, J. Munitz, G. Prévot, A. V. Verschuur, S. A. Nauta, E. M. van Leeuwen, E. L. Fisher, K. A. M. de Jong, Y. Zhao, Y. C. Toner, G. Soultanidis, C. Calcagno, P. H. H. Bomans, H. Friedrich, N. Sommerdijk, T. Reiner, R. Duivenvoorden, E. Zupančič, J. S. D. Martino, E. Kluza, M. Rashidian, H. L. Ploegh, R. M. Dijkhuizen, S. Hak, C. Pérez-Medina, J. J. Bravo-Cordero, M. P. J. de Winther, L. A. B. Joosten, A. van Elsas, Z. A. Fayad, A. Rialdi, D. Torre, E. Guccione, J. Ochando, M. G. Netea, A. W. Griffioen, W. J. M. Mulder, *Cell* **2020**, *183*, 786.

17. W. J. M. Mulder, J. Ochando, L. A. B. Joosten, Z. A. Fayad, M. G. Netea, *Nat Rev Drug Discov* **2019**, *18*, 553.

18. D. J. Hines, D. L. Kaplan, *Crit Rev Ther Drug Carrier Syst* **2013**, *30*, 257.

19. N. Kamaly, B. Yameen, J. Wu, O. C. Farokhzad, *Chem Rev* **2016**, *116*, 2602.

20. X. Lu, L. Miao, W. Gao, Z. Chen, K. J. McHugh, Y. Sun, Z. Tochka, S. Tomasic, K. Sadtler, A. Hyacinthe, Y. Huang, T. Graf, Q. Hu, M. Sarmadi, R. Langer, D. G. Anderson, A. Jaklenec, *Science Translational Medicine* **2020**, *12*, DOI 10.1126/scitranslmed.aaz6606.

21. B. A. Bailey, L. J. Ochyl, S. P. Schwendeman, J. J. Moon, *Advanced Healthcare Materials* **2017**, *6*, 1601418.

22. T. Nakagawa, Q. Zhu, S. Tamrakar, Y. Amen, Y. Mori, H. Suhara, S. Kaneko, H. Kawashima, K. Okuzono, Y. Inoue, K. Ohnuki, K. Shimizu, *J Nat Med* **2018**, *72*, 734.

23. P. Saz-Leal, C. del Fresno, P. Brandi, S. Martínez-Cano, O. M. Dungan, J. D. Chisholm, W. G. Kerr, D. Sancho, *Cell Reports* **2018**, *25*, 1118.

24. S. Fanucchi, J. Domínguez-Andrés, L. A. B. Joosten, M. G. Netea, M. M. Mhlanga, *Immunity* **2021**, *54*, 32.

25. J. Quintin, S. Saeed, J. H. A. Martens, E. J. Giamarellos-Bourboulis, D. C. Ifrim, C. Logie, L. Jacobs, T. Jansen, B.-J. Kullberg, C. Wijmenga, L. A. B. Joosten, R. J. Xavier, J. W. M. van der Meer, H. G. Stunnenberg, M. G. Netea, *Cell Host Microbe* **2012**, *12*, DOI 10.1016/j.chom.2012.06.006.

26. R. J. W. Arts, L. A. B. Joosten, M. G. Netea, *Seminars in Immunology* **2016**, *28*, 425.

27. S.-C. Cheng, J. Quintin, R. A. Cramer, K. M. Shepardson, S. Saeed, V. Kumar, E. J. Giamarellos-Bourboulis, J. H. A. Martens, N. A. Rao, A. Aghajanirefah, G. R. Manjeri, Y. Li, D. C. Ifrim, R. J. W. Arts, B. M. J. W. van der Meer, P. M. T. Deen, C. Logie, L. A. O'Neill, P. Willems, F. L. van de Veerdonk, J. W. M. van der Meer, A. Ng, L. A. B.

Joosten, C. Wijmenga, H. G. Stunnenberg, R. J. Xavier, M. G. Netea, *Science* **2014**, *345*, 1250684.

28. P. Guo, D. Liu, K. Subramanyam, B. Wang, J. Yang, J. Huang, D. T. Auguste, M. A. Moses, *Nature Communications* **2018**, *9*, 130.

29. S. M. Quinn, K. Cunningham, M. Raverdeau, R. J. Walsh, L. Curham, A. Malara, K. H. G. Mills, *Front. Immunol.* **2019**, *10*, DOI 10.3389/fimmu.2019.01109.

30. M. Jeljeli, L. G. C. Riccio, L. Doridot, C. Chêne, C. Nicco, S. Chouzenoux, Q. Deletang, Y. Allanore, N. Kavian, F. Batteux, *Nature Communications* **2019**, *10*, 5670.

31. I. Mitroulis, K. Ruppova, B. Wang, L.-S. Chen, M. Grzybek, T. Grinenko, A. Eugster, M. Troullinaki, A. Palladini, I. Kourtzelis, A. Chatzigeorgiou, A. Schlitzer, M. Beyer, L. A. B. Joosten, B. Isermann, M. Lesche, A. Petzold, K. Simons, I. Henry, A. Dahl, J. L. Schultze, B. Wielockx, N. Zamboni, P. Mirtschink, Ü. Coskun, G. Hajishengallis, M. G. Netea, T. Chavakis, *Cell* **2018**, *172*, 147.

32. J. Chen, M. Qiu, Z. Ye, T. Nyalile, Y. Li, Z. Glass, X. Zhao, L. Yang, J. Chen, Q. Xu, *Science Advances* **2021**, *7*, eabf1244.

33. P. de Graaff, C. Berrevoets, C. Rösch, H. A. Schols, K. Verhoef, H. J. Wichers, R. Debets, C. Govers, *Cancer Immunol Immunother* **2020**, DOI 10.1007/s00262-020-02707-4.

34. M. Liu, F. Luo, C. Ding, S. Albeituni, X. Hu, Y. Ma, Y. Cai, L. McNally, M. A. Sanders, D. Jain, G. Kloecker, M. Bousamra, H. Zhang, R. M. Higashi, A. N. Lane, T. W.-M. Fan, J. Yan, *J Immunol* **2015**, *195*, 5055.

35. L. Kalafati, I. Kourtzelis, J. Schulte-Schrepping, X. Li, A. Hatzioannou, T. Grinenko, E. Hagag, A. Sinha, C. Has, S. Dietz, A. M. de Jesus Domingues, M. Nati, S. Sormendi, A. Neuwirth, A. Chatzigeorgiou, A. Ziogas, M. Lesche, A. Dahl, I. Henry, P. Subramanian, B. Wielockx, P. Murray, P. Mirtschink, K.-J. Chung, J. L. Schultze, M. G. Netea, G. Hajishengallis, P. Verginis, I. Mitroulis, T. Chavakis, *Cell* **2020**, *183*, 771.

36. Y. Ning, D. Xu, X. Zhang, Y. Bai, J. Ding, T. Feng, S. Wang, N. Xu, K. Qian, Y. Wang, C. Qi, *Int J Cancer* **2016**, *138*, 2713.

37. R. A. Maldonado, R. A. LaMothe, J. D. Ferrari, A.-H. Zhang, R. J. Rossi, P. N. Kolte, A. P. Griset, C. O'Neil, D. H. Altreuter, E. Browning, L. Johnston, O. C. Farokhzad, R. Langer, D. W. Scott, U. H. von Andrian, T. K. Kishimoto, *PNAS* **2015**, *112*, E156.

38. D. Essa, P. P. D. Kondiah, Y. E. Choonara, V. Pillay, *Frontiers in Bioengineering and Biotechnology* **2020**, *8*.

39. P. W. Lee, J. K. Pokorski, *Wiley Interdiscip Rev Nanomed Nanobiotechnol* **2018**, *10*, e1516.

40. C. Thomas, A. Rawat, L. Hope-Weeks, F. Ahsan, *Mol. Pharmaceutics* **2011**, *8*, 405.

41. M. Yu, Z. Chen, W. Guo, J. Wang, Y. Feng, X. Kong, Z. Hong, *Int J Nanomedicine* **2015**, *10*, 1743.

42. W.-J. Bai, C.-G. Li, C.-C. Zhang, L.-H. Xu, Q.-Z. Zeng, B. Hu, Z. Hong, X.-H. He, D.-Y. Ouyang, *Front. Immunol.* **2018**, *8*.

43. S. Walachowski, G. Tabouret, M. Fabre, G. Foucras, *Front Immunol* **2017**, *8*, 1089.

44. A. E. Geller, R. Shrestha, M. R. Woeste, H. Guo, X. Hu, C. Ding, K. Andreeva, J. H. Chariker, M. Zhou, D. Tieri, C. T. Watson, R. A. Mitchell, H. Zhang, Y. Li, R. C. G. Martin II, E. C. Rouchka, J. Yan, *Nat Commun* **2022**, *13*, 759

45. M. F. Frasco, G. M. Almeida, F. Santos-Silva, M. do C. Pereira, M. A. N. Coelho, *Journal of Biomedical Materials Research Part A* **2015**, *103*, 1476.

5. Single Dose Vaccine Platform via Delayed Release from Multi-Layer Polymeric Particles

5.1 Summary

Most current vaccines require a primer/boost system to achieve high efficacy. However, achieving high boost uptake has persisted in current pandemic for those with limited resources. Creating technologies which allow single-dose vaccination eliminates the need for booster injections and helps increase the implementation of vaccines. Previous methods of single-dose vaccination have yet to achieve a separated, delayed release of immunological stimuli, which is the hallmark of the boost regimen. To that end, we developed a vaccine particle platform that uses a double polymer coating to delay the release of the core particles' payload to the immune system for 42 days. The double-coated particles successfully acted as a boost in a model vaccine showing promise for use with other subunit vaccines.

5.2 Introduction

Vaccines have revolutionized medicine and contributed to eliminating various diseases such as polio and smallpox within the United States[1]. Part of increasing vaccine's efficiency is reducing the number of booster shots needed. Booster injections help develop or sustain immunity via additional exposure to the vaccine. These shots are taken months or years after receiving the primary dosage.[2] The time commitment is difficult for those with limited resources as repeated visits for injections may not be feasible. Creating a single administration vaccine containing multiple, time-delayed doses eliminates the need for separate booster injections and may help increase the implementation of vaccines.

Few general platforms for single administration vaccines have been developed.[3] The World Health Organization spearheaded a campaign to develop a single-dose tetanus vaccine in the early 1990s. However, their efforts proved expensive due to the implementation of clean-room good manufacturing practice (GMP).[4] The Jaklene group at MIT has published two different methods for single-dose vaccinations that use 3D printing and a second formulation that timed PLGA's burst release for primary and secondary doses. In each case, the main challenge was delaying or validating the delay of the onset immune responses from each boost despite the delayed release of the cargo in vitro. [5,6] While high antibody levels are important in vaccination, a single-dose vaccination that replicates the powerful effects of a boosting regimen must also involve the additive effect of multiple doses staggered in time. We sought to address this challenge through a combination of materials approaches wherein multiple-coatings could temporarily delay a second dose to ensure nearly absolute isolation immune stimulation.

Rather than creating pulsatile release based on the molecular weight of our core polycaprolactone (PCL) particle, we developed a multi-layer coating procedure that utilized the degradation characteristics of multiple mismatched polymers. The coating delayed access to the contents of the core particles – thereby delaying the activation of a second response. A mixture of these uncoated and coated particles in a vaccine might mimic a primary and booster dose. The coating procedure proposed in our study is a simple two-pot synthesis for creating double-coated microparticles. The biocompatibility, degradation rate, and polymerization conditions were key considerations in designing a multiple layer coating. PCL has a melting temperature (T_m) of around 56-65 ^oC. We selected polymerization reactions that did not exceed the T_m to maintain the PCL particle morphology throughout the process.[9]

We selected siloxane as the first layer owing to its biocompatibility and functionality. Our lab has previously reported a polymerization technique for microspheres at room temperature using TEOS-mercaptosilane. [10] We determined that the TEOS coating on its own only delayed the release by 15 days (Figure 3a). To ensure a longer delay and better fidelity, we decided to add a second layer. To achieve this second layer, we polymerized L-lactide to form a layer of poly(lactide) coating. The thiols from the siloxane polymer coating were used as initiators for the ring opening polymerization of L-lactide. Like the primary coating, the secondary coating polymerizes at room temperature and uses a bifunctional thiourea organic catalyst.[11] The secondary coating further hinders the degradation of the core PCL diol particles (Figure 3A,3B.)

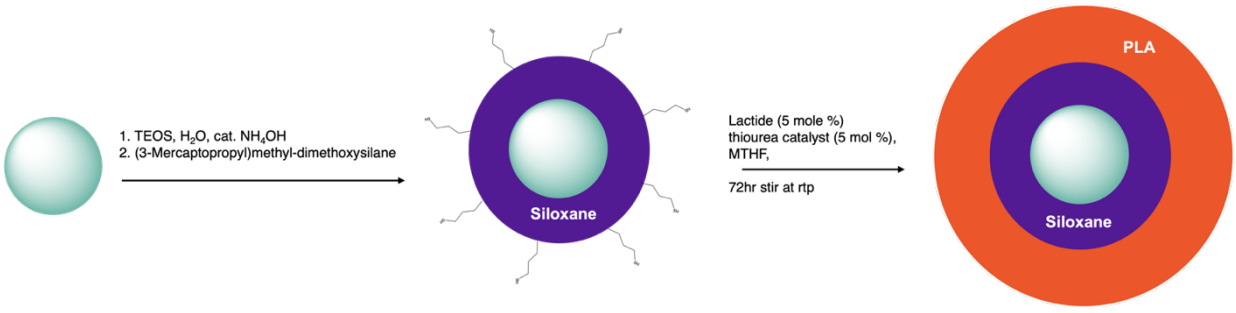

Figure 5.1 Multiple layer coating procedure of PCL microparticles. First, microparticles are coated with TEOS-mercaptosilane and then poly(lactide).

In this study, we present evidence that a double-coated particle delays release compared to both the core particle and single-coated both in vitro and in vivo. The promising delayed release profile led us to test these particles in a subunit vaccine model using the antigen OVA and adjuvant, CpG-1826. The *in vivo* experiment, the coated particles, when used on their own, resulted in a delayed

peak antibody response compared to the core. When combined, the two resulted in high antibody titers throughout the experiment.

5.3 Results and Discussion

To create the complex multilayer system, we had to establish a core particle. This particle required tolerance and compatibility with multiple coating chemistry as well as being bio-compatible itself. To achieve all these criteria, we selected PCL as the core layer owing to its proven biocompatibility and its amenability to multiple processing conditions. Microparticles were created using the double emulsion technique. The precipitated microparticles were collected and lyophilized overnight before characterization. Analysis by SEM confirmed that the particles possess a sphere-like morphology with an average diameter of 6.60 μm ± 2.2 (**Figure 5.1A**).

To add the second polymer layer, we performed a siloxane coating. Particles were suspended in a Pickering emulsion. Afterward, TEOS, aqueous ammonia, and 3-mercaptosilane were added, and the reaction was left stirring for 4 hours. Subsequently, the particles were centrifuged and collected. The remaining were dried under vacuum. SEM analysis of the PCL particles before and after the TEOS coating revealed a clear difference in the surface characteristics of the particles (**Figure 5.1A and 5.1B**) as well as a slight, non-significant change in the measured diameter of 7.00 μm ± 1.4 **(Appendix C1**). This small change indicates that the TEOS-mercaptosilane coating is exceptionally thin. Additionally, SEM-EDS analysis indicated silicone and sulfur were present only on the surface of the TEOS-mercaptosilane treated particles (hereafter referred to as PS particles) (**Figure 5.1D-F**).

The TEOS-mercaptosilane coated (PS) particles were subjected to further coating with poly(lactide). The particles were left stirring for 72 hours with the thiourea catalyst and L-lactide, resulting in a three-layer particle containing a PCL core, a siloxane middle, and a polylactide exterior. We will refer to these as PSL particles for abbreviation through the remainder of the manuscript. SEM images showed that the microparticles surface morphology significantly changed and FTIR spectrum showed an enhanced carbonyl stretch (~1720 cm^{-1}) compared to PS (**Figure C1**) Given the complex nature of these multi-layer particles, we sought to determine how the secondary coating might impact the immunogenicity of particles. We performed a RAW blue assay with the core, primary, and secondary coated particles. The PSL particles had minimal activation of NF-κb, similar to the siloxane-coated particles previously reported (**Figure 5.1G**).[10]

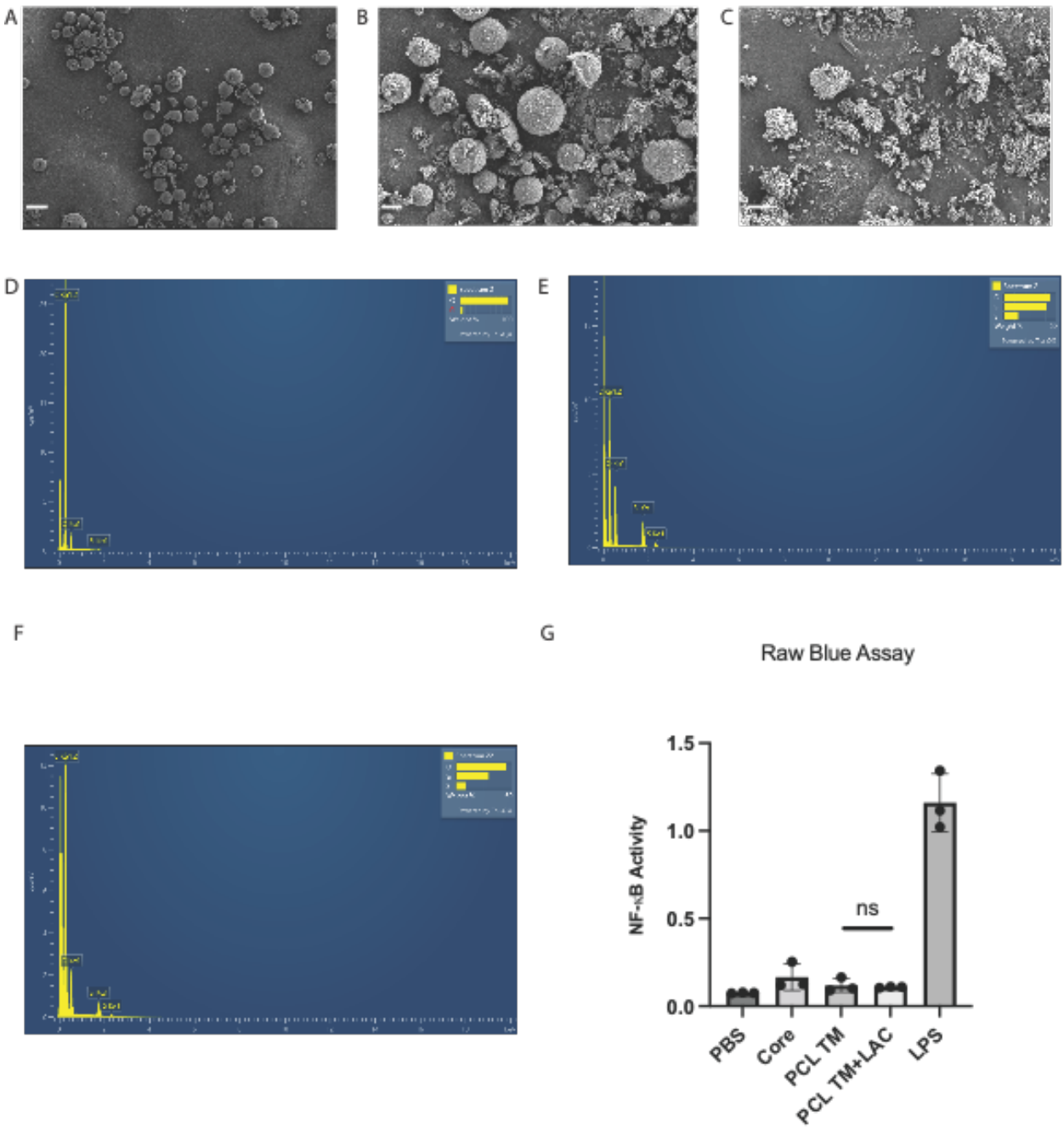

Figure 5.2 Characterization of particles. SEM image of A) PCL core microparticles B) TEOS-mercaptosilane coated microparticles, C) TEOS-mercaptosilane and PLA coated microparticles. SEM-EDS spectrum of a microparticle from D) PCL core microparticles E) TEOS-mercaptosilane coated microparticles F) TEOS-mercaptosilane and PLA coated microparticles. G) Raw Blue Assay of particles showing no significant difference in NF-κB activity between single and double coated particles. N=3.

To understand the degree to which these polymers delay the release of the payload from PCL microparticles, an in vitro release study was performed to measure the release of OVA to compare to previous control and delayed release systems. A dram vial containing 2 mg of the desired polymer-coated OVA microparticles was treated with 0.5 mL of pH 7.45 PBS buffer. The vials were gently stirred at 37 ^{o}C in an oil bath. The particle solution was collected by centrifuging and storing the PBS solution at -20 ^{o}C for later analysis. The OVA concentration was determined via Qubit Protein assay. The *in vitro* release data showed that the core particles immediately started to degrade and release OVA continuously. The PS particles showed a minor burst release (5%) and began to release OVA starting on day 15.

In contrast, the PSL particles did not start to significantly release OVA until day 55. To date, we believe this may represent the longest in vitro delayed release recorded. We attribute the minor burst release observed in the primary and secondary coated particles to a small number of improperly or poorly coated microparticles undergoing a secondary degradation pathway. However, given that it was only 5% and occurred almost instantaneously, we washed the particles an additional time before injection. (**Figure 5.3A**).

With promising *in vitro* data, we next moved to test the release of the particles using *in vivo* biofluorescence imaging. A series of identical core particles were encapsulated with OVA labeled Texas-Red [ThermoFisher] at a similar concentration. To determine the release rate, we tracked the depletion of the labeled OVA as the measure of OVA release from our particles via IVIS. The IVIS measurements correlated closely to the trends observed *in vitro*. The PCL particles showed immediate decay in the fluorescent signal. In contrast, the PSL, double coated particles had an increase in fluorescence before reaching a peak on day 42 and then showing a

decrease in fluorescence. We attribute the modest increase in the case of PSL to adjustments in the particle placement and location within the animal over that long time frame. In conclusion, the IVIS measurements provided further evidence that the coating delayed the release of OVA content in vivo and in vitro (**Figure 5.3B-C**).

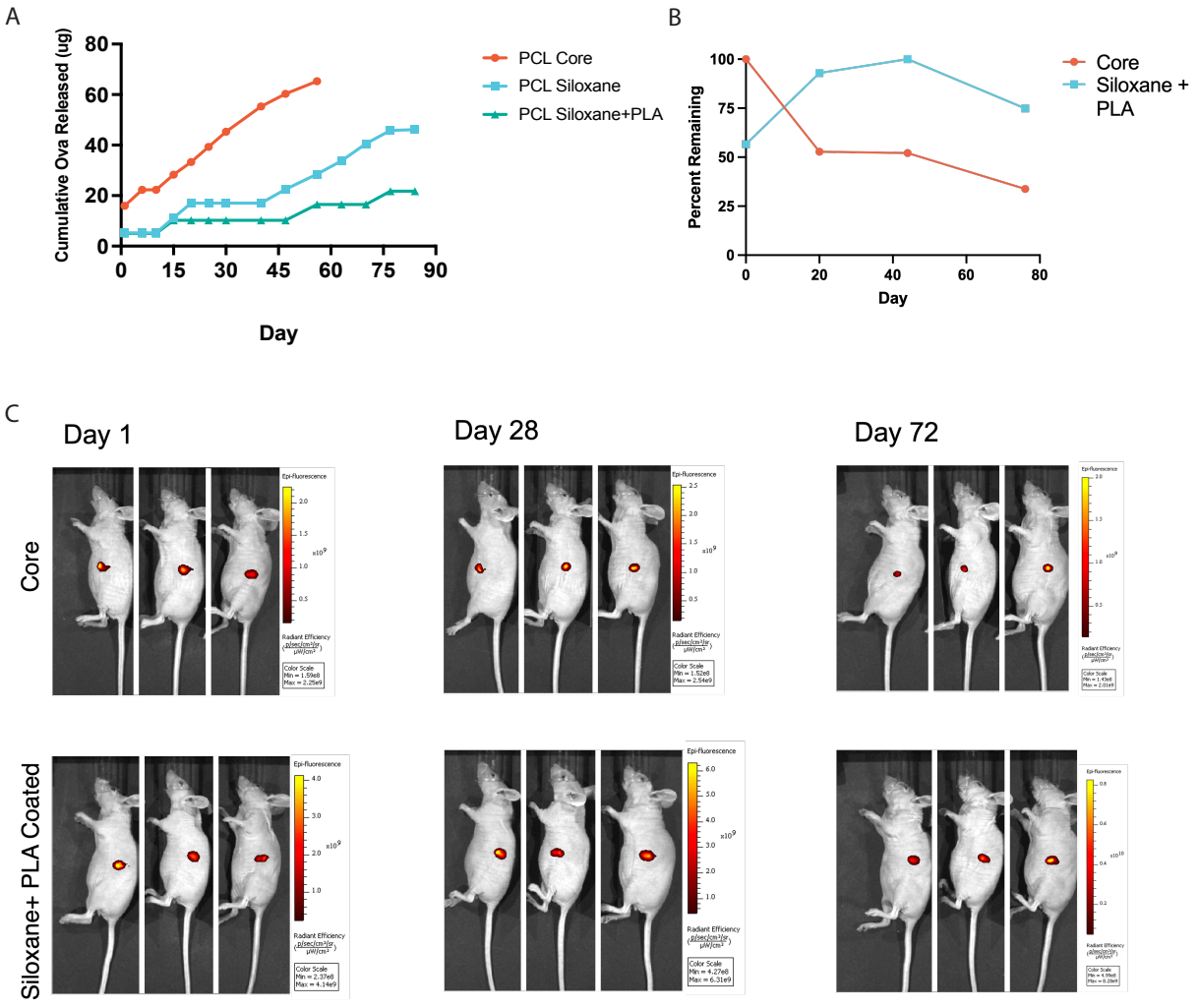

Figure 5.3 Release kinetics of Core and Coated Particles A) in vitro release of core and coated particles. B) in vivo release of core and coated particles. C) Biofluorescence images of the core and coated particles over time.

With these two pieces of evidence in hand, as they were the established measures of the field, we tested the particles in a single administration vaccine with C57BL/6 mice. Five groups were tested: PBS, core PCL particle, PS particle with no payload, core and PSL particles, and unencapsulated control. The core and coated particles were loaded with an adjuvant and antigen, CpG 1826, and OVA. The unencapsulated control was dosed matching the concentration of the core, and coated particles were injected on day 0 and day 42. Unloaded PCL particles were added to the coated particle group to impact the degradation of the coated microparticles. We were curious to see how our single-dose vaccine affected antibody levels and T cell activity over time. As a result, serum was taken weekly and on day 49, draining lymph nodes were harvested and stained with MHCI and MHCII tetramers. The antibody levels for the core particles had high titers remained at day 14 and persisted throughout our 4-month study.

In contrast, the coated particles had peak antibody levels at a later point, day 35, and persisted at high levels throughout the experiment. Combined, the core and the coated particles exhibited a synergism effect, having high titers throughout the experiment starting on day 14 (**Figure 5.4G**). Unfortunately, there was no significant difference for both MHC I and MHC II tetramers between groups (**Figure 5.4B-C**)**.**

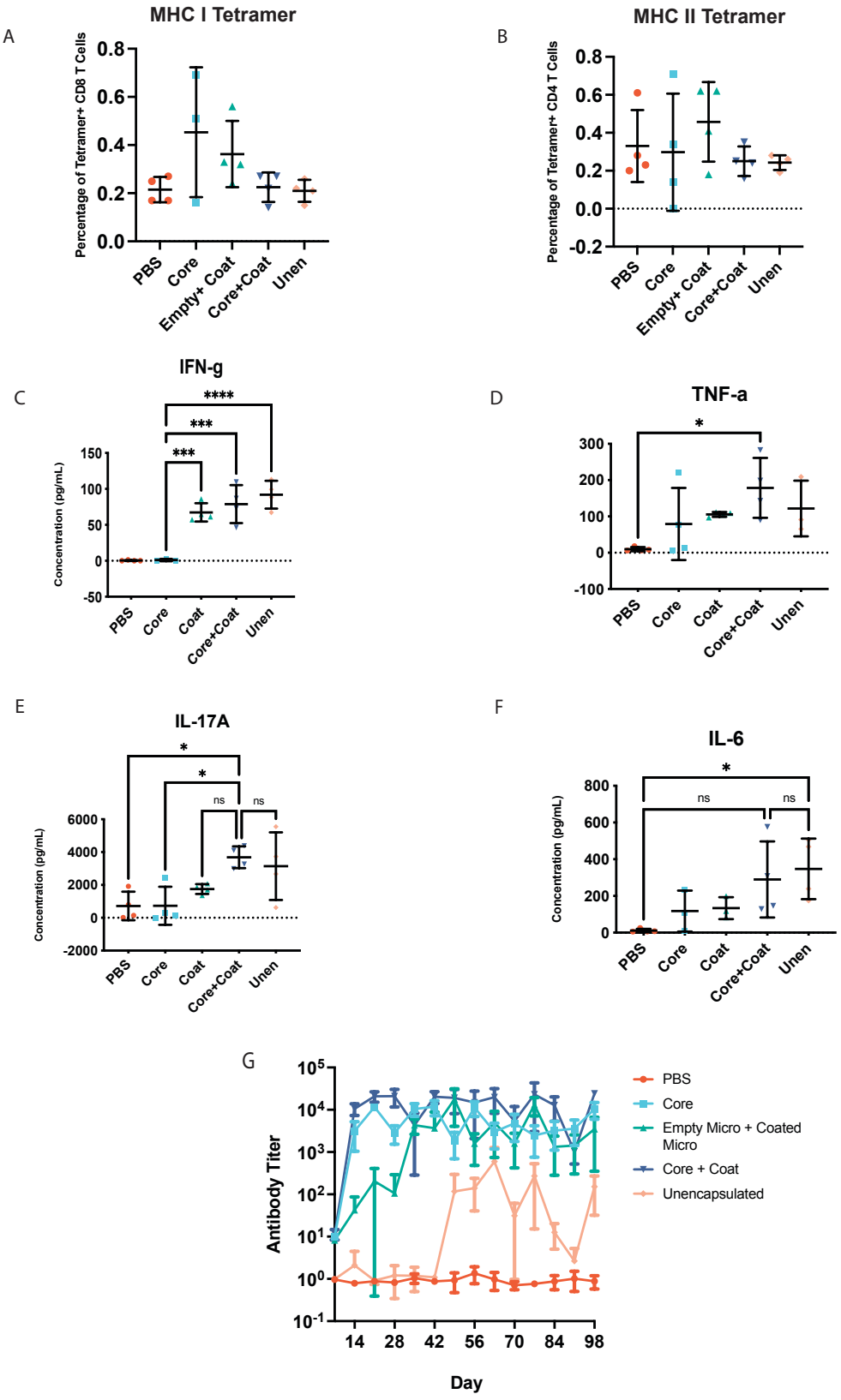

Figure 5.4 *in vivo* vaccination experiment with single dose vaccine

Figure 5.4 continued
A) $OVA^{257-264}$MHC I B) $OVA^{323-339}$MHC II tetramers staining performed on lymphocytes harvested on day 21. N=4. C) IFN-g D) TNF-a E) IL-17A F)IL-6 cytokine levels measured from supernatant taken from OVA simulated lymphocytes after 48 hours. N=4 C) Anti-ovalbumin IgG1 antibody measured weekly from serum over 98 days. N=4. One-Way-Anova performed with Tukey's test. *$P < 0.05$, **$P < 0.01$, and ***$P < 0.001$. n.s., not significant.

However, cytokines secreted by these T cells were measured and revealed that the boost vaccination significantly impacted the core particles. Core+ Coated Particles possessed elevated IFN-g and IL-17A levels compared to the core particles. The Core+ Coated particles also possessed elevated levels of TNF-a and IL-6. But the increased TNF-a and IL-6 levels were not significantly hirer than the core particles (**Figure 5.4 C-F**). The boosted particles provided an elevated TH1/TH2/TH17 profile for the vaccination. This change allows the potential for different adjuvants or immunopotentiators to be incorporated into the coated particles to provide the desired immune response in a single administration vaccine.

5.4 Conclusion

Multiple layer coating of polycaprolactone particles can be accomplished using TEOS-mercaptosilane and PLA. The double layer coating maintains biocompatibility levels similar to the PCL core particles and successfully delays the core particles' release. The delayed release was confirmed in both *in vitro* and *in vivo* models. In a murine animal experiment, the coated particles displayed a delayed peak antibody titer response. Combined with the core particles, the coated particles can act as a boost for an overall single administration vaccine. In our murine experiment, the core and coated particles had high antibody titers that persisted throughout the experiment. Although we report the multiple layer coating with a model antigen, OVA, and

adjuvant, CpG, there is potential for the platform to be applied to various other subunit vaccines that can be encapsulated. Therefore, there is potential for this approach to assist in creating single administration vaccines that solve vaccine compliance issues.

5.5 Materials and Methods

Polycaprolactone Microparticle Synthesis

The payload was added in 300 μL to 3 mL of 100 mg/mL of PCL Diol in methylene chloride. The mixture was ultrasonicated at 40% amplitude for 3 minutes (30 seconds stirring following 30 seconds of rest). After ultrasonification, a determined amount of 5% (w/v) PVA solution was added to the primary w/o emulsion and vortexed for 30 seconds to produce the w/o/w double emulsion. The w/o/w emulsion was poured into 200 mL of chilled 1% (w/v) PVA and stirred at room temperature for 6 hours. The microspheres were either centrifuged and the pellet were washed three times with ultrapure deionized water and then lyophilized

Siloxane Coating

The emulsion was formed by sonicating cyclohexane (22.5 mL), 1-hexanol (5.4 mL), DI water (1 mL), and Triton X-114 (5.4 mL) for 20 minutes. PCL microparticles (100 mg) were added to the suspension and sonicated for an additional 40 minutes. TEOS (200 uL) was added dropwise, and 14 M ammonia hydroxide (600 uL) while being stirred at 1000 rpm for 30 minutes. Afterward 3-mercaptosilane (100 uL) was added dropwise, and the reaction was left stirring for 4 hours. The reaction was centrifuged at 4000 rpm for 10 minutes. The supernatant was removed, and pellet was washed three times with ethanol before being dried in vacuo.

Poly(lactide) Coating

TEOS-mercaptosilane particles (50 mg) were combined with L-lactide (5 mol %), 1-[3,5-bis(trifluoromethyl)phenyl]-3-[(1R,2R)-(-)-2-(dimethylamino)cyclohexyl]thiourea (5 mol%) and in 2-methyl tetrahydrofuran (2.5 mL). The reaction was left stirring for 72 hours. Afterward the reaction was quenched with benzoic acid (5mg) and crashed out in iced cold methanol. The reaction was then spun down, the supernatant was removed, and the pellet was dried in vacuo.

SEM and SEM-EDS

Microparticles were sputter coated with 12 nm of Pt/Pd using Sputter Coater - Cressington 208HR. SEM images were taken with Carl Zeiss Merlin SEM at 5.0 kV. SEM-EDS images were prepared by sputtering the sample with 8 nm of Carbon using a Leica EM Ace600 and imaged with Carl Zeiss Merlin SEM.

Raw Blue Assay

RAW-Blue™ NF-κB cells (Invivogen) were passaged and plated in a 96 well flat bottom plate at 100k cells/ well in 180 µL DMEM with 10% HIFBS. OVA-loaded particles were added at 100 ug/mL, and the final volume of media in the wells reached 200uL. The plate was incubated overnight at 37° C at 5% CO_2. The following day, 20 µL of supernatant was added to 180 µL of Qaunti- Blue (Invivogen) in a 96 well plate. The plate was incubated for two hours before reading on a spectrophotometer at 620 nm.

In Vitro Release Measurements

Gram vials containing 2 mg of OVA-loaded particles were treated with 0.5 mL of pH 7.45 PBS. The vials were gently stirred at 200 rpm at 37 °C in an oil bath. The particle solution was collected by centrifuging the vials at 4000 rpm for ten minutes and stored at -20 °C. The ova concentration was determined by using a Qubit Protein Assay.

Loading Analysis

Loading analysis was performed in triplicate using a previously reported extraction method[12]. CpG and immune potentiators concentrations were measured on reverse phase high-performance liquid chromatography (HPLC). Protein levels were calculated with Qubit Fluorometer.

Biofluorescence Imaging

Particles containing Texas OVA Red were imaged periodically using Xenogen IVIS 200 Imaging System. Fluorescence intensity was measured at F stop=2, 1 second Exposure, Ex= 570 nm, and Em= 620 nm.

Animal Experiment

8-10 week old C57BL/6 mice were anesthetized and injected subcutaneously with the respective particle vaccine group (n=12). Serum from the submandibular vein was collected weekly in rotation between cages to allow two-week recovery.

T cell Staining and Cytokine Secretion Analysis

Murine lymphocytes were harvested on day 21. $OVA_{323-339}$ and $OVA_{257-264}$ Tetramer staining (MBL Tetramer) was conducted on 1 million lymphocytes and processed using flow cytometry. From each sample, one million lymphocytes were plated on a 96-well plate and treated with ovalbumin. The cells were allowed to rest for 48 hours in a cell incubator at 37 ^{o}C and 5% CO_2. The supernatant was collected and cytokines were analyzed via LegendPlex.

Antibody Titer

96 well plate was treated with 100 µL of 100 µg/mL of OVA plated in PBS overnight. The following day the plate was washed twice with PBST, and 250 µL of blocking buffer was added

to the wells. The plate was left at room temperature for two hours and washed twice. Diluted Serum has added the wells and incubated for 2 hours at 37 C. The plate was washed three times before (1:1000) diluted monoclonal IgG antibody was added. The plate was incubated for 1 hour at 37 C and then washed three times. 100 μL of TMBD (Thermofisher) for 15 minutes. The reaction was stopped with 2M H2SO4 (Thermofisher), and the plate was read on a spectrophotometer at 450 nm.

5.6 References

1. Greenwood, B. The contribution of vaccination to global health: past, present and future. *Phil. Trans. R. Soc. B* **369**, 20130433 (2014).

2. Slifka, M. K. & Amanna, I. How advances in immunology provide insight into improving vaccine efficacy. *Vaccine* **32**, 2948–2957 (2014).

3. Jain, D., Raturi, R., Jain, V., Bansal, P. & Singh, R. Recent technologies in pulsatile drug delivery systems. *Biomatter* **1**, 57–65 (2011).

4. Johansen, P., Gómez, J. M. M. & Gander, B. Development of synthetic biodegradable microparticulate vaccines: a roller coaster story. *Expert Review of Vaccines* **6**, 471–474 (2007).

5. McHugh, K. J. *et al.* Fabrication of fillable microparticles and other complex 3D microstructures. *Science* **357**, 1138–1142 (2017).

6. Tzeng, S. Y. *et al.* Stabilized single-injection inactivated polio vaccine elicits a strong neutralizing immune response. *PNAS* **115**, E5269–E5278 (2018).

7. Ekanem, E. E., Nabavi, S. A., Vladisavljević, G. T. & Gu, S. Structured Biodegradable Polymeric Microparticles for Drug Delivery Produced Using Flow Focusing Glass Microfluidic Devices. *ACS Appl. Mater. Interfaces* **7**, 23132–23143 (2015).

8. Makadia, H. K. & Siegel, S. J. Poly Lactic-co-Glycolic Acid (PLGA) as Biodegradable Controlled Drug Delivery Carrier. *Polymers* **3**, 1377–1397 (2011).

9. Labet, M. & Thielemans, W. Synthesis of polycaprolactone: a review. *Chem. Soc. Rev.* **38**, 3484 (2009).

10. Moser, B. A., Steinhardt, R. C. & Esser-Kahn, A. P. Surface Coating of Nanoparticles Reduces Background Inflammatory Activity while Increasing Particle Uptake and Delivery. *ACS Biomater Sci Eng* **3**, 206–213 (2017).

11. Pratt, R. C. *et al.* Exploration, Optimization, and Application of Supramolecular Thiourea−Amine Catalysts for the Synthesis of Lactide (Co)polymers. *Macromolecules* **39**, 7863–7871 (2006).

12. Saez, V. *et al.* Extraction of PLGA-Microencapsulated Proteins Using a Two-Immiscible Liquid Phases System Containing Surfactants. *Pharm Res* **30**, 606–615 (2013).

Appendix A: Chapter 3

Table A1 Encapsulation efficiency of microparticle formulations

	CpG 1826 (%)	OVA(%)	SN50(%)	Honokiol(%)	Capsaicin(%)
CpG OVA Micro	71.2	75.9	-	-	-
CpG OVA SN50 Micro	58.6	81.2	32.8	-	-
CpG OVA Hon	31.2	65.8	-	0.07	-
CpG OVA Cap	40.7	86.8	-	-	59.6
Empty Microparticles	-	-	-	-	-

Table A2 Payload injections for SN50 *in vivo* experiment

Group	**N**	CpG (**µ**g)	OVA(**µ**g)	SN50 (**µ**g)	Particles (mg)	Empty Particles (mg)
PBS	10	-	-	-	-	-
CpG OVA Micro	10	6.50	52.0	-	1.00	0.13
Unencapsulated CpG OVA Micro	10	6.50	52.0	-	-	-
CpG OVA SN50 Micro	10	6.50	45.0	17.2	1.13	-
Unencapsulated CpG OVA SN50 Micro	10	6.50	45.0	17.2	-	-

Table A3 Payload injections for small molecule *in vivo* experiment

Group	**N**	CpG (**μ**g)	OVA(**μ**g)	Capsaicin (**μ**g)	Honokiol (**μ**g)	Particles (mg)	Empty Particles (mg)
PBS	10	-	-	-	-	-	-
CpG OVA Micro	10	5.70	41.9	-	-	-	-
CpG OVA Capsaicin Micro	10	5.70	61.2	22.3	-	1.00	0.120
Unencapsulated CpG OVA Capsaicin Micro	10	5.70	61.2	22.3	-	0.802	0.318
CpG OVA Honokiol Micro	10	5.70	64.6	-	.0367	1.12	-
Unencapsulated CpG OVA Honokiol Micro	10	5.70	64.6	-	.0367	-	-

Appendix B: Chapter 4

Figure B1: Dynamic light scattering (DLS) for synthesized nanoparticles

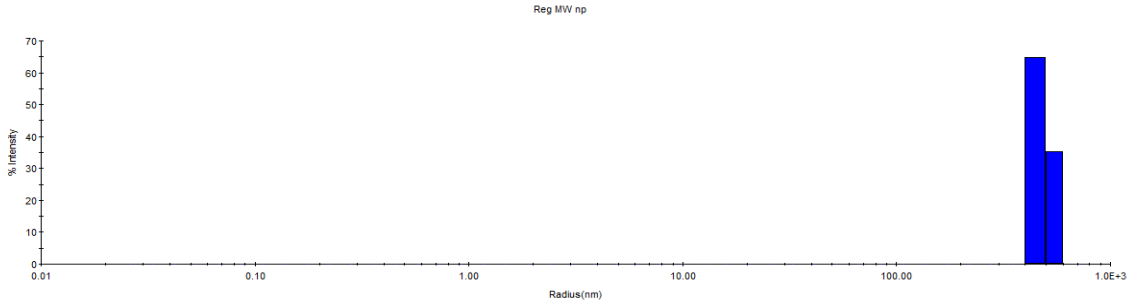

Figure B2: HEKmTLR4 assay for synthesized nanoparticles confirming no endotoxin.

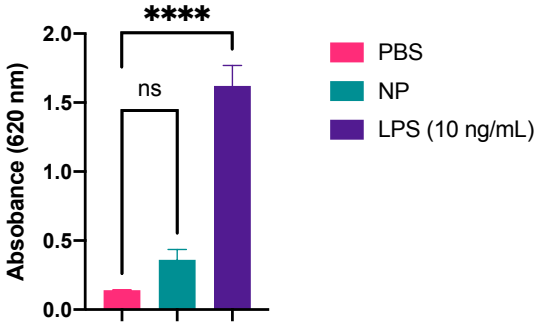

Figure B3: BMDMs were trained for 24 h with indicated materials (untrained or PBS (black bars), equivalent amount of free β-glucan (pink bars), empty or unencapsulated nanoparticles (green bars), mixture of empty nanoparticles and equivalent amount of free β-glucan (purple bars) or nanoparticles (lilac bars)) and rested for 5 days. On day 6, trained cells were challenged with 10 ng/mL of LPS and IL-6 and TNF-a levels from the supernatant were quantified using ELISA.

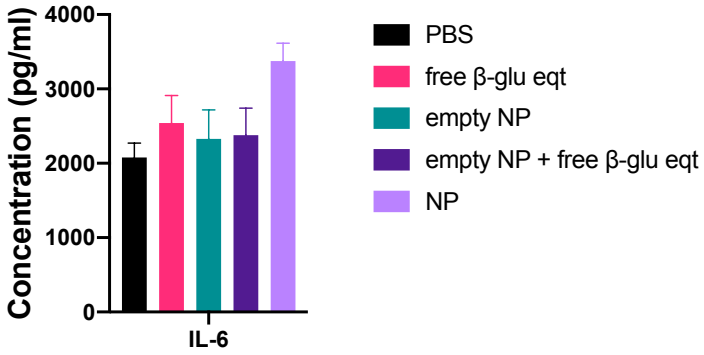

Figure B4: Uptake of free Fitc-labelled β-glucan and Fitc-labelled β-glucan encapsulated in nanoparticles by flow cytometry- representative plots shown. (n=3)

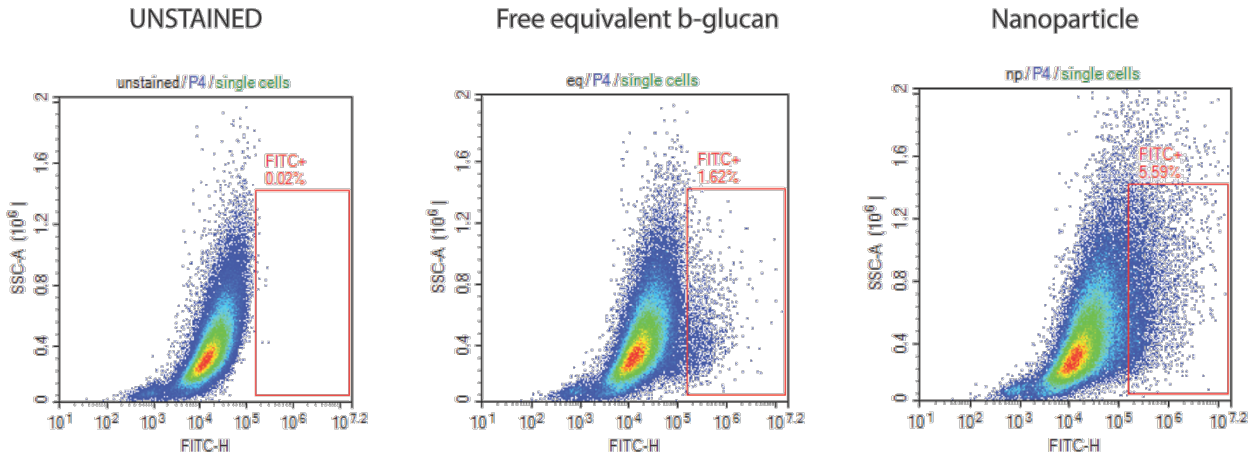

Figure B5: Day 35 serum cytokines for mice trained with indicated materials (PBS (black), equivalent amount of free β-glucan (pink), free 1 mg β-glucan (green) or nanoparticles (purple)) 1 h after challenge with LPS. No significant changes in cytokines were observed after LPS challenge 35 days post training.

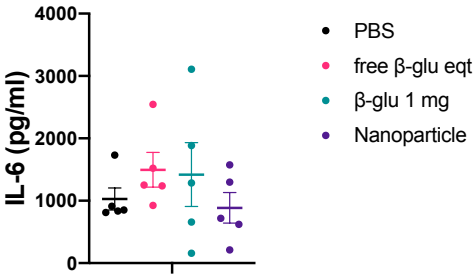

Figure B6: Ruling out innate immune priming for nanoparticles *in-vivo*: Mice that were trained with indicated materials (PBS (pink), equivalent amount of free β-glucan (green), free 1 mg β-glucan (purple) or nanoparticles (lilac)) and serum cytokines were analyzed prior to LPS challenge on day 27. No significant changes in cytokines were observed in any of the groups before LPS challenge.

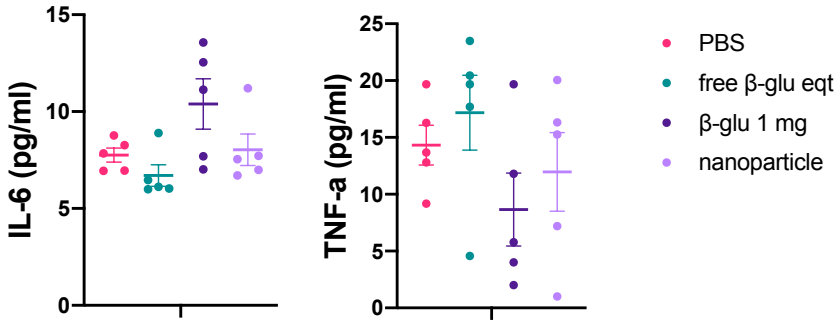

Figure B7: Mice were trained with either PBS (black) or NIR labelled PLGA encapsulating β-glucan (pink). *in-vivo* degradation profile was recorded until 21 days later. The mice were then challenged with LPS and serum cytokines were quantified 3 h later.

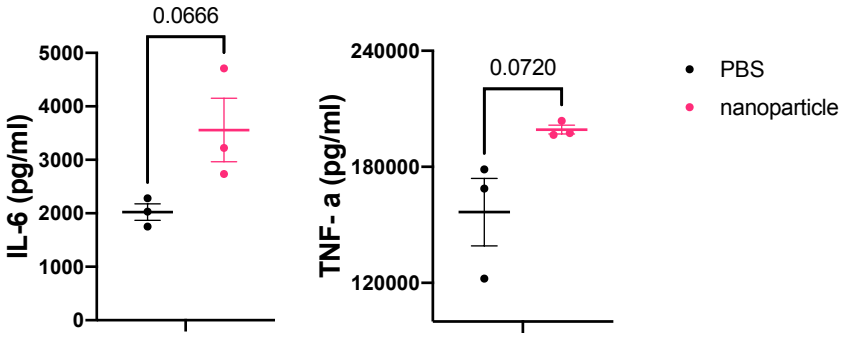

Figure B8: Gating strategy for small peritoneal macrophages (SPM) characterized as $CD11b^{+}MHC2^{high}$ $F4/80^{-1}$

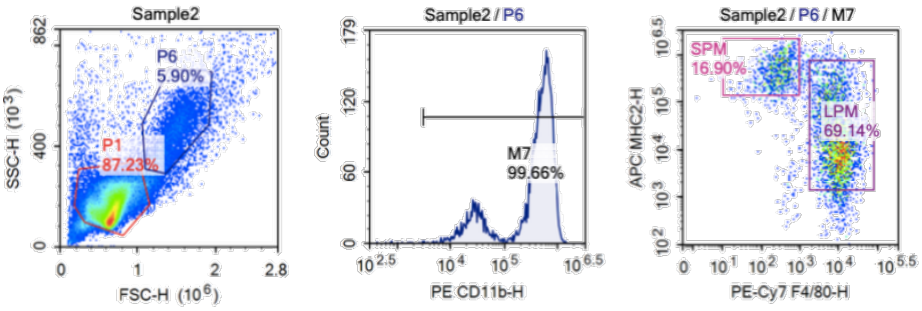

Representative flow cytometry plots for % SPMs in different groups tested (n=5)

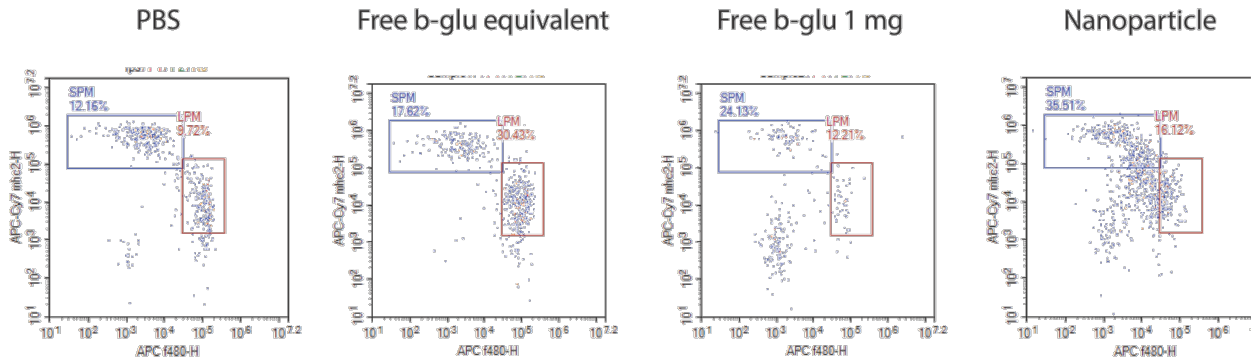

Figure B9: Mice were trained with indicated materials (PBS (black), equivalent amount of free β-glucan (pink), free 1 mg β-glucan (green) or nanoparticles (purple)) and challenged with LPS 7 days later. Spleens were harvested and analyzed. Splenic macrophages ($CD45^{+}B220^{-}$ $CD11b^{+}F4/80^{+}$) were higher in nanoparticle trained mice whereas neutrophils ($CD45^{+}B220^{-}$ $CD11b^{+}Ly6G^{+}$) were higher in the conventional 1 mg β-glucan trained mice.

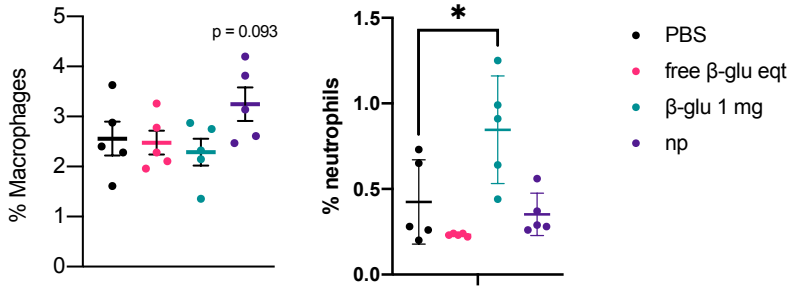

Figure B10: Mice were trained with indicated materials (PBS (black bars), 1 mg of nanoparticles on day 0 only (pink bars), 0.5 mg of nanoparticles on both day 0 and day 4 (green bars), equivalent amount of free β-glucan (purple), free 1 mg β-glucan (lilac). After 7 days, bone marrow was harvested and differentiated into BMDMs. 6 days after culture, cells were re plated at a density of 100,000 cells/ well and were challenged ex-vivo with LPS (10 ng/mL) and cytokines were quantified. Only mice trained with 1 mg of free β-glucan showed increased IL-6 levels confirming that nanoparticles did not act at the bone marrow.

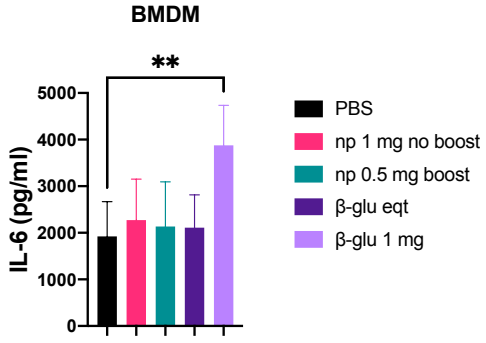

Figure B11: Tumor microenvironment analysis: At day 46, tumors were excised, and single cell suspensions were prepared. Gating strategy for tumor associated macrophages ($CD45^+CD11b^+F4/80^+$) and tumor associated neutrophils ($CD45^+CD11b^+Ly6G^+$) and representative flow cytometry plots for % TAMs and % TANs in tumor micro-environment in the groups tested (n=5).

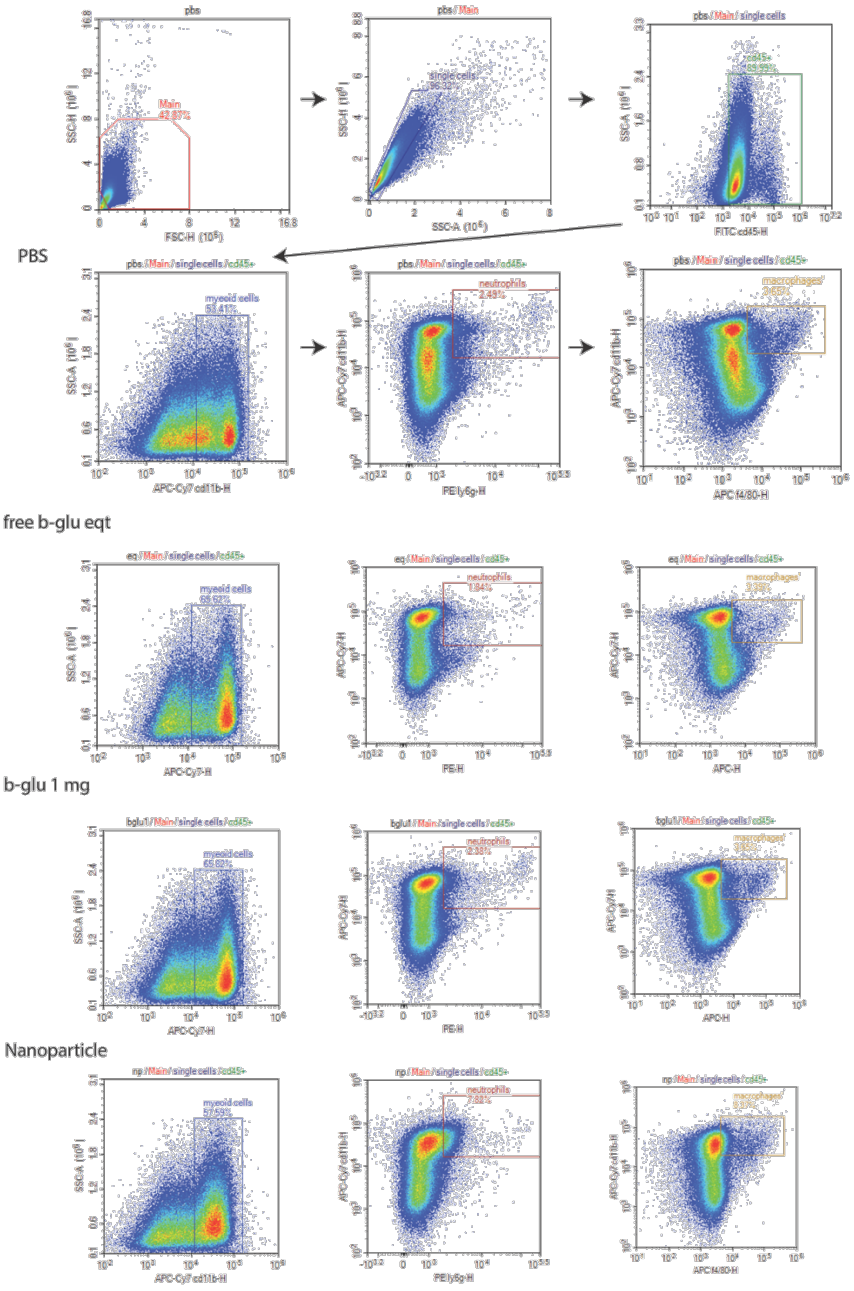

Figure B12: Mice were trained with indicated materials (PBS (pink), equivalent amount of free β-glucan (green), free 1 mg β-glucan (purple) or nanoparticles (lilac)) and were challenged with B16.F10 tumors after 3 weeks. Mice were sacrificed at day 46 and spleen weights were measured. Splenomegaly was observed for all groups except nanoparticle trained mice.

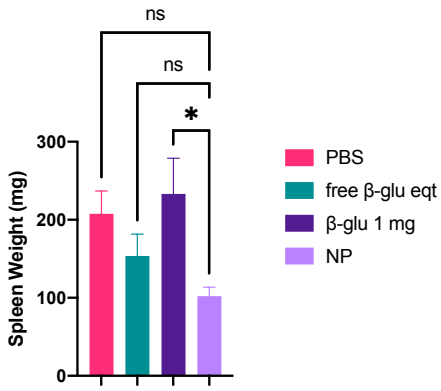

Figure B13: EG7.OVA tumor challenge. Mice were trained with indicated materials- PBS (black and pink), 1 mg of free β-glucan (purple) or 0.5 mg nanoparticles (lilac). One week after training, all groups except untreated (black) received CpG/OVA vaccination and were then challenged with EG7.OVA tumor after 2 weeks. Tumor growth was measured and quantified.

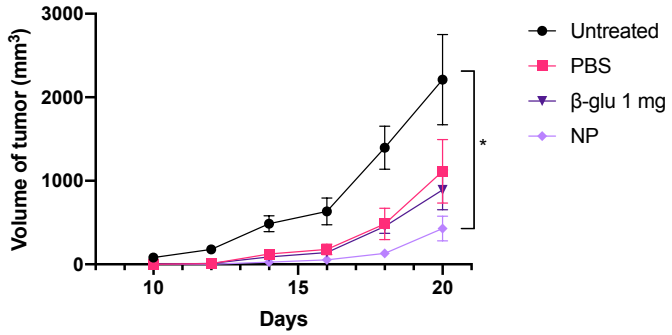

Figure B14a: DLS and SEM data for low molecular weight acid-terminated nanoparticles

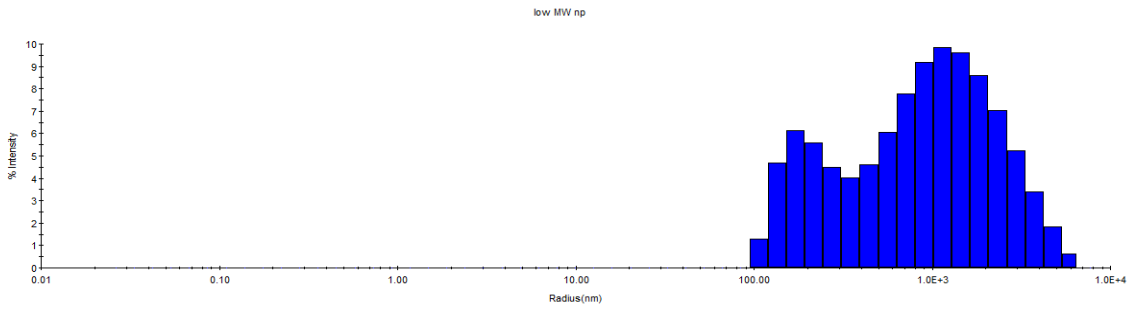

Figure B14a continued

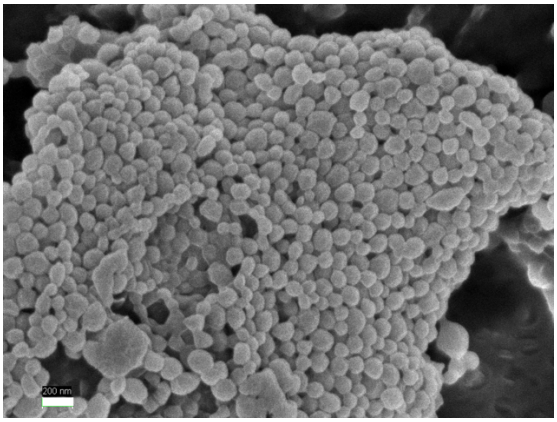

Figure B14b: DLS and SEM data for medium molecular weight ester-terminated nanoparticles (NIR-PLGA nanoparticles used for imaging)

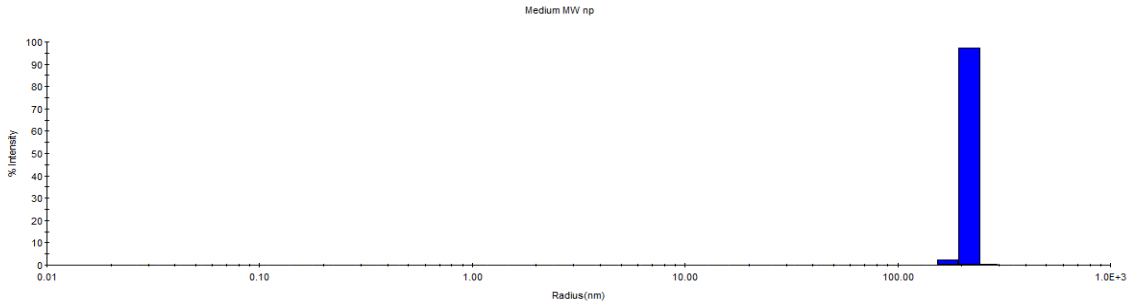

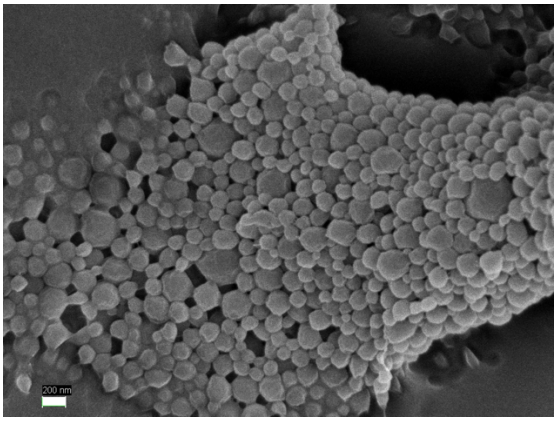

Figure B14c: DLS and SEM data for high molecular weight acid-terminated nanoparticles

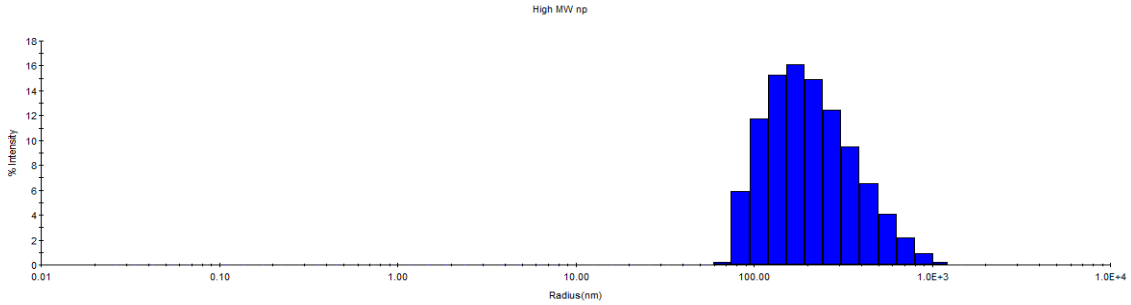

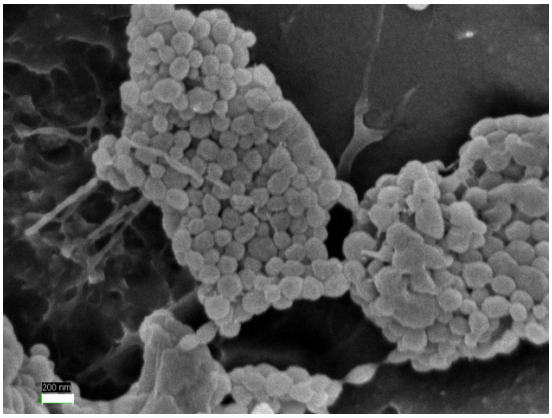

Figure B14d: DLS and SEM data for low molecular weight ester-terminated nanoparticles

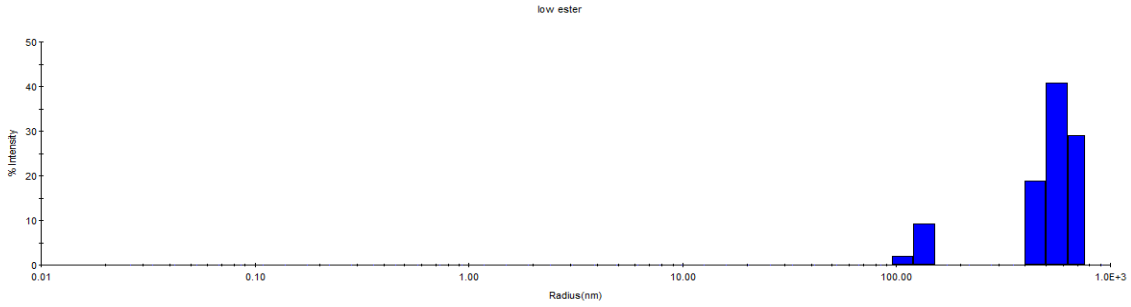

Figure B14d continued

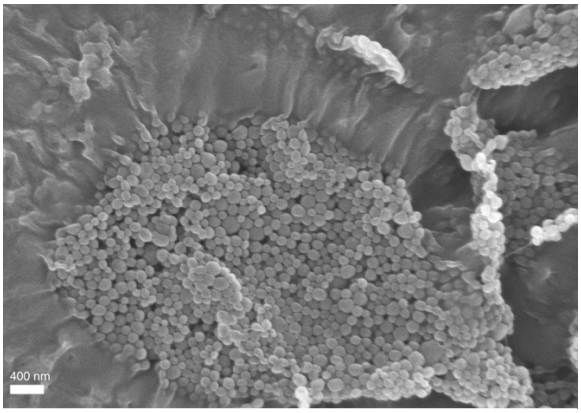

Figure B14e: DLS and SEM data for high molecular weight ester-terminated nanoparticles

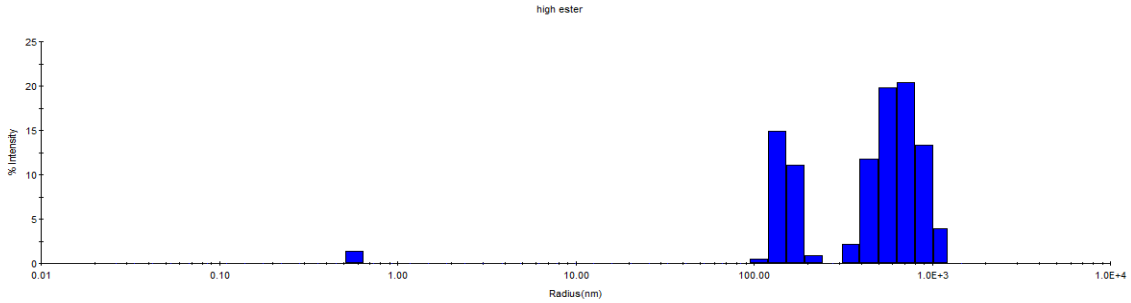

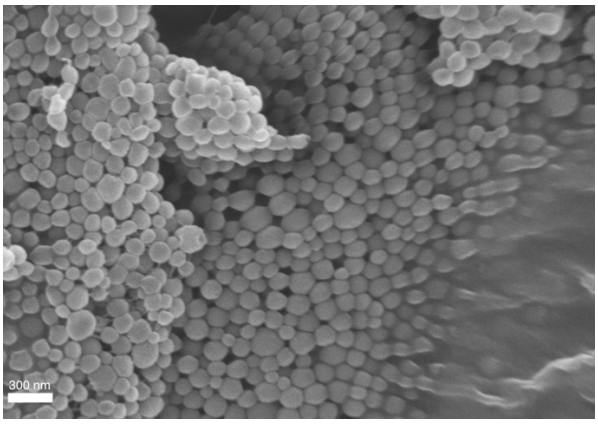

Table B1: Characterization data for synthesized nanoparticles

	Scale	Recovered(mg)	Loading (mg β-glucan/mg of particle)	SEM radius (nm)	DLS radius size (nm)	encapsulation efficiency (%)
Regular ester	200	140	52.4	67.2	487.9	73.4
Low acid	100	44	41.0	66.8	687	72.4
Medium ester	100	57	56.4	100	217	63.8
High acid	100	43	24.0	104	245	41.3
Low ester	100	50	43.0	137	468	63.3
High ester	100	66	120	130	413	55.6

Figure B15: Mice were trained once on day 0 with the desired training materials – PBS (black), low molecular weight acid terminated nanoparticles (pink), low molecular weight ester-terminated nanoparticles (green), high molecular weight acid terminated nanoparticles (purple) or low molecular weight ester-terminated nanoparticles (lilac). Different set of mice were challenged with LPS at different time points- IL-6 levels from serum of mice challenged on day 30 showed no difference from untrained mice.

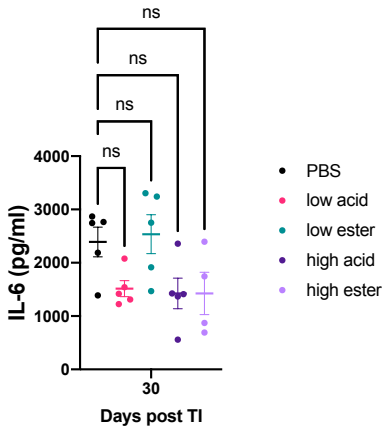

Appendix C: Chapter 5

Table C1 Characterization Data of Microparticles

Group	Diameter (µm)	Standard Deviation (µm)
PCL Core	6.61	2.03
PCL + Siloxane	7	1.41
PCL + Siloxane +PLA	8.45	1.26

Figure C1 FTIR of PS (purple) and PSL (yellow) coated microparticles. Both particles posses stretching at 1044 cm^{-1} representing the Si-O-Si stretch from the siloxane coating. The stronger stretch at 1720 cm^{-1} are from the carbonyl groups in the poly(lactide) secondary coating.